A new model for cold climate source rock preservation in the Arckaringa Basin

Thesis submitted in accordance with the requirements of the University of Adelaide for an Honours Degree in Geology

Natalie Debenham
November 2014

THE UNIVERSITY of ADELAIDE

TITLE

A new model for cold climate source rock preservation in the Arckaringa Basin

ABSTRACT

The controls on organic carbon preservation in sediments are poorly understood, however there is a first order association between high total organic carbon concentration (TOC), warm climates and fine grained sediments with mature mineralogy in the geologic record. Permo-Carboniferous marine sediments in the Arckaringa Basin, however, present an exception with anomalous organic carbon concentration (<11% TOC) occurring within mineralogically immature siltstones deposited in deep, narrow (marine) fjords during glacial conditions. Organic matter (OM) is not refractory terrigenous material, but rather hydrogen-rich and labile, thus identifying an active preservational mechanism that differs from conventional organic carbon enrichment controlled by mineral preservation effects. Energy Dispersive Spectrometry (EDS) reveal an association between labile OM and high sulphur concentrations, and EDS mineral mapping identifies a cyclic millimetre alteration between sulphur/OM rich laminae and manganese carbonate (kutnohorite) laminae, identifying oscillating benthic redox conditions similar to annual varves in proglacial environments. Framboidal pyrite (<5 µm) is abundant only within organic-rich laminae, indicating sulphate reduction in euxinic conditions resulting from restricted sea water exchange and the development of strong density stratification. Seisimic profiles indicate that deposition occurred in fjord-shaped troughs, with restriction resulting from end moraines acting as sills to the open ocean. Thus, organic carbon enrichment is attributed to restriction in the ancient fjords, leading to periods of hydrogen sulphide build up within the water column that were annually flushed with seasonal change in temperature and runoff. The reducing conditions of the fjord provided a chemical trap for S leading to its enrichment in organic matter. Similarly, Mn within carbonates was enriched in the same manner. Excess dissolved sulphur build up in the water column and sediments resulted in vulcanization (sulfurization) reactions polymerizing labile organic compounds (lipids and carbohydrates) and their preservation as organosulphur compounds during early diagenesis.

KEYWORDS

Arckaringa Basin, organic carbon, preservation, vulcanization, icehouse, source rock

TABLE OF CONTENTS

Title i
Abstract i
Keywords i
List of Figures 3
List of Tables 6
Introduction 7
Geological Setting/Background 9
Formation of basin troughs and influences on deposition 14
Methods 14
Sample Collection 14
Geochemical Analysis 15
Mineralogical Analyses 16
Petrographical Analyses 16
Observations and Results 17
Facies 1: Proglacial facies 24
Facies 2: Pelagic facies 25
Sub-facies 2a (Cyclic varve unit) 32
Sub-facies 2b (Massive black shale) 32
Sub-facies 2c (Lensed mudstone) 33
Facies 3: Bioturbated facies 34
Facies 4: Mass flow facies 35
Source Rock Characterisation 36
Discussion 40
Conclusions 50
Acknowledgments 52
References 52
Appendix A: Extended basin history and influences on deposition 57
Appendix B: Extended methods 60
1 Sample collection and preparation 60
2 Analyses 62
2.1 Total Organic Carbon (TOC) analysis 62
2.1.1 Pressure Calcimeter standard procedure 63
2.1.2 Elemental Analyser 64

2.2 Source Rock Analyser (SRA) and RockEval Analysis 65
2.2.1 Sample preparation standard procedure 65
2.3 GC-MS Analysis 67
2.3.1 MSSV-GC-MS thermal maturity analysis 67
2.3.2 Palaeoredox determination 68
2.3.3 Solvent extraction preparation 69
2.4 X-ray Diffraction (XRD) analysis 69
2.4.1 Bulk mineralogy and mineral identification 69
2.4.1 Clay fraction 70
2.5 Thin section analysis 74
2.6 Organic petrography analysis 75
2.7 Scanning Electron Microscope (SEM) analysis 77
Appendix C: XRD Results 78
Appendix D: Supporting sub-sample data 79

LIST OF FIGURES

Figure 1: Location map of the Arckaringa Basin in South Australia (inset) and the position of the Boorthanna Trough and Southern Arckaringa Troughs. The locations of Arck 1 and Cootanoorina 1 within the Boorthanna Trough are also shown, intersected by section line A–B. Permian isopach lines illustrate the thickness of the subsurface Permian sediments across the basin. Modified after Hibburt (1995) and Menpes (2012). 10
Figure 2: Schematic cross section through the Arckaringa Basin along section line A–B, showing the geometry of the Boorthanna Trough and the formations intersected by Arck 1 and Cootanoorina 1. The sedimentation of the Permo-Carboniferous succession extends from the depocentres and covers the less disturbed areas of the basement highs. Unconformably underlying this succession is the Cootanoorina Formation, which is restricted to the Boorthanna Trough. Modified after Hibburt (1995) and Harvey and Hibburt (1999).....11
Figure 3: Scanning electron microscope (SEM) photomicrographs showing the compositionally immature nature of the detrital mineral component within the Stuart Range Formation and its relationship organic matter (OM). OM is bounded by sub-angular quartz (qz) grains and detrital mica surrounded by a clay and quartz (cl+qz) matrix that is likely dominated by illite and kaolinite. Altered mica grains show extensive fraying and contain pyritic (py) replacement. Gypsum (gyp) within close proximity of OM is also apparent. Kutnohorite (kut) is observed in some samples. (a) Sample 2053188 (sub-facies 2b, TOC: 8.18); (b) 2053194 (sub-facies 2a, TOC: 3.04); (c) 2053196 (sub-facies 2b, TOC: 7.74); (d) 2053198 (sub-facies 2c, TOC: 4.64); (e) OM-rich sample (2053191 sub-facies 2b, TOC: 8.24) with sporinite and minor lamalginite; and inset (f) indicating no association between OM and diagenetic components, which are only minor in the high TOC samples. 18
Figure 4: Representative images and characteristic features of the four facies identified within the lower Stuart Range Formation, Arck 1: (a) Facies 1, proglacial facies; (b) Sub-facies 2a, cyclic varve unit (pelagic facies); (c) Sub-facies 2b, mass black shale (pelagic facies); (d) Sub-facies 2c, lensed mudstone (pelagic facies); (e) Facies 3, bioturbated facies; and (f) Facies 4, mass flow facies. 20
Figure 5: The abrupt upper boundary (at 960 m) between the mass flow facies, heading into the cyclic varve sub-facies (pelagic facies) within the lower Stuart Range Formation, Arck 1. High resolution total organic carbon (TOC) data was obtained from slivers of core (<4 mm) and has been plotted against depth, indicated by the scale bar on the left. The colours in the legend represent sedimentological observ-ations. The calcareous zone subsamples (within the mass flow facies) and the kutnohorite laminae subsamples (within the cyclic varve 2a, pelagic facies) have low TOC values. The light mudstone, as part of the transition to the dark varve laminations, has a medium TOC value, and the dark laminations have high TOC values.....21
Figure 6: Core logs of Arck 1 and Cootanoorina 1, illustrating lithological and geochemical variability. The Arck 1 log comprises the upper Boorthanna Formation to the lower Mount Toondina Formation, and the Cootanoorina 1 log comprises the upper Cootanoorina Formation to the lower Stuart Range Formation. Total organic carbon (TOC) data from core and cutting sub-samples was plotted with depth. Note that the Arck 1 depth scale is double the Cootanoorina 1 depth scale. Lithological observations presented in Harris and McGowran (1968) were followed as core for lithological analyses of Cootanoorina 1 was limited. 22
Figure 7: Core log of Arck 1 illustrating lithological and geochemical variability (left), with total organic carbon (TOC) data from core sub-samples plotted against depth. A subsection from 970–940 m was studied at higher resolution (right) and four facies were identified. Note that the subsection depth scale is three times the Arck 1 core log depth scale. 23
Figure 8: Scanning electron microscope (SEM) and integrated energy dispersive X-ray spectroscopy (EDS) photomicrographs of polished blocks taken from the pelagic facies in Arck 1. (a) SEM photomicrograph of sample I at 958 m (sub-facies 2a) and (b) accompanying EDS map of elemental distributions, where red = iron, green = calcium, and blue = manganese. This confirms the dominant mineralogy of the thin, light kutnohorite intervals that occur after every

dark couplet. The important minerals identified are gypsum (gyp) and kutnohorite (kut), surrounded by a primarily clay and quartz (cl+qz) matrix with framboids of pyrite (py). (c) SEM photomicro-graph of sample 2053196 at 959.97 m (sub-facies 2b) and (d) accompanying EDS map of elemental distributions, where red = silicon, green = calcium, and blue = manganese. The small red ovoid shapes correspond to pyrite. (e) SEM photomicrograph of sample 2053198 at 955.79 m (sub-facies 2c) and (f) accompanying EDS map of elemental distributions, where red = manganese, green = phosphorus, and blue = calcium. Apatite (ap) was present within the matrix and pyrite (py) is represented by light yellow-green. 26
Figure 9: Clay mineral fraction X-ray diffractogram of Arck 1 core samples 2053194 (red, sub-facies 2b) and 2053198 (blue, sub-facies 2b), with both air dried (solid line) and ethylene glycol (dashed line) treatments. The diffractograms have been shifted upwards for clarity. The phyllosilicate mineral compositions were determined by applying the United States Geological Survey (USGS) Clay Mineral Flow Diagram of Poppe *et al.* (2001). Mixed layer illite-smectite (mixed I-S), illite (I), kaolinite (kao), natrojarosite (nj), and quartz (qz) were identified in both samples. Data based on Appendix C, Table C2.....27
Figure 10: Reflected light (left) and ultra-violet (right) photomicrographs showing the organic components within the Stuart Range Formation, from low total organic carbon (TOC) contents (a, b) to 9 TOC contents (e, f). (a, b) Sample 2053339 at 923.03 m, with a TOC value of 2.11, Facies 3. Dominated by a terrigenous source of organic matter, comprising sub-angular and unstructured telinite (tel) and semifusinite (sf). Sporinite (sp), also of terrestrial origin, is present in minor quantities. A high proportion of carbonates are present, which is typical of low TOC samples. (c, d) Sample 2053197 at 957.60 m, with a TOC value of 4.78, sub-facies 2a. Semifusinite surrounded by abundant sporinite, framboidal pyrite (py), lamalginite (lam), and minor telinite. (e, f) Sample 2053196 at 959.97 m, with a TOC value of 7.74, sub-facies 2b. Abundant lamalginite, sporinite, and framboidal pyrite, with minor alginate (alg) and telinite. Lamalginite, alginate, and framboidal pyrite are of marine origin. No carbonates are present within the higher TOC samples. The classification table for the identification of organic macerals in Appendix B, Table B3, was followed during analysis.....28
Figure 11: Scanning electron microscope (SEM) photomicrograph of polished blocks taken from Arck 1. Energy dispersive spectroscopy (EDS) spot analysis within discrete particles of organic matter was performed to determine elemental compositions. The results are illustrated graphically to the right. Peaks indicate the presence of carbon (C), oxygen (O), aluminium (A), silicon (Si), sulphur (S), potassium (K) and iron (Fe). 'Clay matrix' indicates where spot analysis has also analysed the clay matrix, and 'Matrix' indicates where the carbonate matrix has been analysed. (a) 2053196 at 959.97 m, total organic carbon (TOC): 7.74, sub-facies 2b; (b) 2053188 at 966.35 m, TOC: 8.18, sub-facies 2b; (c) 2053307B at 952.59 TOC: 1.76, Facies 3. 30
Figure 12: Solvent extracted, gas chromatography-mass spectrometry (GC-MS) chromatogram of sample 2053334, with a high total organic carbon content of 5.97 mg/g. Octacyclosulphur (S_8) is the major peak, with sulphur allotropes hexacyclosulphur (S_6) and heptacyclosulphur (S_7) as minor peaks. The double peak for S_6 is likely to be an artefact of instrument error. The background peaks indicate the hydrocarbon profile for this sample. Inset is an ion chromatogram of the S_8 peak (*m/z* 64) showing cyclic sulphur complexes and ions associated with S_8. 31
Figure 13: Quantitative Evaluation of Minerals by Scanning electron microscopy (QUEMSCAN® by FEI Company) mineral map of a polished block taken from the massive black shale (sub-facies 2b) in Arck 1 (sample 2053196 at 959.97 m) using energy-dispersive X-ray spectroscopy (EDS) for data acquisition. The legend to the right illustrates the colour assignment of the minerals present. The inset further details mineral associations and distributions to a higher resolution. The repetitive laminae (50–800 μm width) illustrated by the blue–purple shades that primarily represent gypsum ± anhydrite (purple), and rhondochrosite (± anhydrite), and kutnohorite (blue). The higher resolution mineral map inset also demonstrates the compositionally immature nature of the detrital mineral component within the Stuart Range

Formation, with sub-angular to sub-rounded quartz grains, poorly sorted K-feldspar, and detrital mica surrounded by a clay and quartz matrix dominated by illite and kaolinite. 34
Figure 14: Sealed vessel thermal extraction (TH-GC-MS) and micro-scaled sealed vessel pyrolysis coupled to gas chromatography-mass spectrometry (MSSV-GC-MS) chromatograms of a representative high total organic carbon (TOC) sample (2053188, at 966.35 m, TOC: 8.18, sub-facies 2b) and a low-medium TOC sample (2053367, at 975.60 m, TOC: 4.23) from the Arck 1 core. (a) TH-GC-MS chromatograms of samples 2053188 (red) and 2053367 (grey), and MSSV-GC-MS chromatogram of sample 2053367 (blue) which is a close approximation of what would be expected if sample 2053367 had naturally undergone further maturation to produce free hydrocarbons. (b) TH-GC-MS chromatogram of sample 2053188, focussing on the pristane (pr) and phytane (ph) biomarker parameter for the assessment of redox conditions. A pr/ph value >1 indicates oxic conditions and a pr/ph value <1 reflects anoxic conditions at the sediment/water interface, following Didyk *et al.* (1978). In this case, pr/ph = 0.92, suggesting deposition during anoxic to sub-oxic conditions. (c) MSSV-GC-MS chromatogram of sample 2053367, showing that pr/ph = 2.37, suggesting deposition during oxic conditions. 37
Figure 15: The types of hydrocarbons and the maturity of a selection of Arck 1 and Cootanoorina 1 core samples, based on source rock analysis (SRA). The Stuart Range Formation (box), taken from the Arck 1 core, is primarily Type II–III oil-gas-prone to Type III gas-prone as indicated by the low hydrogen index (HI) values. It is immature to mature, heading into the oil generation window. The Stuart Range Formation samples have been coloured according to their facies. Samples without an assigned facies have not been coloured. The Cootanoorina Formation (red triangle), taken from the Cootanoorina 1 core, is Type IV inert to Type III gas-prone as indicated by the extremely low HI values. This formation has no potential to very minimal potential to produce hydrocarbons. 39
Figure 16: Representative source rock potential pyrograms of the Stuart Range Formation and the Cootanoorina 1 Formation based on source rock analysis (SRA). The plots show the proportions of free (S1) and potential (S2) hydrocarbons as artificial maturation is induced by incrementally increasing temperature over a period of time. (a) The Stuart Range Formation (2053193 at 963.04 m), taken from the Arck 1 core, has a significant hydrocarbon potential, as indicated by the large S2 peak. The comparatively low S1 peak indicates a low proportion of free hydrocarbons. (b) The Cootanoorina Formation (2066664 at 948.06 m), taken from Cootanoorina 1, has multiple S2 peaks, suggesting multiple stages of maturation and multiple phases of migration. 40
Figure 17: Schematic diagrams illustrating the interpreted depositional environments for the six facies identified in the lower Stuart Range Formation in the Arck 1 core. Features within these models are further detailed in Figure 19. The pycnocline (water density gradient) is represented by the red dashed line. (a) Proglacial facies depositional model. Very low sea level, shallow sill conditions due to the presence of glaciers and icebergs. Rare deep water renewal and a shallow pycnocline, with occasional fresh water replenishment as ice melts. (b) Mass flow facies depositional model. Low sea level, shallow sill conditions. Rare deep water renewal and a shallow pycnocline, promotes the development of stratified, euxinic bottom water conditions. Though this is disrupted with mass flow events that result in a surge of sediment deposition and brief bottom water oxygenation. (c) Bioturbated facies depositional model. High sea level, deep sill conditions. Frequent deep water renewal and a pycnocline within the interstitial waters a few centimetres below the sediment–water interface. Mixing of the water column with oxygen and nutrients promotes benthic fauna activity within the oxic sediments (bioturbation). (d) Pelagic facies depositional model. Low sea level, shallow sill conditions. Rare deep water renewal and a shallow pycnocline, promotes the development of stratified, euxinic bottom water conditions. However, this is episodically interrupted by oxic conditions following the bioturbated marl depositional model, on a seasonal timescale. 42
Figure 18: Interpretation of seismic line 86AK-7 of the Southern Arckaringa Basin troughs (West Trough and Phillipson Trough), showing the current geometry of the troughs

(unflattened). These troughs have been interpreted as incised glacial valleys, i.e. fjords. From Menpes *et al.* (2010). 45
Figure 19: Schematic diagram illustrating the changes in water exchange across the sill and changes in bottom water redox conditions, as sea level rises and falls. Connection with the open ocean water across the sill allows sulphate (SO42-) replenishment. This diagram also shows the fluxes of fresh water, terrigenous material, and organic matter (OM) during deposition of the Stuart Range Formation, within the Arckaringa Basin troughs. (a) Low sea level, shallow sill conditions. Rare deep water renewal and a shallow pycnocline, promotes the development of stratified, euxinic bottom water conditions. The sulphur cycle, occurring within the euxinic zone, shows the partial removal of SO42- by bacterial sulphate reduction to make sulphide or hydrogen sulphide (H2S). H2S can then react with the iron (Fe) minerals within the water column to precipitate pyrite (FeS2). Fine-grained sediments are deposited as laminations in this undisturbed setting. (b) High sea level, deep sill conditions. Frequent deep water renewal and a pycnocline within the interstitial waters a few centimetres below the sediment–water interface. Mixing of the water column with oxygen and nutrients promotes benthic fauna activity within the oxic sediments (bioturbation). 47

LIST OF TABLES

Table 1: Stratigraphic descriptions of the Arckaringa Basin formations and underlying Cootanoorina Formation, including age based on palynology and interpreted sedimentary environment of deposition. …….11
Table 2: Summary of the drill core and sampling information for Cootanoorina 1 and Arck 1, acquired from the Cootanoorina 1 and Arck 1 well completion reports. ……....14
Table 3: Characteristics and interpretations of the six facies identified within the lower Stuart Range Formation, as observed within Arck 1. ……...18
Table 4: Typical mineralogy of the six facies identified within the lower Stuart Range Formation, X-ray diffraction (XRD) of bulk powders (Appendix C, Table C1). The presence (%samples) of mineral phases has been grouped into 'all samples', 'most samples', and 'few samples', and 'N/A' has been assigned to facies with only 2 XRD sample results. The number of XRD samples is bracketed beside each facies number. ……....23

INTRODUCTION

Periods of anomalous organic-rich source rock deposition are evident within the stratigraphic record, and are commonly thought to be associated with warm greenhouse Earth conditions (Klemme and Ulmishek 1991; Weissert and Mohr 1996). These periods are often linked to stratified, oxygen-depleted waters in which biotic productivity is enhanced due to accelerated chemical weathering and nutrient influx. Organic matter (OM) preservation is consequently improved through reduced degradation of OM as a result of oxygen depletion (Sun *et al.* 2002; Moodley *et al.* 2005) and through association with partial soil-derived detrital clay minerals favoured in warm climates (Mayer 1994; Kennedy *et al.* 2002). A review by Klemme and Ulmishek (1991) suggested that there are only six stratigraphic intervals that account for around 90% of the world's effective and exploitable petroleum reserves, with almost 60% derived from OM enriched source rocks deposited during the greenhouse conditions of the Late Jurassic and middle Cretaceous.

Though more rarely, there are also source rocks deposited during icehouse conditions. Icehouse glacial and subsequent paraglacial periods are characterised by sediment build up from physical weathering and mechanical erosion, resulting in unstable landscapes, increased sedimentation rates and sediment gravity flows (Jasper and Gagosian 1989; Summerfield 1991; Ballantyne 2002). These types of environments are not conducive to OM enrichment. Higher organic productivity, leading to more enriched sediments, has been related to nutrients released from deglacial waters (Macquaker and Keller 2005) and deep-water to coastal nutrient upwelling (Lüning *et al.* 2000; Algeo *et al.* 2014) in response to coastal currents enhanced by latitudinal temperature gradients.

Economically significant source rocks deposited during icehouse conditions occur in Ordovician successions in North Africa and Middle East regions, in marine glacial fjord basins such as the Rub al Khali (Saudi Arabia), Murzuq (Libya) and Illizi (Algeria) basins, (Ballantyne 2002). Organic carbon (OC) preservation in these basins is poorly understood, however, and is not obviously the result of enhanced nutrient influx from upwelling or runoff. Predictive models for source rock prospecting in icehouse periods are comparatively poorly developed.

In Australia, a number of basins contain economically important source rocks of Permian age, corresponding with icehouse conditions, including the Arckaringa, Carnarvon, Canning, Officer, Pedirka, and Cooper basins (Bradshaw *et al.* 2012). Source rocks in the adjacent Arckaringa and Cooper Basins fall within the supersource rock category with a high proportion (<11%) of total organic carbon (TOC; Kennedy and Wagner 2011). These sediments were deposited under restricted marine conditions in the Arckaringa Basin, in contrast to the lacustrine conditions within the Cooper Basin, during the waning stages of glaciation in the Pennsylvanian to early Permian (Wopfner 1970; Alexander *et al.* 1998). Little is known about the preservation mechanisms responsible for the significant organic enrichment evident in these successions.

In this thesis I show, from whole core to micron scale, the distribution and variation of OM and mineral phases in Permo-Carboniferous succession of the Arckaringa Basin in order to identify the mechanisms responsible for one of Australia's most organic rich source rock. More specifically I determine mineral surface preservation effects, and the

role of restriction and anoxia associated with marine sill development in a fjord. I show that marine restriction of the basin troughs led to periods of hydrogen sulphide build up, promoting vulcanization reactions to preserve OM through the incorporation of inorganic S into lipids and carbohydrates to form organosulphur compounds during early diagenesis.

GEOLOGICAL SETTING/BACKGROUND

The Arckaringa Basin is a Permo-Carboniferous intracratonic basin that covers an area of approximately 100,000 square kilometres in central northern South Australia (Figure 1; Wopfner 1970; Wohling *et al.* 2013). Five thick depocentres with infill sediments exceeding 1,000 metres in depth (Hibburt 1995) are situated around a basement high associated with the Mount Woods Inlier. The two main depocentres within the basin are the broad Boorthanna Trough in the east and the narrow Southern Arckaringa Troughs (Wallira, Penrhyn, Phillipson, and West) in the south. The Permo-Carboniferous succession of the Boorthanna Trough is partially underlain by early Palaeozoic Cootanoorina Formation and Neoproterozoic sediments of the Adelaide Rift complex, while the succession of the Southern Arckaringa Troughs is underlain by Archaean to Early Mesoproterozoic rocks of the Gawler Craton (Hibburt 1984). An abbreviated succession of late Jurassic to early Cretaceous Eromanga Basin sediments unconformably overlie the Permo-Carboniferous succession, thickening to the north east, which is in turn overlain by a thin veneer of Tertiary sediments (Hibburt 1984).

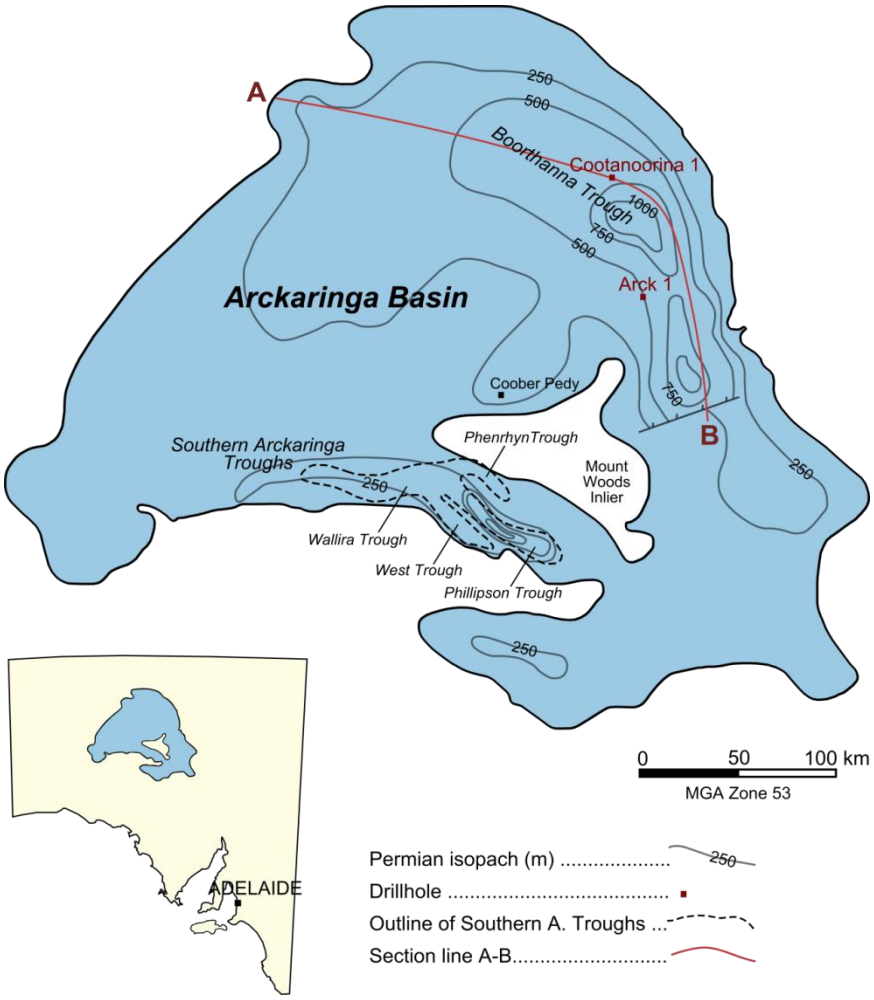

Figure 1: Location map of the Arckaringa Basin in South Australia (inset) and the position of the Boorthanna Trough and Southern Arckaringa Troughs. The locations of Arck 1 and Cootanoorina 1 within the Boorthanna Trough are also shown, intersected by section line A–B. Permian isopach lines illustrate the thickness of the subsurface Permian sediments across the basin. Modified after Hibburt (1995) and Menpes (2012).

The Permo-Carboniferous succession of the Arckaringa Basin comprises three formations defined by drillcores, outcrop mapping, and geophysical exploration (Ludbrook 1961; Townsend and Ludbrook 1975; Wopfner 1980). These formations, in ascending stratigraphic order, are the Boorthanna, Stuart Range, and Mount Toondina Formations (Figure 2; Table 1). Source rock studies of the Permo-Carboniferous succession indicate that the basal Stuart Range Formation and Boorthanna Formation contain oil-prone potential source rocks. Additionally, pre-Permian strata deposited

within the Boorthanna Trough may also contain potential source rocks (Moore 1982; Bishop 2013). Within the Boorthanna Trough, Permo-Carboniferous sediments with increasing thermal maturity are found in the deeper southern parts of the trough where burial has been sufficient for hydrocarbon generation. Sediments with a higher thermal maturity are also found within the Phillipson Trough, possibly due to a high heat flow event 150 million years ago (Harvey and Hibburt 1999). Coal deposits in the upper Mount Toondina Formation are currently being assessed for potential in situ gasification and Coal Seam Gas production, and the basin is also being investigated for conventional and unconventional oil and gas plays (Wohling *et al.* 2013).

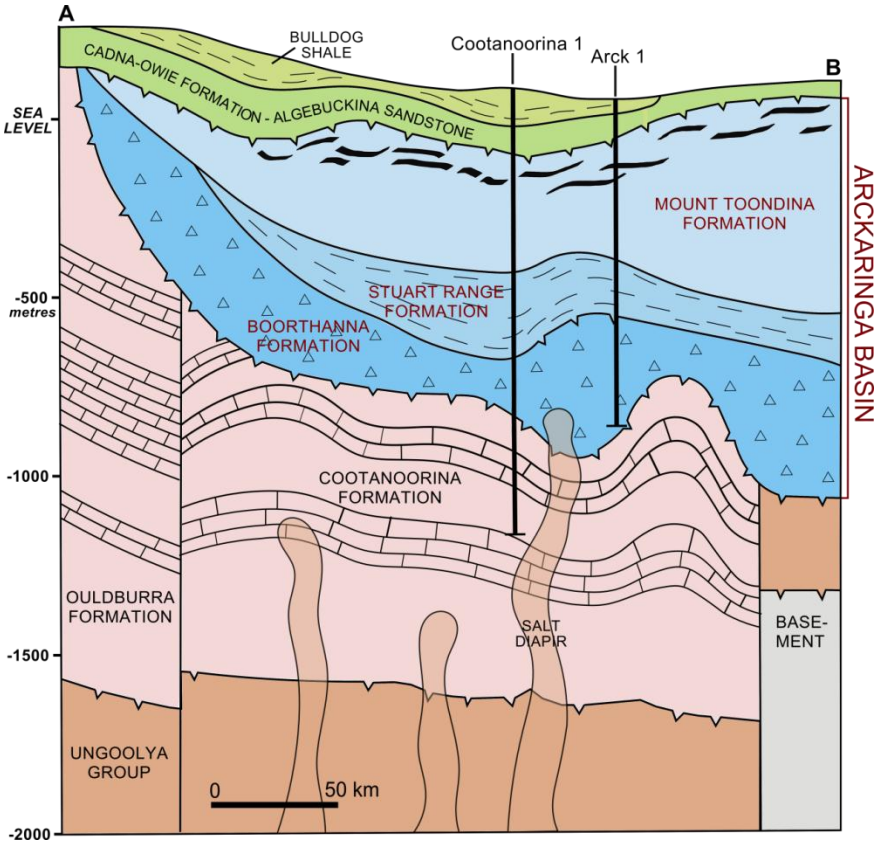

Figure 2: Schematic cross section through the Arckaringa Basin along section line A–B, showing the geometry of the Boorthanna Trough and the formations intersected by Arck 1 and Cootanoorina 1. The sedimentation of the Permo-Carboniferous succession extends from the depocentres and covers the less disturbed areas of the basement highs. Unconformably underlying this succession is the Cootanoorina Formation, which is restricted to the Boorthanna Trough. Modified after Hibburt (1995) and Harvey and Hibburt (1999).

Table 1: Stratigraphic descriptions of the Arckaringa Basin formations and underlying Cootanoorina Formation, including age based on palynology and interpreted sedimentary environment of deposition.

Unit	Age based on palynology (Price et al. 1985; Wohling et al. 2013)	Description	Interpreted sedimentary environment
Mount Toondina Formation	295.0 to 290.1 Ma (Sakmarian), or palynostratigraphic zone PP2	The Mount Toondina Formation overlies the Stuart Range Formation with a conformable to disconformable relationship; however the formation may also unconformably overlie the Stuart Range Formation and the Boorthanna Formation in some areas within the Boorthanna Trough (Hibburt 1984). The Mount Toondina Formation is prevalent across much of the basin, with the thickest intersection of 598 metres in the Boorthanna 1 well. Two units can be identified within the formation; The lower unit consists of interbedded siltstones and clays with minor fine sands, and contains minimal carbonaceous material and is absent of coals. The upper unit is comprised of interbedded siltstones, shales and thin 10 metre thick coal seams with minor sands, and contains an increased abundance of carbonaceous material.	The formation comprises an overall coarsening upward succession that is capped by coals, consistent with the prograding deltaic to fluvial-lacustrine deposition with intermittent coal swamp development suggested by Menpes (2012), derived from interpretations made by Wopfner (1970) and Townsend and Ludbrook (1975) and geophysical observations from recent drilling activity.
Stuart Range Formation	The lower Stuart Range Fm. has been assigned to zone PP1 (Asselian) and the upper Fm. has been assigned to zone PP2 (Sakmarian), suggesting 298.9 to 290.1 Ma	The Stuart Range Formation conformably overlies the Boorthanna Formation in most areas throughout the basin, although seismic sections indicate an unconformable boundary within the Boorthanna Trough (Hibburt 1984; Hibburt 1995). The formation is widely distributed and encountered in most wells, and has a maximum thickness of 491 metres that was intersected by the Lake Phillipson Bore (Ludbrook 1967; Townsend and Ludbrook 1975). It comprises homogenous shale with occasional thinly laminated siltstone and minor sandstone, and can be micromicaceous, calcareous and pyritic (Hibburt 1984). The sediments were deposited during a marine transgressive phase (Jones 1987), and sequence stratigraphic studies by Menpes (2012) indicate that the maximum flooding surface can be considered as a reasonable marker for the top of the Stuart Range Formation.	Alternating restricted marine and lacustrine depositional conditions are suggested in a number of wells across the basin (Hibburt 1995) by changes in lithology and microfauna assemblages (Harris and McGowran 1968; Hibburt 1984; Hawkes 2014).
Boorthanna Formation	298.9 to 295 Ma (Asselian), or palynostratigraphic zone PP1	The Boorthanna Formation was defined using the Boorthanna 1 well (Townsend and Ludbrook 1975), which provides the representative 419.1 metres thick subsurface type section of the formation. Two units can be identified within the formation which grade from a glaciogene sequence to a marine facies	The lower unit of the Boorthanna Formation represents subaqueous glacial debris that may have been transported by mudflows (Hibburt

		stratigraphically higher. The lower unit appears to be restricted to the deeper parts of the basin, such as within the Southern Arckaringa Troughs and the southern half of the Boorthanna Trough. It consists of a glaciogene diamictite of sandy clays and pebble to boulder clays with occasional carbonate intercalations (Wohling et al. 2013), and in some wells conglomerates from the local erosion of basement highs have been identified (Ludbrook 1961; Townsend and Ludbrook 1975; Moore 1982). The upper unit is more ubiquitous and is comprised of rhythmically bedded marine clastics with grain sizes that range from silt to boulders. Medium to coarse grained sandstone dominates the unit, often grading to conglomerates composed of basement rock lithologies and occasionally grading into siltstones (Hibburt 1984; Hibburt 1995). Kellett et al. (1999) described the Boorthanna Formation sediments as mostly weakly indurated with local calcareous, ferruginous and pyrite cementation.	1995). Many studies suggest the glaciogene sediments were transported and deposited by rivers, mudflows and turbidity currents under fluvial and marine conditions (Wopfner 1970; Townsend and Ludbrook 1975; Hibburt 1995).
Cootanoorina Formation	Early Palaeozoic	The Cootanoorina Formation that unconformably underlies the Permo-Carboniferous succession within the Boorthanna Trough comprises a shallow marine siliciclastic to dolomitic and anhydritic sequence and is laterally equivalent to the Ouldburra Formation of the Officer Basin (Jones 1988; Hibburt 1995). The anhydrite shows evidence of significant post-depositional mobilisation (Moore 1982) which could potentially be a result of the Mount Toondina diapiric structure (Allchurch et al. 1973; Jones 1988). Gently undulating Neoproterozoic sediments of the Adelaide Rift complex underlie the Cootanoorina Formation. The formation can range up to 1000 metres thick toward the centre of the Boorthanna Trough.	Interpreted to have been deposited as a predominately shallow marine and evaporitic tidal flat sequence (Moore 1982).

Formation of basin troughs and influences on deposition

According to Wopfner and Allchurch (1967), and Townsend (1976), the Arckaringa Basin troughs developed primarily along north-west trending lineaments (further detailed in Appendix A), which were re-activated during the Devonian to Early Permian. The Boorthanna Trough was initially interpreted as a failed rift arm and is considered to be the largest basinal depocentre, (Jones 1988). Alternatively, Ludbrook (1967), and more recently Menpes *et al.* (2010), based on seismic data, considered the Arckaringa Basin troughs to have formed as erosional features (fjords) resulting from glacial scour augmented by syngenetic faulting (Wopfner 1970; Harvey and Hibburt 1999; Jensen-Schmidt *et al.* 2006). The basin sediments have been dated from 298.9 to 290.1 Ma (Price *et al.* 1985) on the basis of palynological information. Palynology indicates that connection to the ocean was episodically restricted and oxygen depleted (Jones 1987). The Boorthanna Formation and lower Stuart Range Formation were deposited during glaciation and subsequent deglaciation (Wopfner 1970; Jones 1987; Veevers 2006). Eustatic fall and/or crustal isostatic recovery resulted in deltaic progradation evident in the Mount Toondina Formation (Menpes *et al.* 2010; Menpes 2012).

METHODS

Sample Collection

Core samples were collected from Arck 1 and Cootanoorina 1 at the DMITRE drill core library, South Australia. Both cores were drilled within the Boorthanna Trough (Figure 1) at similar depths (Table 2), although Arck 1 has undergone deeper burial. The thicknesses of core studied were 118 m (Arck 1) and 75 m (Cootanoorina 1), with 168m

of cuttings inspected from Cootanoorina 1. Samples were selected for geochemical, mineralogical, and petrographical analyses to illustrate the geochemical and diagenetic variability across the Arckaringa Basin formations and the underlying Cootanoorina Formation. Higher resolution studies were performed on 30 m of Arck 1 core within the lower Stuart Range Formation to further elucidate geochemical and sedimentological trends.

Table 2: Summary of the drill core and sampling information for Cootanoorina 1 and Arck 1, acquired from the Cootanoorina 1 and Arck 1 well completion reports.

	Cootanoorina 1	Arck 1
Max. drilled date	15-06-1967	17-08-2011
Operator	S.A. Dept. Mines and Energy	Linc Energy Ltd.
Exploration tenement	–	PEL 122
Latitude	28° 00.5′ 23.218″ S	28° 30′ 12.48″ S
Longitude	135° 19′ 59.632″ S	135° 29′ 10.37″ E
Formations intersected	Lower Stuart Range Formation to upper Cootanoorina Formation	Mount Toondina Formation to upper Boorthanna Formation
Core depth sampled	380.09–948.06 m	876.13–994.10 m
Cutting depth sampled	701.04–871.73 m	–
Inspection number	4278	4194, 4337

Geochemical Analysis

A total of 260 sub-samples (comprising 179 core samples from Arck 1, and 25 core and 56 cutting samples from Cootanoorina 1) were milled to a fine powder for geochemical analysis (detailed in Appendix B). Total carbon (TC) content was measured using a PerkinElmer® 2400 Series II CHNS/O Elemental Analyser and inorganic carbon (IC) content was determined using the modified pressure-calcimeter method of Sherrod *et al.* (2002). Total organic carbon (TOC) was calculated by subtraction, i.e. TOC (%) = TC (%) – IC (%). Source rock characterisation was performed using a Weatherford® Laboratories Source Rock Analyser (SRA) TPH workstation to evaluate the proportion

of free hydrocarbons (S_1) and hydrocarbon generation potential (S_2), based on the Rock-Eval pyrolysis method of Espitalié *et al.* (1977), and thermal maturity (Jarvie *et al.* 2001). The hydrocarbon distributions of the S_1 and S_2 fractions and the palaeoredox conditions were elucidated by applying micro-scale-sealed-vessel thermal extraction and pyrolysis technologies hyphenated to gas chromatography mass spectrometry (MSSV-GC-MS; detailed in section 2.3, Appendix B; Hall *et al.* 2011). Conventional while oil GC-MS was conducted on a selected sample following solvent extraction using a Thermo Fisher Accelerated Solvent Extractor (ASE) 350 (detailed in section 2.3.3, Appendix B). All GC-MS were conducted using a HP 6890/5973 Quadrupole system.

Mineralogical Analyses

The bulk mineralogy of a selection of representative and high TOC samples was ascertained by a Bruker D8 ADVANCE Powder X-ray Diffraction (XRD) with a Cu-radiation source, using Bruker DIFFRAC.EVA software and Crystallography Open Database reference patterns for identifying mineral phases. XRD analysis of the clay fraction, with various treatments (orientated air dried and ethylene glycol expanded), was subsequently carried out (detailed in section 2.4, Appendix B). Mineralogy was also examined by optical and scanning electron microscope (SEM) analysis (detailed further below).

Petrographical Analyses

Variations in composition, texture, porosity and diagenetic alteration were investigated by examining representative thin sections and polished blocks. Transmitted and polarised light optical petrography was conducted using a Nikon Eclipse CiPOL

polarising microscope on thin sections (~30 μm) prepared by Prograding Rock Services Ltd. Backscattered SEM imaging was performed on a selection of polished blocks using the FEI Quanta 450 SEM and Joel Neoscope JCM 6000 SEM, both equipped with energy dispersive x-ray spectroscopy (EDS) systems for elemental analysis. Samples were cut perpendicular to the bedding plane and the polished blocks were milled using a Fischione 1010 Argon Ion Mill. Reflected white light and fluorescence (UV and blue light) microscopy was performed using a Nikon Eclipse CiPOL polarising microscope for organic petrography analyses in order to identify the organic matter present. Sample preparation and analyses were conducted following the methodology and identification standards of Taylor *et al.* (1998) and Suárez-Ruiz *et al.* (2012) based on the ICCP (International Committee for Coal Petrology) System 1994 (section 2.6, Appendix B).

Observations and Results

The Stuart Range Formation is predominately an organic-rich feldspathic micaceous siltstone that is compositionally immature and prone to diagenetic alteration (Figure 3). Evidence of bioturbation is sparse, with a prevalence of undisturbed parallel lamination throughout the formation, suggesting oxygen depleted conditions inhibitive of benthic macrofauna. The formation is texturally and mineralogically heterogeneous, as demonstrated by four facies that have been identified within the Arck 1 subsection (summarised in Table 3 and represented in Figure 4). These facies appear to be linked to paraglacial and oceanographic changes, and are defined compositionally by the detrital mineral component more so than the diagenetic component. All facies contain detrital quartz, and illite/mica and kaolinite as the two primary clay phases.

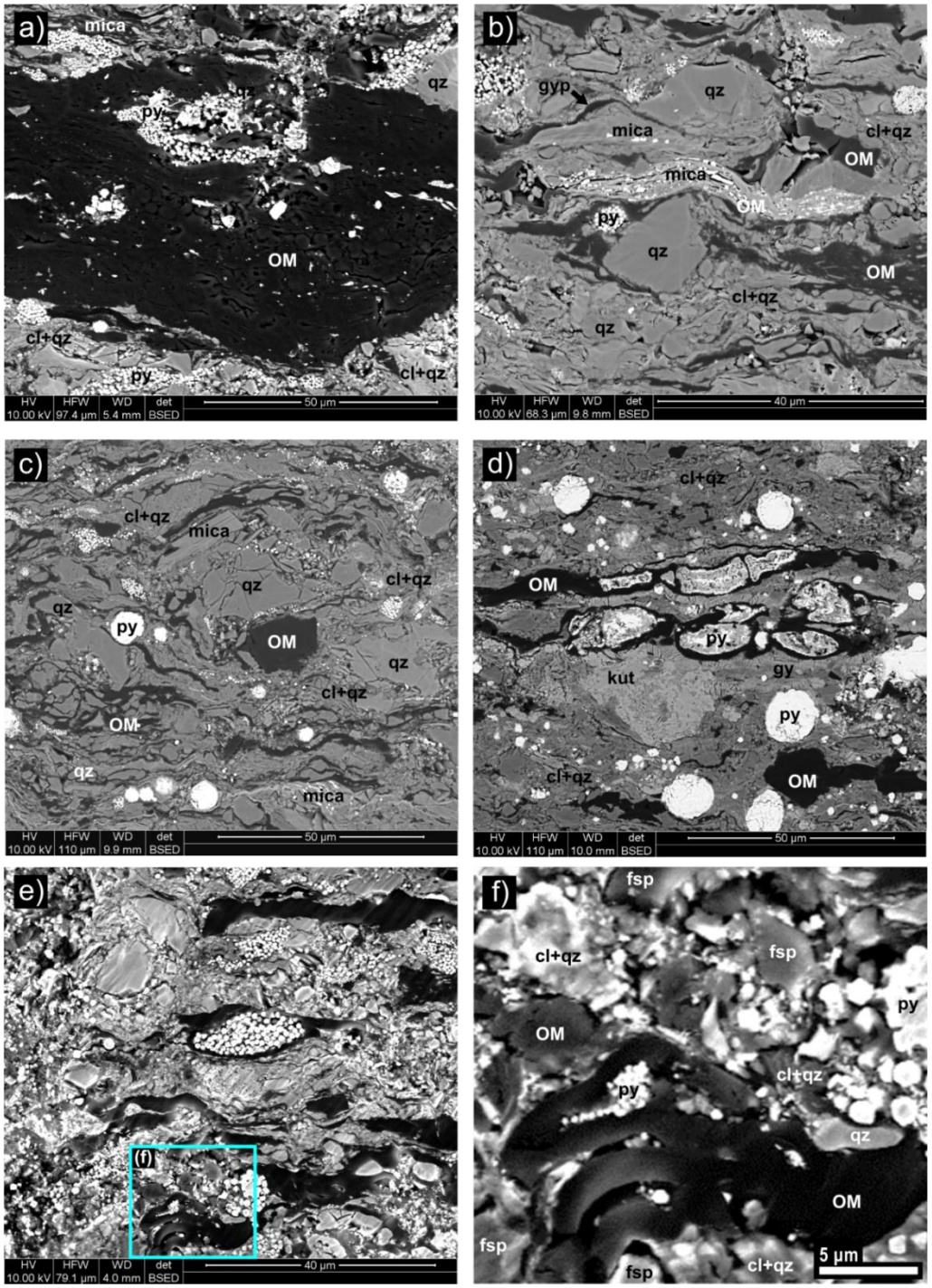

Figure 3: Scanning electron microscope (SEM) photomicrographs showing the compositionally immature nature of the detrital mineral component within the Stuart Range Formation and its relationship organic matter (OM). OM is bounded by sub-angular quartz (qz) grains and detrital mica surrounded by a clay and quartz (cl+qz) matrix that is likely dominated by illite and kaolinite. Altered mica grains show extensive fraying and contain pyritic (py) replacement. Gypsum (gyp) within close proximity of OM is also apparent. Kutnohorite (kut) is observed in some samples. (a) Sample 2053188 (sub-facies 2b, TOC: 8.18); (b) 2053194 (sub-facies 2a, TOC: 3.04); (c) 2053196 (sub-facies 2b, TOC: 7.74); (d) 2053198 (sub-facies 2c, TOC: 4.64); (e) OM-rich sample (2053191 sub-facies 2b, TOC: 8.24) with sporinite and minor lamalginite; and inset (f) indicating no association between OM and diagenetic components, which are only minor in the high TOC samples.

Table 3: Characteristics and interpretations of the six facies identified within the lower Stuart Range Formation, as observed within Arck 1.

Facies		Description	Interpretation
Facies 1: Proglacial facies		Dark grey mudstone laminated at approximately 1 cm scales, with thin interbeds of very fine grained sandstone (particularly lower down in stratigraphy). High abundance of fine euhedral pyrite disseminated in mudstone. Occasional clasts (<4 mm) and sparse dropstones (< 1/m) causing with soft sediment deformation of mudstone. Dropstones can be sub-angular to rounded igneous and meta-igneous clasts.	Gradational contact of Boorthanna and Stuart Range Formations. The presence of dropstones suggests the melting of glaciers or floating icebergs within the water column, and the transition to dominantly deglacial conditions.
Facies 2	**Sub-facies 2a:** Couplet facies	Repetitive asymmetrical laminations of a thicker medium to dark grey mudstone, in sharp contact with a thinner very fine brown carbonaceous mudstone. The mudstone laminae appear paired, i.e. couplets or rhythmites, and vary in thickness from 0.1–1 cm. Generally these laminae grade from a lighter grey to a darker grey stratigraphically upward. The finer carbonaceous mudstone is pale pink and varies in thickness from 0.001–0.1 cm. Overall very fissile and heterogeneous.	The gradual increase to darker shades of grey within the thicker mudstone laminations suggests a gradual increase in OM content or OM preservation. The paler carbonaceous mudstone may indicate oxidation and a change in bottom water chemistry. This may ultimately indicate pronounced seasonality in productivity or sediment supply.
	Sub-facies 2b: Massive black shale	Massive black shale with abundant euhedral pyrite. ~10 cm broad alternating bands of light and dark grey mudstone, interlaminated by discrete mm-scale laminae. Darker mudstone is texturally more complex with more laminae.	Interpreted as being similar to sub-facies 2a (described above), but with a less pronounced seasonality.
	Sub-facies 2c: Lensed mudstone	Alternating bands of dark and light grey mudstone, varying in thickness from mm- to cm-scales. Laminae are homogenous with minimal internal gradation and are often discontinuous. Common lensoid and lenticular segregations forming parallel to laminae and replaced by subhedral calcite. Often grades from Facies 5.	Homogeneity and discontinuity of laminae suggests some bottom water reworking or upwelling. Calcite crystals in segregations are interpreted to have precipitated after the deposition of siliclastic and organic material and prior to major compaction.
Facies 3: Bioturbated facies		Light grey massive calcareous mudstone with interrupted laminae, gradually becoming more laminated toward the top. More pervasive laminae through upper part of unit in comparison to Facies 2. However, remnant laminae throughout unit can be distinguished in some intervals. Rip-up clasts (0.5–2.0 cm) and soft sedimentary deformation are present at the base of the unit. Lower boundary surface is often undulating and non-horizontal.	Bioturbated oxic marl. Bioturbation evidenced by homogeneity of the unit and by the interruption and displacement of pre-existing laminae. Laminae may be becoming more pervasive toward the top as bioturbation activity is inhibited by oxygen depletion.
Facies 4: Mass flow facies		Massive moderately-calcareous mudstone. Homogenous light grey-brown mudstone with occasional discontinuous dark laminae, gradually becoming more laminated toward the top. Very abrupt lower boundaries that are horizontal. Lonestone identified at 960.58 m.	Mass flow deposits. Laminae may be becoming gradually laminated toward the top as mass flow slows down and the sediments become more stratified. Abrupt boundary suggests rapid onset of mass deposition.

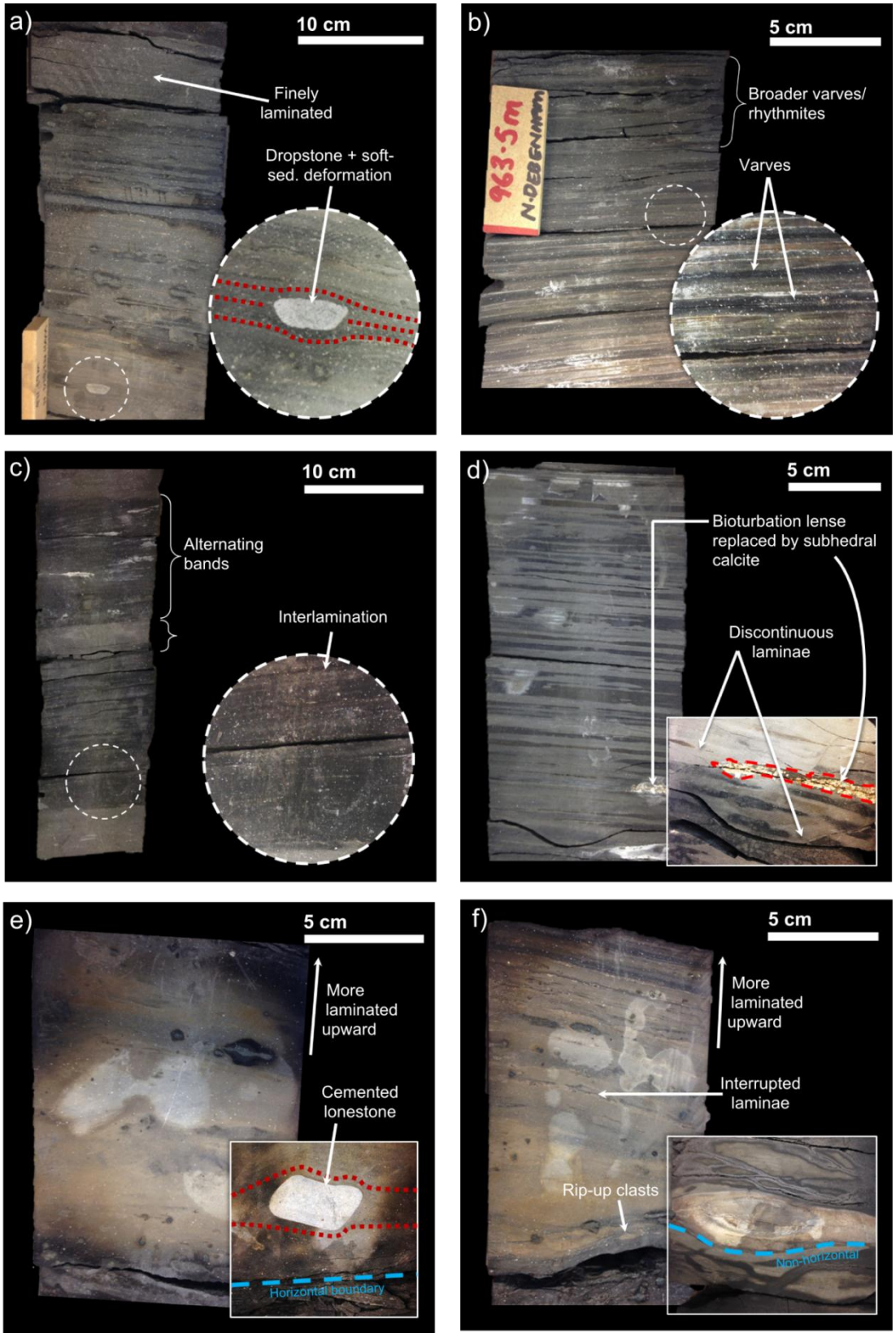

Figure 4: Representative images and characteristic features of the four facies identified within the lower Stuart Range Formation, Arck 1: (a) Facies 1, proglacial facies; (b) Sub-facies 2a, cyclic varve unit (pelagic facies); (c) Sub-facies 2b, mass black shale (pelagic facies); (d) Sub-facies 2c, lensed mudstone (pelagic facies); (e) Facies 3, bioturbated facies; and (f) Facies 4, mass flow facies.

Geochemical analyses revealed millimetre- to metre-scale cyclic variations in total organic carbon (TOC) content across the Stuart Range Formation within Arck 1, though the metre-scale cyclicity may be an artefact of sampling density. The heterogeneity of the Stuart Range Formation at sub-micron scale implies that the sampling density (approximately 1 sample/50 cm) during this study was insufficient to capture detailed geochemical trends. For instance, Figure 5 illustrates the lower mass flow facies with lower TOC and the upper pelagic facies (cyclic varve unit). The upper cyclic couplet facies demonstrates the mm-scale variability in mineralogy and geochemistry. Sample resolution in Cootanoorina 1 was lower than Arck 1 as continuous core was not collected during drilling (Figure 6). The high resolution sub-section of Arck 1, was sufficient for detailed facies analysis (Figure 7).

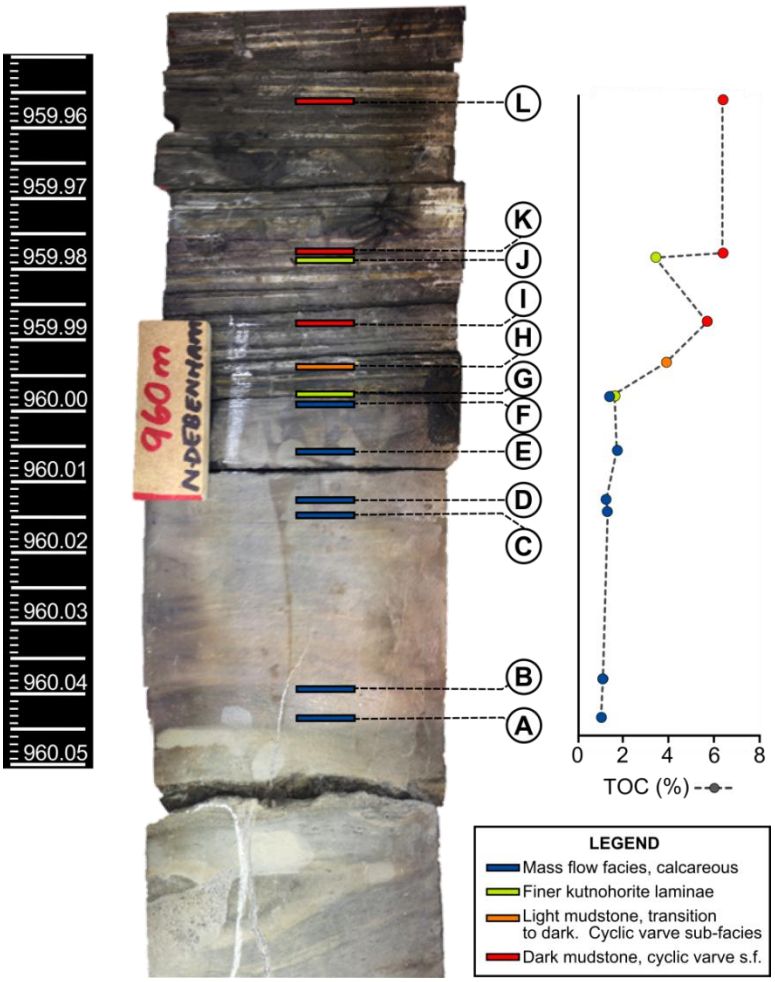

Figure 5: The abrupt upper boundary (at 960 m) between the mass flow facies, heading into the cyclic varve sub-facies (pelagic facies) within the lower Stuart Range Formation, Arck 1. High resolution total organic carbon (TOC) data was obtained from slivers of core (<4 mm) and has been plotted against depth, indicated by the scale bar on the left. The colours in the legend represent sedimentological observ-ations. The calcareous zone subsamples (within the mass flow facies) and the kutnohorite laminae subsamples (within the cyclic varve 2a, pelagic facies) have low TOC values. The light mudstone, as part of the transition to the dark varve laminations, has a medium TOC value, and the dark laminations have high TOC values.

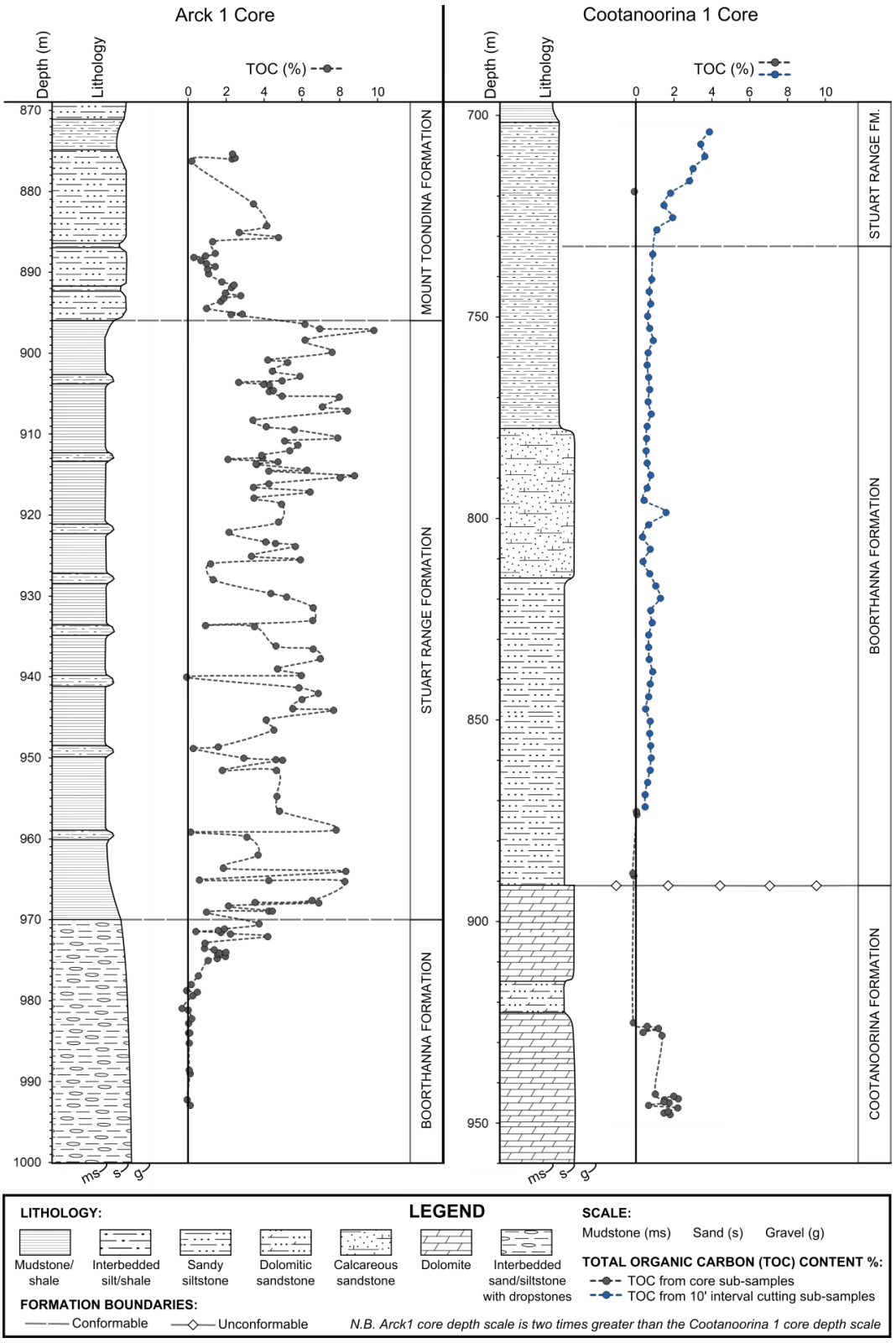

Figure 6: Core logs of Arck 1 and Cootanoorina 1, illustrating lithological and geochemical variability. The Arck 1 log comprises the upper Boorthanna Formation to the lower Mount Toondina Formation, and the Cootanoorina 1 log comprises the upper Cootanoorina Formation to the lower Stuart Range Formation. Total organic carbon (TOC) data from core and cutting sub-samples was plotted with depth. Note that the Arck 1 depth scale is double the Cootanoorina 1 depth scale. Lithological observations presented in Harris and McGowran (1968) were followed as core for lithological analyses of Cootanoorina 1 was limited.

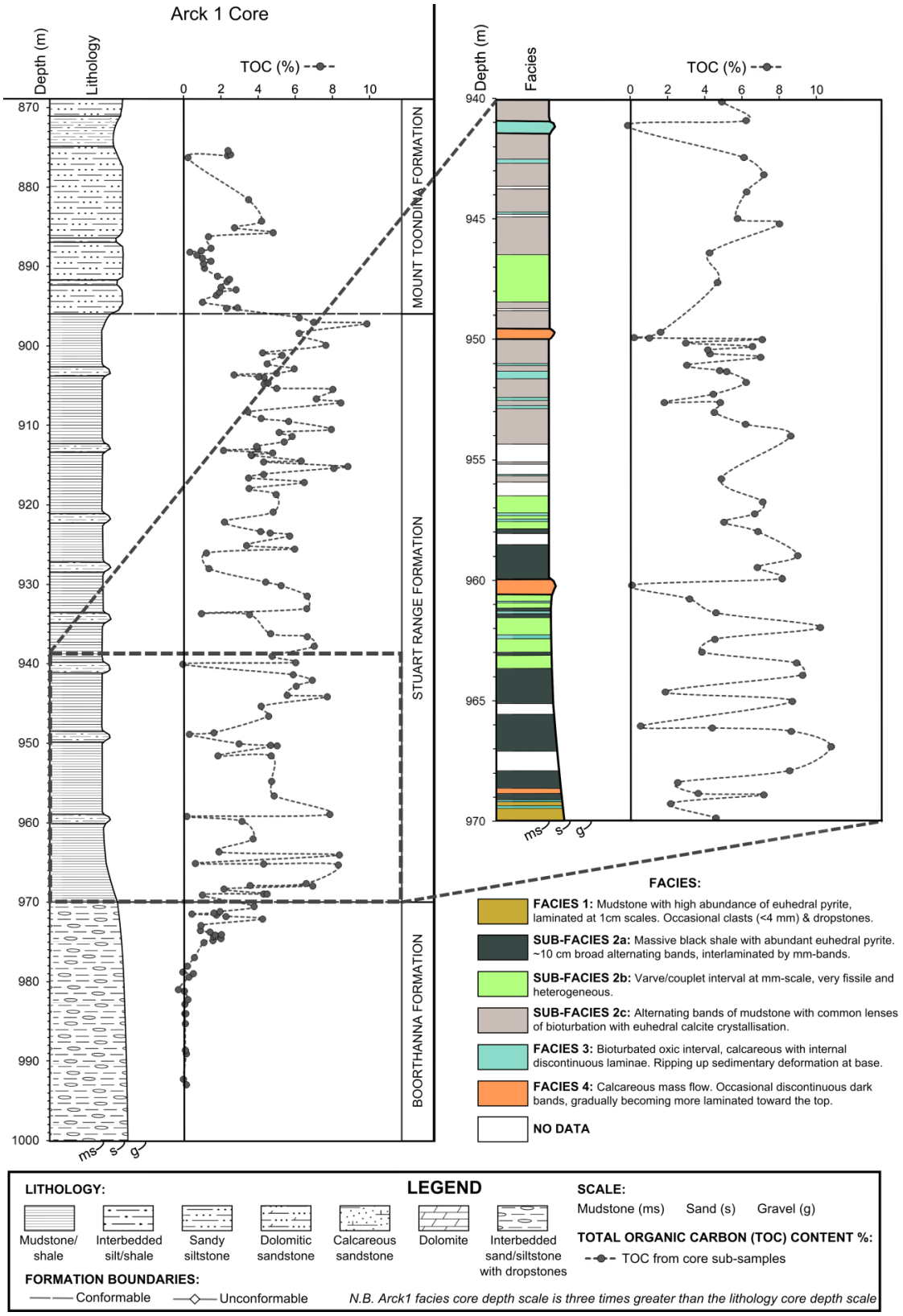

Figure 7: Core log of Arck 1 illustrating lithological and geochemical variability (left), with total organic carbon (TOC) data from core sub-samples plotted against depth. A subsection from 970–940 m was studied at higher resolution (right) and four facies were identified. Note that the subsection depth scale is three times the Arck 1 core log depth scale.

Facies 1: Proglacial facies

The most basal facies identified within the Stuart Range Formation is a laminated mudstone, with thin interbeds of very fine grained sandstone, that contains occasional clasts (<4 mm) and sparse dropstones (Figure 4a), suggesting the continuation of ice rafting and glacial conditions. X-ray diffraction (XRD) identified clays, quartz, feldspars, carbonates, jarosite, chlorite, and pyrite. Carbonate phases include dolomite and kutnohorite, and clay phases include illite/mica, kaolinite and chlorite. The proglacial facies contained a high proportion of silicates with minimal carbonates in both samples analysed. Table 4 summarises the typical mineralogy of the four facies based on bulk powder XRD and shows the percentage of samples within each facies that contain a given mineral.

Table 4: Typical mineralogy of the six facies identified within the lower Stuart Range Formation, X-ray diffraction (XRD) of bulk powders (Appendix C, Table C1). The presence (%samples) of mineral phases has been grouped into 'all samples', 'most samples', and 'few samples', and 'N/A' has been assigned to facies with only 2 XRD sample results. The number of XRD samples is bracketed beside each facies number.

	Typical Mineralogy (Presence %samples in XRD Samples)		
Facies	All samples (100%)	Most samples (99–31%)	Few Samples (30%)
Facies 1: (2) Proglacial facies	Quartz, albite, illite/mica, K-feldspar, kaolinite, chlorite, kutnohorite, jarosite, pyrite	Dolomite	N/A
Sub-facies 2a: (2) Cyclic varve unit	Quartz, albite, illite/mica, kaolinite, jarosite, gypsum, pyrite, chlorite	Dolomite, kutnohorite, apatite	N/A
Sub-facies 2a: (5) Massive black shale	Quartz, albite, illite/mica, kaolinite, jarosite, gypsum, pyrite	Chlorite	K-feldspar
Sub-facies 2a: (3) Lensed mudstone	Quartz, albite, illite/mica, kaolinite, jarosite, gypsum, pyrite	K-feldspar	Mixed I-S, kutnohorite, apatite
Facies 3: (2) Bioturbated facies	Quartz, illite/mica, kaolinite, dolomite, apatite	Albite, K-feldspar, chlorite, magnesite, kutnohorite, jarosite, gypsum, pyrite	N/A
Facies 4: (2) Mass flow facies	Quartz, albite, kaolinite, chlorite, siderite, dolomite, kutnohorite, pyrite	Magnesite, jarosite	N/A

Facies 2: Pelagic facies

Based on whole core observations, the pelagic facies had initially been divided into individual three facies. However, the similarity of these facies, mineralogically and texturally, implies a common detrital source and depositional setting, and thus these facies have been grouped together. This facies is the most prevalent across the high resolution Arck 1 subsection, and due to its primary sedimentary features, pervasiveness and composition, it is interpreted to represent background pelagic settling. The pelagic facies has been studied in greater detail in order to determine mineral surface preservation effects and to establish a depositional model for the Arckaringa Basin.

Mineral distribution mapping, by integrating EDS with BSEM, identified kutnohorite and gypsum bands separated by a clay and quartz matrix zone occurring repetitively through all sub-facies (Figure 8). The pale kutnohorite bands vary in thickness and extent within each sub-facies, and it may be the scale of oxic bottom water conditions and associated bioturbation that is inducing any differences (detailed below). Sub-facies 2a comprises the most pronounced and uniform rhythmicity of all three sub-facies, which therefore implies constant cyclicity. For each pelagic sub-facies, energy-dispersive X-ray spectroscopy (EDS) coupled with BSEM was used to map the distribution of mineral phases including minor mineral phases that were not detected during XRD. XRD analysis of clay separates (Figure 9) of each sub-facies indicated the presence of illite, smectite (presence uncertain in sub-facies 2a), mixed layer illite-smectite (identified using ethylene glycol treatment), kaolinite, and chlorite. Typically, darker mudstone laminae comprised varying abundances of quartz, pyrite, illite/mica, kaolinite, chlorite, and K-feldspar, and the lighter laminae comprised quartz, kutnohorite, dolomite, jarosite, and gypsum.

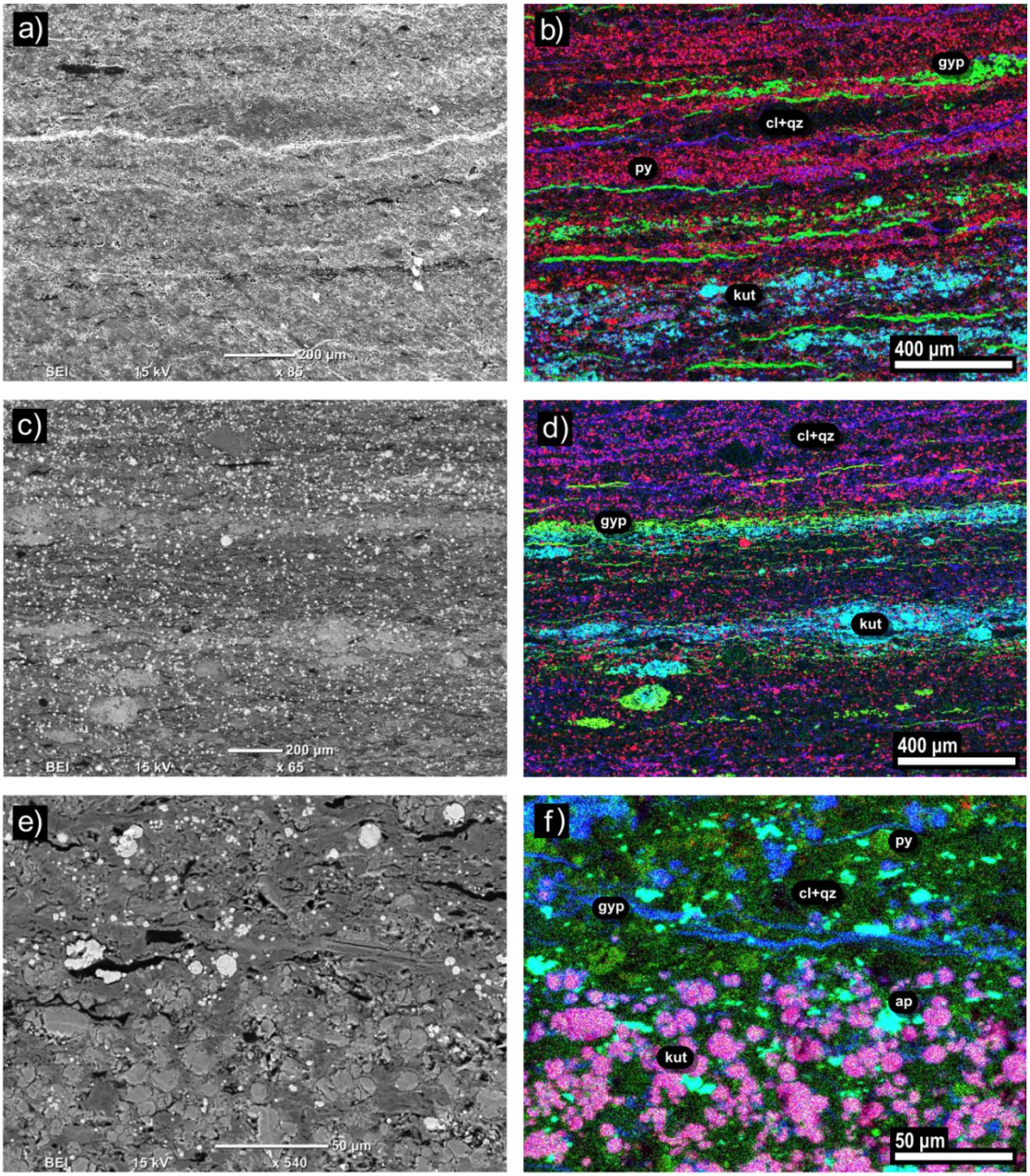

Figure 8: Scanning electron microscope (SEM) and integrated energy dispersive X-ray spectroscopy (EDS) photomicrographs of polished blocks taken from the pelagic facies in Arck 1. (a) SEM photomicrograph of sample I at 958 m (sub-facies 2a) and (b) accompanying EDS map of elemental distributions, where red = iron, green = calcium, and blue = manganese. This confirms the dominant mineralogy of the thin, light kutnohorite intervals that occur after every dark couplet. The important minerals identified are gypsum (gyp) and kutnohorite (kut), surrounded by a primarily clay and quartz (cl+qz) matrix with framboids of pyrite (py). (c) SEM photomicrograph of sample 2053196 at 959.97 m (sub-facies 2b) and (d) accompanying EDS map of elemental distributions, where red = silicon, green = calcium, and blue = manganese. The small red ovoid shapes correspond to pyrite. (e) SEM photomicrograph of sample 2053198 at 955.79 m (sub-facies 2c) and (f) accompanying EDS map of elemental distributions, where red = manganese, green = phosphorus, and blue = calcium. Apatite (ap) was present within the matrix and pyrite (py) is represented by light yellow-green.

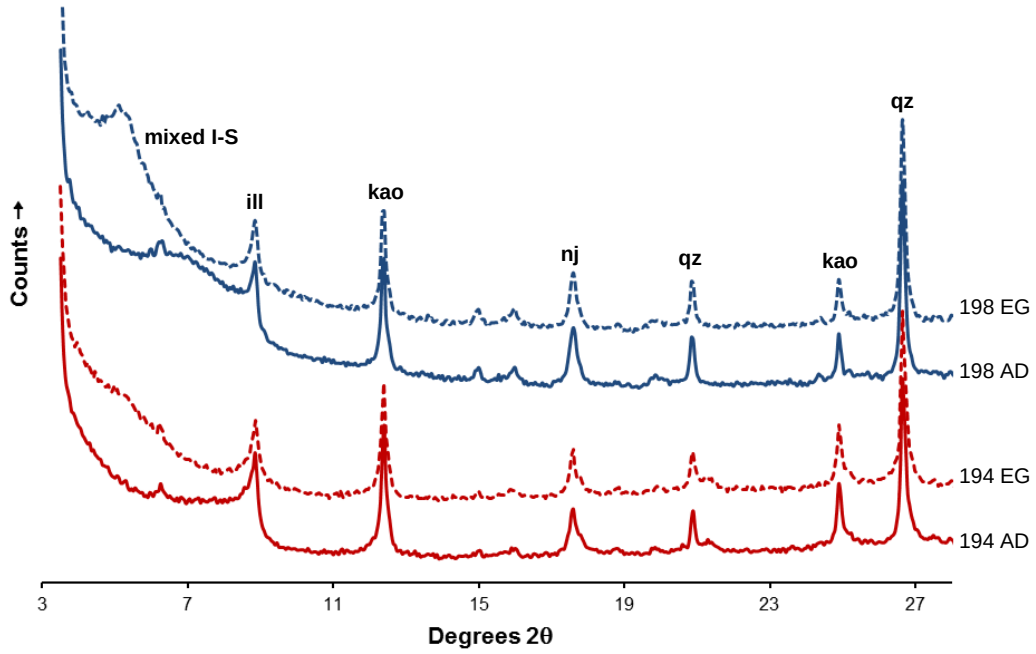

Figure 9: Clay mineral fraction X-ray diffractogram of Arck 1 core samples 2053194 (red, sub-facies 2b) and 2053198 (blue, sub-facies 2b), with both air dried (solid line) and ethylene glycol (dashed line) treatments. The diffractograms have been shifted upwards for clarity. The phyllosilicate mineral compositions were determined by applying the United States Geological Survey (USGS) Clay Mineral Flow Diagram of Poppe *et al.* (2001). Mixed layer illite-smectite (mixed I-S), illite (I), kaolinite (kao), natrojarosite (nj), and quartz (qz) were identified in both samples. Data based on Appendix C, Table C2.

Petrographic observations in ultra-violet/fluorescence mode and reflected white light mode indicated a predominance of liptinite, with sporinite (terrigenous origin), alginite, and lamalginite (both marine origin) as the main macerals. Figures 10c and 10d are of sub-facies 2a and Figures 10e and 10f are of sub-facies 2b. 20 µm sized ellipsoidal shapes with quartz, clay, and pyritic centres defined by thick, distinct walls were identified as a plant spore (sporinite). These were often deformed, likely due to burial compaction. Alginite (Figure 10f) was defined by its 'cauliflower' appearance suggesting algal colonies (up to 50 µm). Long and finely banded, thin-walled lamellar OM was identified as lamalginite (Figures 10d and 10f). Due to the long, string-like nature of this maceral and the way it appears to wrap around mineral grains, it is possible that migrated hydrocarbon phases could be confused with lamalginite.

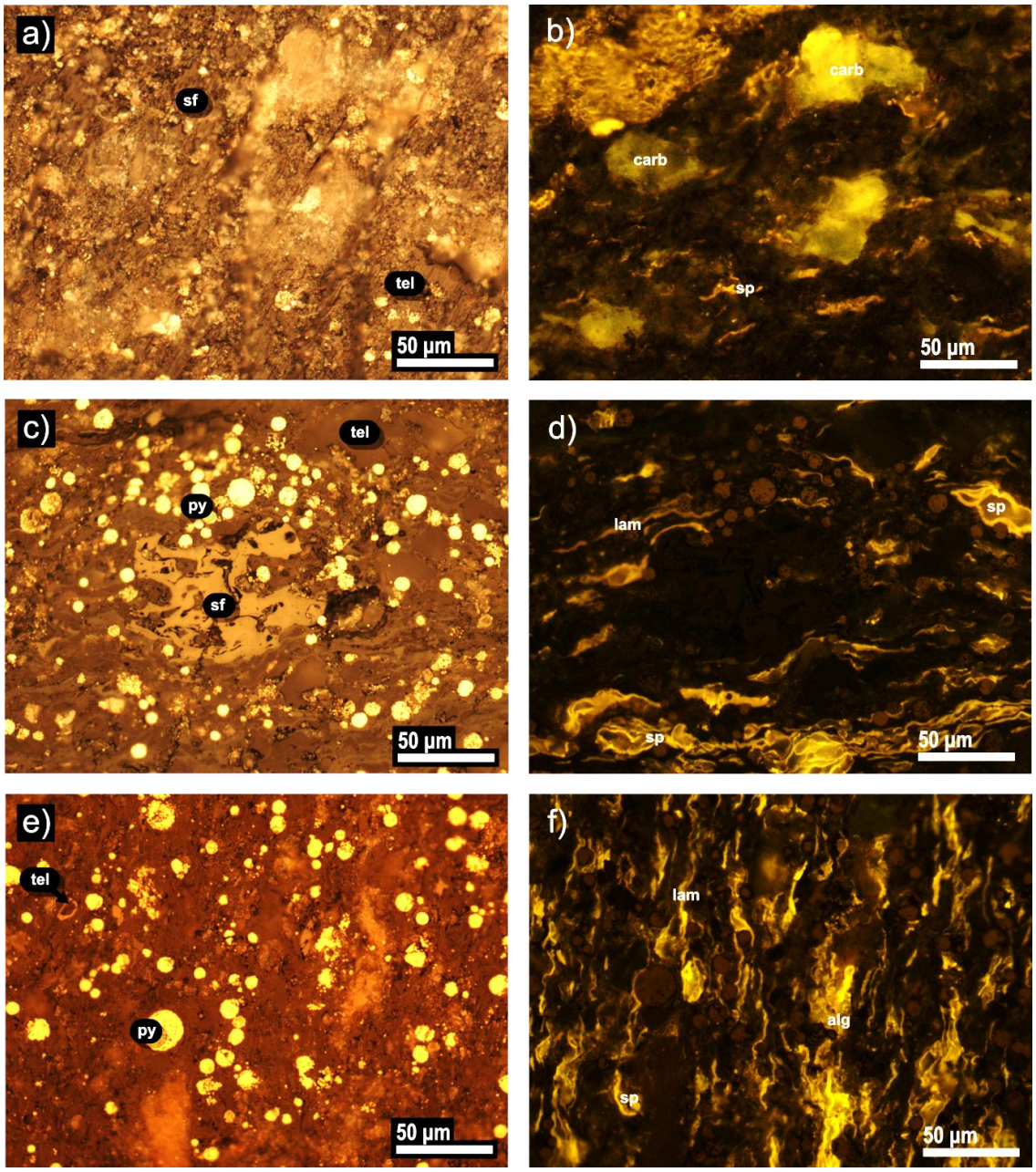

Figure 10: Reflected light (left) and ultra-violet (right) photomicrographs showing the organic components within the Stuart Range Formation, from low total organic carbon (TOC) contents (a, b) to 9 TOC contents (e, f). (a, b) Sample 2053339 at 923.03 m, with a TOC value of 2.11, Facies 3. Dominated by a terrigenous source of organic matter, comprising sub-angular and unstructured telinite (tel) and semifusinite (sf). Sporinite (sp), also of terrestrial origin, is present in minor quantities. A high proportion of carbonates are present, which is typical of low TOC samples. (c, d) Sample 2053197 at 957.60 m, with a TOC value of 4.78, sub-facies 2a. Semifusinite surrounded by abundant sporinite, framboidal pyrite (py), lamalginite (lam), and minor telinite. (e, f) Sample 2053196 at 959.97 m, with a TOC value of 7.74, sub-facies 2b. Abundant lamalginite, sporinite, and framboidal pyrite, with minor alginate (alg) and telinite. Lamalginite, alginate, and framboidal pyrite are of marine origin. No carbonates are present within the higher TOC samples. The classification table for the identification of organic macerals in Appendix B, Table B3, was followed during analysis.

Broken fragments of plant wall were identified as semifusinite (Figure 10c) and comprised sharp and curved cell shapes. Distinct pieces of tabular woody tissue (telinite) occur as angular fragments ranging in size from less than 10 μm to 50 μm.

BSEM imaging of the pelagic facies indicates a poorly sorted, compositionally and texturally immature, feldspathic micaceous siltstone (Figure 3). Sub-angular to sub-rounded quartz grains and detrital mica are surrounded by a silica-rich matrix, dominated by illite/smectite, kaolinite, and mm-scale authigenic quartz determined by EDS and XRD. Abundant framboidal and euhedral pyrite and authigenic gypsum were present in the darker laminae, and the gypsum is often spatially associated with OM particles. TOC is higher in finer grained sediments within the darker laminae, which may simply reflect reduced dilution by siliclastic phases.

EDS spot analysis of discrete OM particles (Figure 11) showed that the OM contains variable quantities of sulphur (S). Greater concentrations of S were identified within sporinite and lamalginite, and minor amounts of S within vitrinite group macerals, predominantly telinite. A pronounced peak in octacyclosulphur (S_8) was also identified following solvent extraction coupled to gas chromatography-mass spectrometry (Figure 12), suggesting a high abundance of free sulphur in the system. This prevalence of S within OM may contribute to OM preservation (discussed below).

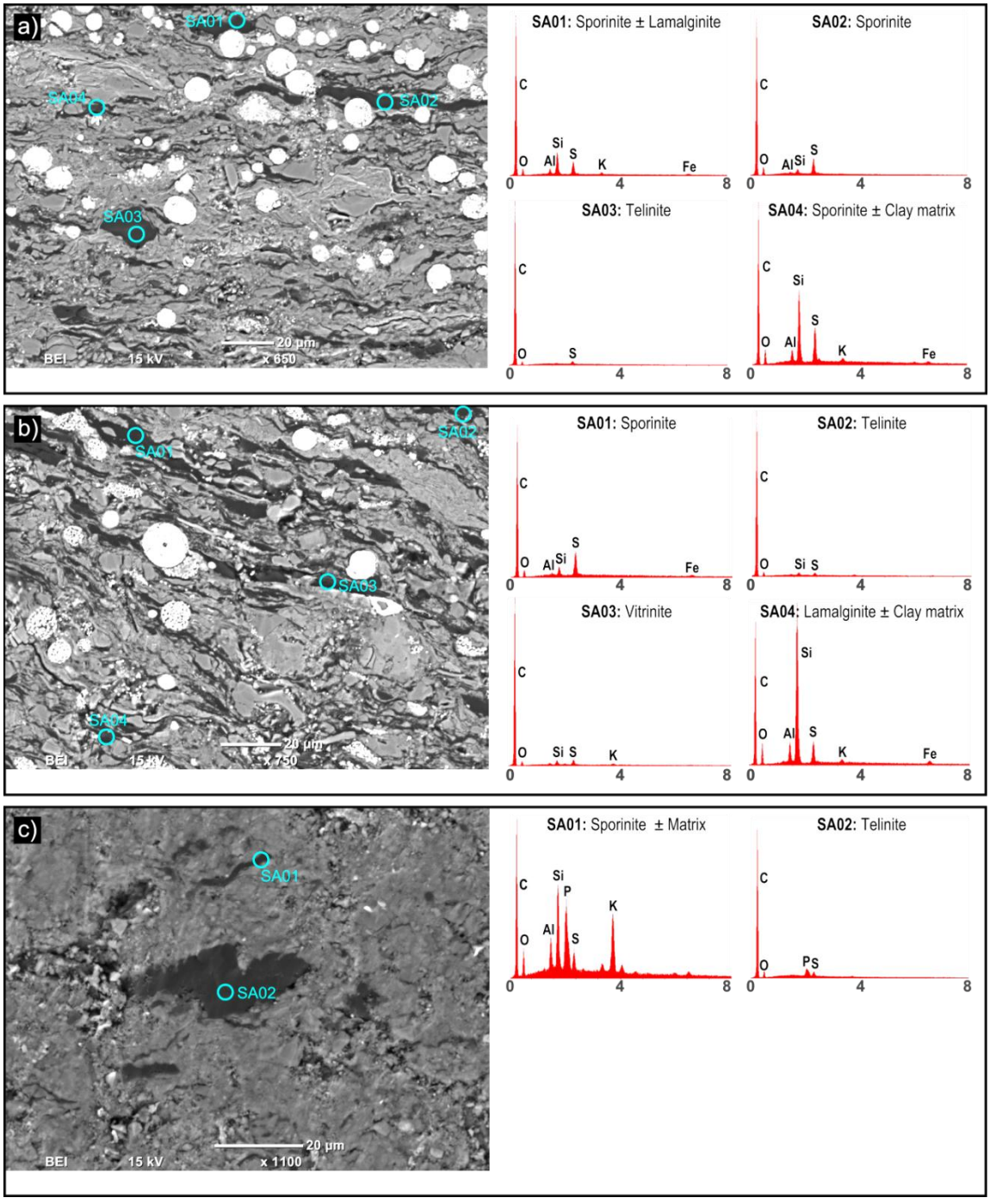

Figure 11: Scanning electron microscope (SEM) photomicrograph of polished blocks taken from Arck 1. Energy dispersive spectroscopy (EDS) spot analysis within discrete particles of organic matter was performed to determine elemental compositions. The results are illustrated graphically to the right. Peaks indicate the presence of carbon (C), oxygen (O), aluminium (A), silicon (Si), sulphur (S), potassium (K) and iron (Fe). 'Clay matrix' indicates where spot analysis has also analysed the clay matrix, and 'Matrix' indicates where the carbonate matrix has been analysed. (a) 2053196 at 959.97 m, total organic carbon (TOC): 7.74, sub-facies 2b; (b) 2053188 at 966.35 m, TOC: 8.18, sub-facies 2b; (c) 2053307B at 952.59 TOC: 1.76, Facies 3.

It was initially hypothesised that OM preservation within the Stuart Range Formation occurs by the early generation of organic acids resulted in the breakdown of unstable minerals and the precipitation of cements and sub-millimetre encapsulation of migrating hydrocarbons. Hydrocarbons are generated as a result of the maturation of buried OM. There was, however, no obvious textural association between the OM and the diagenetic components (Figure 3f) in the samples analysed. The organic component is dominated by detrital particles, rather than generated hydrocarbons. Cement precipitation is minor within the high TOC samples (darker laminae) and does not envelop OM particles. Cement is more pervasive in the low TOC samples (kutnohorite-dominated laminae). There was no evidence for migration of hydrocarbons during SRA analysis (described below), which also refutes OM preservation by encapsulation.

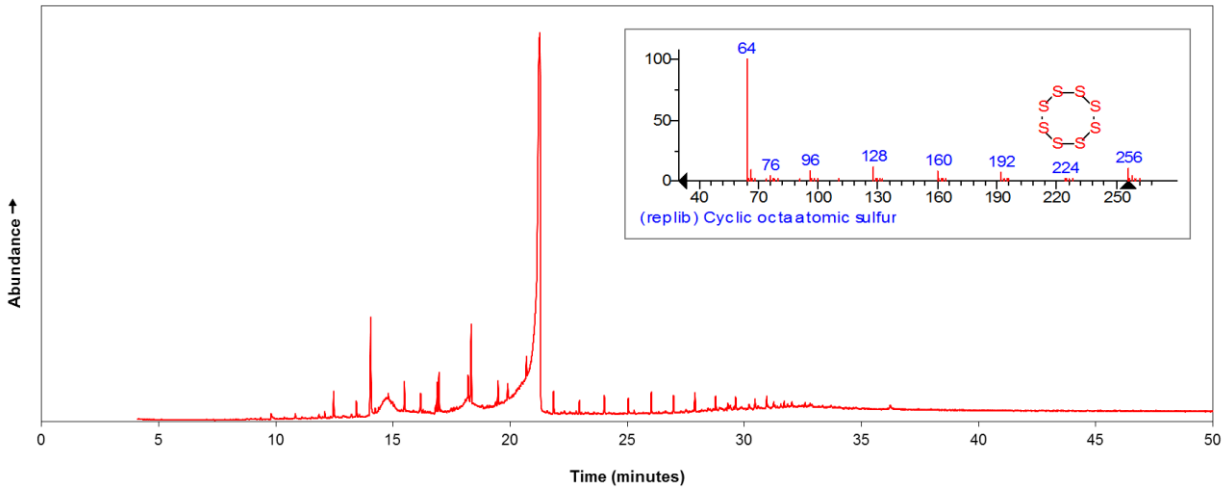

Figure 12: Solvent extracted, gas chromatography-mass spectrometry (GC-MS) chromatogram of sample 2053334, with a high total organic carbon content of 5.97 mg/g. Octacyclosulphur (S_8) is the major peak, with sulphur allotropes hexacyclosulphur (S_6) and heptacyclosulphur (S_7) as minor peaks. The double peak for S_6 is likely to be an artefact of instrument error. The background peaks indicate the hydrocarbon profile for this sample. Inset is an ion chromatogram of the S_8 peak (*m/z* 64) showing cyclic sulphur complexes and ions associated with S_8.

SUB-FACIES 2A (CYCLIC VARVE UNIT)

Sub-facies 2a is distinguished by dark laminae forming a rhythmic facies and comprised a repetitive asymmetrical laminations of a thicker medium to dark mudstone (0.1–1 cm), in sharp contact with a thinner and well cemented very fine brown carbonate mudstone (Figure 4b), dominated by Mn carbonate (kutnohorite; 0.001–0.1 cm). The gradual increase to darker shades of grey within the thicker mudstone laminations suggests a gradual increase in OM content with each cycle. The kutnohorite laminae contain less OM. Mineralogically, the cyclic varve unit is very variable (Table 4), which is consistent with the heterogeneous appearance of the sub-facies. XRD identified clays, quartz, albite, carbonates, jarosite, gypsum, and pyrite. Clay phases include illite/mica, kaolinite and, chlorite. Carbonate phases include dolomite and kutnohorite, which were typically restricted to the low TOC laminae as indicated by mineral mapping (Figure 8b).

SUB-FACIES 2B (MASSIVE BLACK SHALE)

Macroscopically, sub-facies 2b appears to be a massive black shale. However, SEM-based mineral distribution mapping identifies heterogeneities and subtle laminations in what otherwise appears a homogenous unit. Sub-facies 2b is confined to the lower 15 m of the Stuart Range Formation within Arck 1. This unit is defined by approximately 10 cm thick alternating bands of lighter and darker mudstone and is interlaminated by mm-scale laminae. The darker mudstone is texturally more complex with more laminae (Figure 4c). EDS mineral mapping (Figure 8d) shows that these finer-scaled laminae comprise alternating bands of kutnohorite and gypsum with clays and quartz. This facies has been interpreted have a less pronounced rhythmicity than sub-facies 2a, but is compositionally similar. Mineralogically, the massive black shale was

heterogeneous and similar to that of sub-facies 2a, with varying presences of chlorite and feldspar.

EDS integrated with Quantitative Evaluation of Minerals by Scanning electron microscopy (QUEMSCAN®), conducted on polished blocks taken from sub-facies 2b, was used to identify spatial patterns of mineral phases (Figure 13). The detrital grains are comprised of poorly sorted, sub-angular to sub-rounded quartz grains (<250 μm) with occasional tabular K-feldspar (<100 μm), illite aggregates (<50 μm) and minor muscovite (<25 μm). The matrix is comprised of by illite, kaolinite, chlorite (clinochlore and chamosite) and authigenic quartz (<5 μm). Abundant pyrite framboids occur only within phyllosilicate intervals.

SUB-FACIES 2C (LENSED MUDSTONE)

Gradational with sub-facies 2b is sub-facies 2c, a lensed mudstone, which is characterised by alternating bands of dark and light mudstone, varying in thickness from millimetre- to centimetre-scales (Figure 4d). Laminae are homogenous with minimal internal gradation and are often discontinuous. Common lensoid and lenticular segregations (2–8 cm length and <2 cm width) form parallel to laminae and are comprised of subhedral calcite, and are interpreted to be bioturbation lenses. This facies dominates, and is restricted to, the upper 16 m of the subsection. On the basis of the homogeneity and discontinuity of laminae, sediment reworking by bioturbation may have been prevalent during deposition. Mineralogically, the lensed mudstone was very similar to the other two sub-facies (Table 4), though also contained K-feldspar and minor mixed layer illite–smectite.

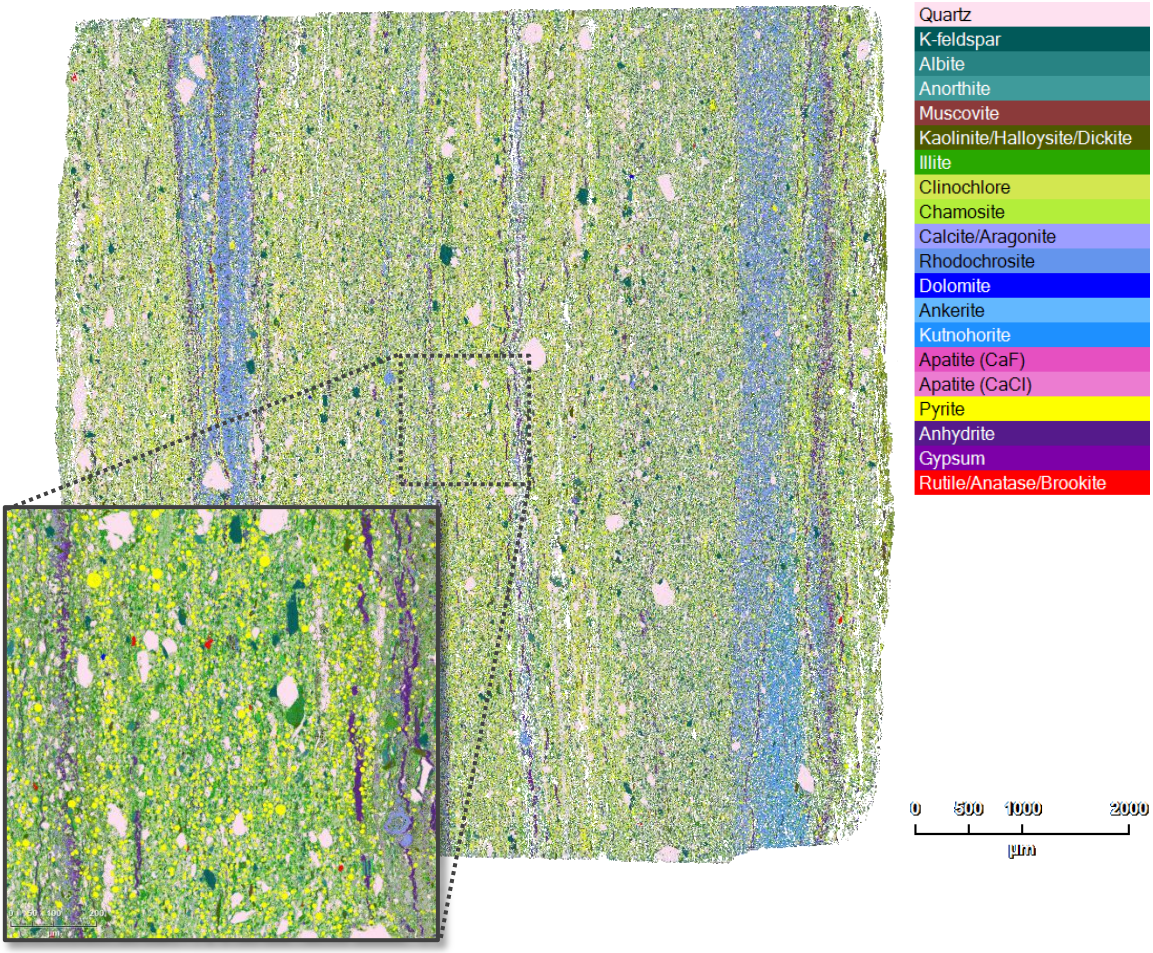

Figure 13: Quantitative Evaluation of Minerals by Scanning electron microscopy (QUEMSCAN® by FEI Company) mineral map of a polished block taken from the massive black shale (sub-facies 2b) in Arck 1 (sample 2053196 at 959.97 m) using energy-dispersive X-ray spectroscopy (EDS) for data acquisition. The legend to the right illustrates the colour assignment of the minerals present. The inset further details mineral associations and distributions to a higher resolution. The repetitive laminae (50–800 µm width) illustrated by the blue–purple shades that primarily represent gypsum ± anhydrite (purple), and rhondochrosite (± anhydrite), and kutnohorite (blue). The higher resolution mineral map inset also demonstrates the compositionally immature nature of the detrital mineral component within the Stuart Range Formation, with sub-angular to sub-rounded quartz grains, poorly sorted K-feldspar, and detrital mica surrounded by a clay and quartz matrix dominated by illite and kaolinite.

Facies 3: Bioturbated facies

Facies 3 is a massive calcareous marl that is more pervasively laminated toward the upper boundary of the unit. Residual structures of primary lamination can be distinguished in most intervals, and rip-up clasts (0.5–2.0 cm) and soft sedimentary deformation are present along the lower boundary surface, which is often undulating

and non-horizontal. Burrow shapes are commonly observed (Figure 4e), and this, together with the homogeneity of the unit and the interruption of pre-existing laminae, suggests bioturbation in oxygenated bottom water conditions. However, relics or traces of benthic organisms are absent. This facies is dominated by dolomite, and typically contains quartz, illite/mica, kaolinite, and apatite (Table 4).

Petrographic observations indicated that terrestrially-derived inertinite (semifusinite) and vitrinite (telinite) were the main macerals, although minor contribution of liptinite was also noted. Distinct, tabular woody tissue (telinite) occurs as angular fragments in high abundances, and range up to 50 μm in size. The different distribution of macerals in this facies, in comparison to the pelagic facies, could result from different input or selective preservation resulting from the greater resistance of terrestrial OM toward oxidation (Freudenthal *et al.* 2001). Thus, the dominance of terrestrial OM in lower TOC intervals may reflect a greater influence of freshwater and terrigenous sediment discharge during deposition, resulting in more oxic bottom water conditions and reduced liptinite (lamalginite and sporinite) OM preservation efficiency.

Facies 4: Mass flow facies

Broad intervals (<60 cm) of a massive, calcareous, low total organic carbon mudstone were identified approximately every 10 m, and more minor intervals (>2 cm) were identified throughout. Internally, it comprised minor discontinuous dark laminae that gradually became more laminated toward the top. A white lonestone (2x3 cm) with compaction-related sediment deflection was identified within one interval at 960.58 m in the Arck 1 core implying the continuation of ice rafting (Figure 4b). Very abrupt, erosive lower boundaries suggest rapid onset deposition. Consequently, this facies was

interpreted as a mass flow deposit. XRD identified quartz, albite, carbonates, pyrite, and minor clays (kaolinite and chlorite) in all samples analysed. Carbonate phases include dolomite, kutnohorite, and siderite.

Source Rock Characterisation

Sealed vessel thermal extraction (TH-GC-MS) and micro-scaled sealed vessel pyrolysis coupled to gas chromatography-mass spectrometry (MSSV-GC-MS) chromatograms, of a representative high TOC (massive black shale) and a low-medium TOC sample (clastic mudstone) from the Arck 1 core, were generated in order to determine the pristane (pr) and phytane (ph) ratios (Figure 14). The pr/ph ratio is a geochemical proxy used to interpret palaeoredox conditions in the water column or shallow sediment environment. A pr/ph value >1 indicates oxic conditions and a pr/ph value <1 reflects anoxic conditions (Didyk *et al.* 1978). The high TOC sample (8.18 mg/g) generated a pr/ph of 0.92, suggesting deposition during anoxic to sub-oxic conditions, whereas the low TOC sample produced a high pr/ph of 2.37, suggesting oxidising conditions in the depositional environment. This association was observed in 3 samples that were analysed, and demonstrates the fluctuating nature of the redox conditions within the shallow depositional environment. This fluctuation also corresponds with framboidal pyrite abundance evident in SEM images. Framboidal pyrite is commonly used as a water column proxy for sulphidic conditions. Higher TOC samples contain greater concentrations of pyrite and lower pr/ph values suggesting that OM preservation may have been influenced by basinal anoxia.

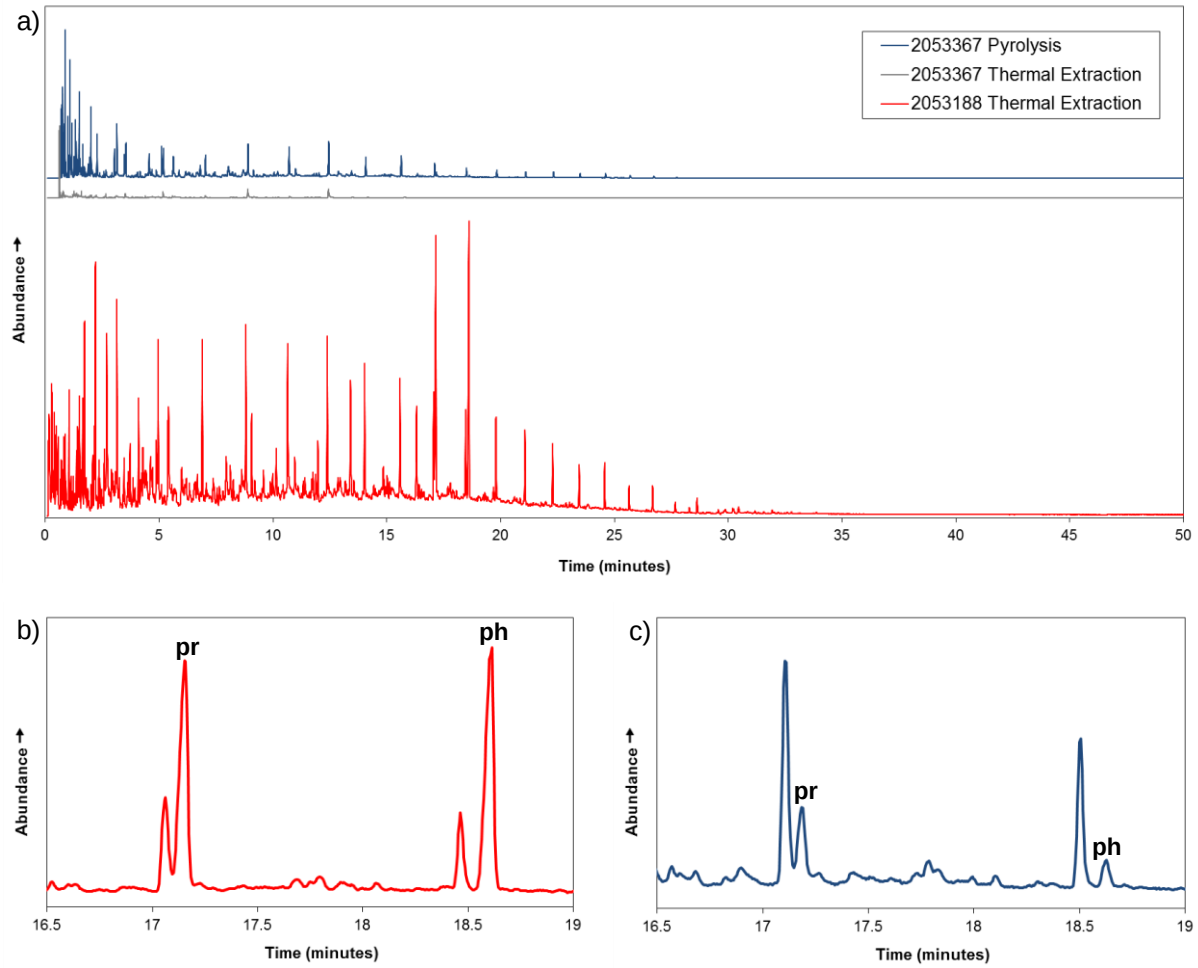

Figure 14: Sealed vessel thermal extraction (TH-GC-MS) and micro-scaled sealed vessel pyrolysis coupled to gas chromatography-mass spectrometry (MSSV-GC-MS) chromatograms of a representative high total organic carbon (TOC) sample (2053188, at 966.35 m, TOC: 8.18, sub-facies 2b) and a low-medium TOC sample (2053367, at 975.60 m, TOC: 4.23) from the Arck 1 core. (a) TH-GC-MS chromatograms of samples 2053188 (red) and 2053367 (grey), and MSSV-GC-MS chromatogram of sample 2053367 (blue) which is a close approximation of what would be expected if sample 2053367 had naturally undergone further maturation to produce free hydrocarbons. (b) TH-GC-MS chromatogram of sample 2053188, focussing on the pristane (pr) and phytane (ph) biomarker parameter for the assessment of redox conditions. A pr/ph value >1 indicates oxic conditions and a pr/ph value <1 reflects anoxic conditions at the sediment/water interface, following Didyk *et al.* (1978). In this case, pr/ph = 0.92, suggesting deposition during anoxic to sub-oxic conditions. (c) MSSV-GC-MS chromatogram of sample 2053367, showing that pr/ph = 2.37, suggesting deposition during oxic conditions.

Organic matter within the Stuart Range Formation is primarily Type II–III oil-gas-prone to Type III gas-prone as indicated by high hydrogen index (HI) values of <400 mg HC/g (Figure 15). It is predominately immature to mature, heading into the oil generation window. Analysis of several samples by micro-scale-sealed-vessel thermal extraction

and pyrolysis technologies hyphenated to gas chromatography mass spectrometry (MSSV-GC-MS) identifies mainly low molecular weight macromolecules, typical of light oil (Figure 14). Rock Eval (SRA analysis) indicates the proportion of free hydrocarbons (S_1) that evolve from a rock sample without cracking kerogen during the first stage (heating at 300 °C) of stimulated maturation. The proportion of hydrocarbons with generative potential (S_2) correspond to hydrocarbons that evolve during the second stage (heating above 300 °C) of stimulated maturation. The S_1 component within the Stuart Range Formation varies between 0 and 0.96 mgHC/gOC and the S2 component varies between 0.53 and 33.02 mgHC/gOC (Figure 16a). The maximum S2 value is very high relative to the S1 value, implying good source rock potential should burial and maturation continue. However, a high S2 is unfavourable in terms of oil production within the Arckaringa basin. Nonetheless, these organic rich shales may also be in the oil generation window where deeper burial has already occurred or where a higher geothermal gradient is present.

The Cootanoorina Formation is Type IV inert to Type III gas-prone as indicated by HI values <100 mg HC/g, but mainly <20 mg HC/g (Figure 15). This formation has no potential to very minimal potential to produce hydrocarbons, and may already be over-mature with hydrocarbons migrating to shallower parts of the basin. Alternatively, this formation may have never had any significant potential to produce hydrocarbons. Rock Eval indicates that the S_1 component varies between 0.01 and 0.03 mgHC/gOC and that the S_2 component varies between 0.02 and 0.08 mgHC/gOC for the Cootanoorina Formation (Figure 16b). The Cootanoorina Formation had multiple S_2 peaks, suggesting multiple stages of maturation and multiple phases of migration, potentially

representing a new source of hydrocarbons for the Arckaringa hydrocarbon system, within the shallower parts of the basin.

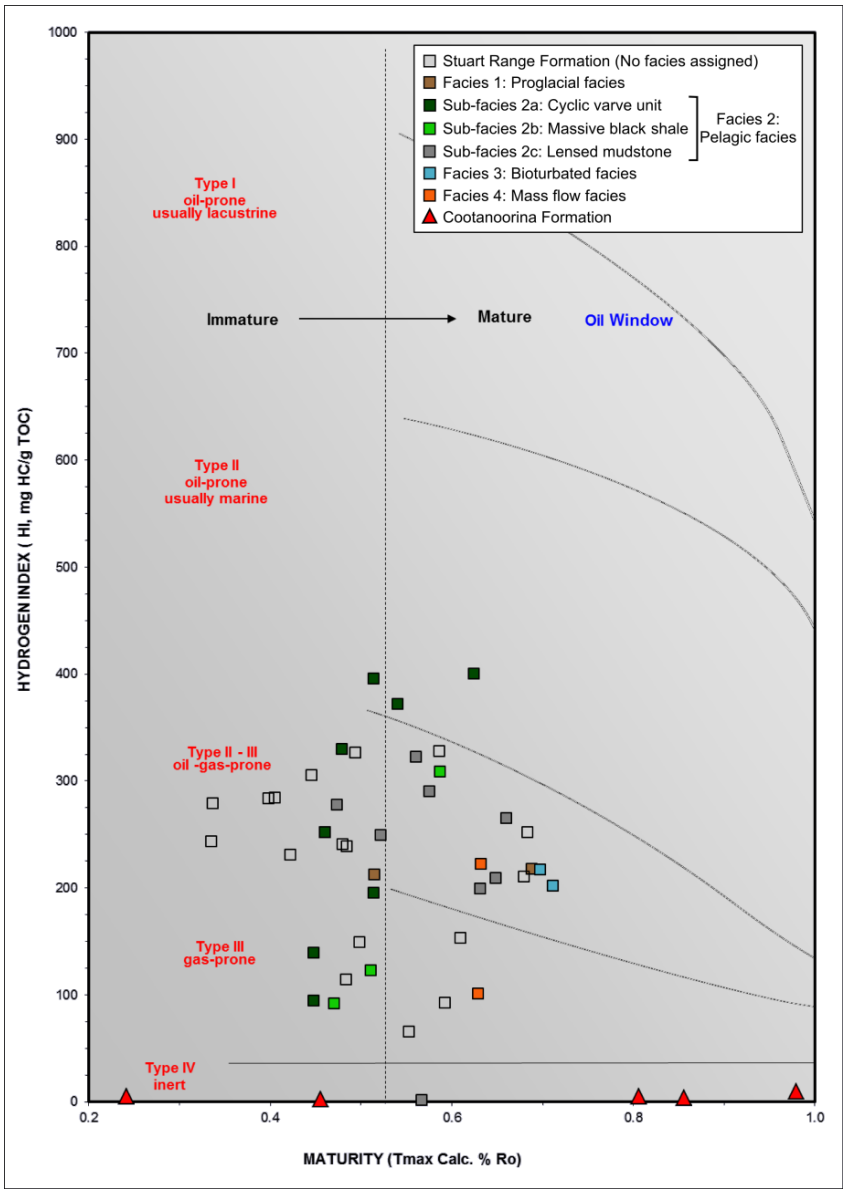

Figure 15: The types of hydrocarbons and the maturity of a selection of Arck 1 and Cootanoorina 1 core samples, based on source rock analysis (SRA). The Stuart Range Formation (box), taken from the Arck 1 core, is primarily Type II–III oil-gas-prone to Type III gas-prone as indicated by the low hydrogen index (HI) values. It is immature to mature, heading into the oil generation window. The Stuart Range Formation samples have been coloured according to their facies. Samples without an assigned facies have not been coloured. The Cootanoorina Formation (red triangle), taken from the Cootanoorina 1 core, is Type IV inert to Type III gas-prone as indicated by the extremely low HI values. This formation has no potential to very minimal potential to produce hydrocarbons.

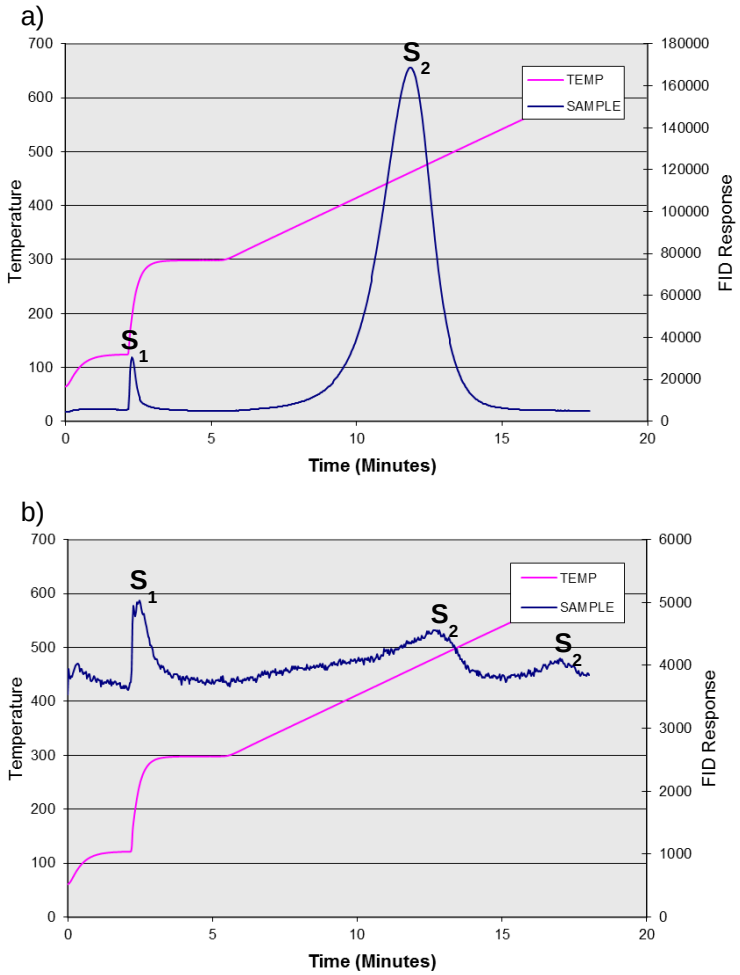

Figure 16: Representative source rock potential pyrograms of the Stuart Range Formation and the Cootanoorina 1 Formation based on source rock analysis (SRA). The plots show the proportions of free (S1) and potential (S2) hydrocarbons as artificial maturation is induced by incrementally increasing temperature over a period of time. (a) The Stuart Range Formation (2053193 at 963.04 m), taken from the Arck 1 core, has a significant hydrocarbon potential, as indicated by the large S2 peak. The comparatively low S1 peak indicates a low proportion of free hydrocarbons. (b) The Cootanoorina Formation (2066664 at 948.06 m), taken from Cootanoorina 1, has multiple S2 peaks, suggesting multiple stages of maturation and multiple phases of migration.

DISCUSSION

These observations and data reveal the heterogeneous nature of the Stuart Range Formation and present a valuable geochemical record of OM deposition and preservation through time. This study attempts to determine the mechanism of OM preservation in the absence of the influences typical of source rocks forming in greenhouse conditions, such as mineral surface (MSA) preservation with mineral surfaces of detrital clay minerals. These source rocks show that MSA provides a form of physical sheltering for otherwise labile organic compounds (Keil *et al.* 1994; Kennedy and Wagner 2011). The organic rich Stuart Range Formation is composed of immature feldspathic silts. This reflects the dominance of physical over chemical

weathering, so that high surface clay minerals typically formed in soils are not significant and thus cannot account for OM preservation in the same way as the class of source rocks deposited during greenhouse conditions**.** Indeed, petrographic analysis shows that OM occurs as micron-scale, discrete particles (Figure 3), rather than as organo-clay aggregates. Organic geochemistry indicates that these particles are hydrogen rich, and thus labile, raising the question of preservational mechanisms in this environment if mineral surfaces were not significant.

Unlike typical source rock deposition during greenhouse conditions, the Arckaringa Basin source rocks are coincident with the waning stages of glaciation. Active glaciation is evidenced by the dominance of physical weathering, by the presence of rainout clastic material and dropstones within the proglacial facies from melting glaciers or icebergs (Figure 17a), and by the lonestone identified within the mass flow facies. The feldspathic micaceous siltstone composition of the Stuart Range Formation is immature and is lacking the mineralogy typical of source rocks, i.e. soil derived clay minerals. In fact, recent and ancient marine shales normally contain 60–80% phyllosilicate minerals (Weaver 1980). This sheds light on the peculiarity of the mechanically-produced Stuart Range Formation sediments, whose presence and distribution, at such fine resolutions, was made available by the novel approach of EDS mineral mapping.

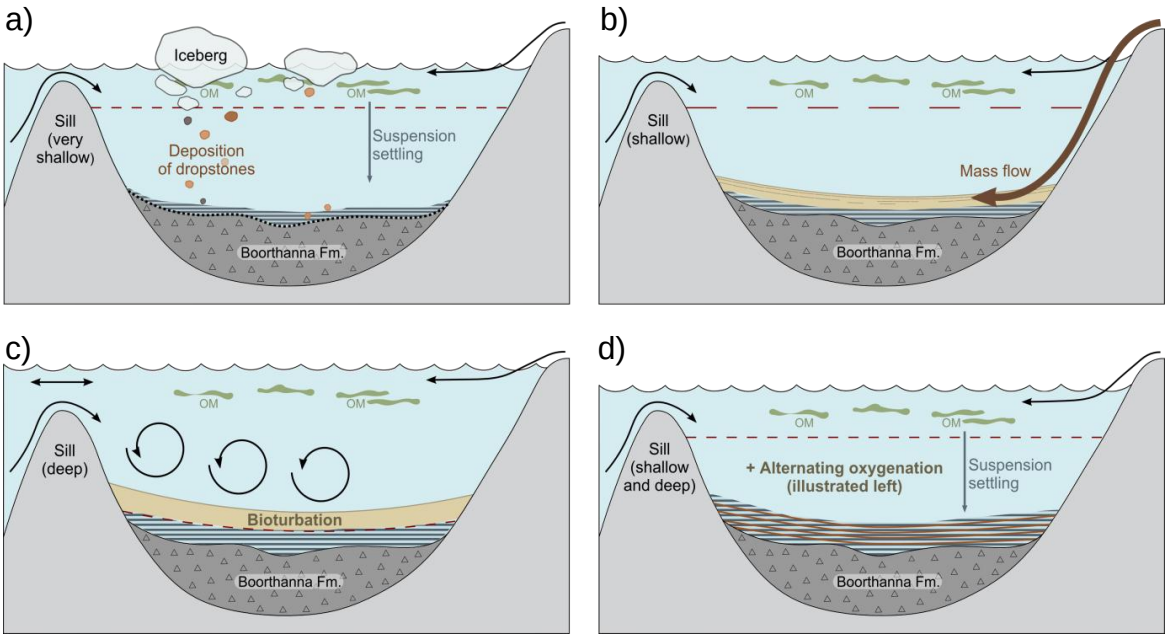

Figure 17: Schematic diagrams illustrating the interpreted depositional environments for the six facies identified in the lower Stuart Range Formation in the Arck 1 core. Features within these models are further detailed in Figure 19. The pycnocline (water density gradient) is represented by the red dashed line. (a) Proglacial facies depositional model. Very low sea level, shallow sill conditions due to the presence of glaciers and icebergs. Rare deep water renewal and a shallow pycnocline, with occasional fresh water replenishment as ice melts. (b) Mass flow facies depositional model. Low sea level, shallow sill conditions. Rare deep water renewal and a shallow pycnocline, promotes the development of stratified, euxinic bottom water conditions. Though this is disrupted with mass flow events that result in a surge of sediment deposition and brief bottom water oxygenation. (c) Bioturbated facies depositional model. High sea level, deep sill conditions. Frequent deep water renewal and a pycnocline within the interstitial waters a few centimetres below the sediment–water interface. Mixing of the water column with oxygen and nutrients promotes benthic fauna activity within the oxic sediments (bioturbation). (d) Pelagic facies depositional model. Low sea level, shallow sill conditions. Rare deep water renewal and a shallow pycnocline, promotes the development of stratified, euxinic bottom water conditions. However, this is episodically interrupted by oxic conditions following the bioturbated marl depositional model, on a seasonal timescale.

The millimetre-scale cyclic variations in TOC may be linked to paraglacial changes within the continental and depositional system. The oscillation between organic enriched laminae and organic lean, carbonate rich laminae describes a repetitive process that is constrained by the timing of the cyclicity acting on the system. In many marine systems, such as the modern restricted basins of east Antarctica (Stickley *et al.* 2005), varves are considered to record seasonal stratification at annual time scales. Storm

disturbances (2–30 years), climate trends (100–300 years), and Milankovitch forcing (19,000 year precession or 41,000 year obliquity periodity) can also be recorded (Anderson 1964; Peizhen *et al.* 2001). Although it is not clear whether the varved sequences within the Arckaringa Basin are seasonal, it is apparent that cyclical processes are acting on short timescales within the system, and it is reasonable to suggest seasonality. The mass flow facies that punctuate the pelagic, laminated facies may be an exception of cyclicity however, they are more likely a function of the frequency of sediment loading and gravitational instability on the trough slopes. In any case, given that they are episodic event deposits, they do not relate to chemical or physical conditions that would lead to OM preservation.

High resolution mineral mapping and spot analysis within the Stuart Range Formation has revealed unique elemental and mineral distributions. Manganese (Mn) and sulphur (S) enrichment are of particular interest and appear to be tied with cyclicity, where kutnohorite (Mn carbonate) laminae alternate with S-enriched OM and pyritic laminae. For instance, within the cyclic varve unit (pelagic facies) the systematic increase from light to dark mudstone laminations indicate an increasing contribution of organic matter resulting from increased productivity, sediment supply, or enhanced OM preservation efficiency due to water column anoxia. Also coincident with the darker mudstone laminations is an abundance of framboidal pyrite. Framboidal pyrite formation is commonly interpreted as the product of bacterial reduction of seawater-derived sulphate, which forms hydrogen sulphide (H_2S) and reacts with dissolved iron in the water column to form pyrite (Berner 1982). Pyrite can only form in the absence of oxygen and the presence of H_2S, and these conditions identify euxinia. As H_2S is only

available under anoxic conditions, this indicates bottom water or water column euxinia at the time dark laminae were deposited. The abundance of framboidal pyrite and the S enrichment in OM (lamalginite and sporinite; Figure 10) within higher TOC samples further indicate euxinia during sediment deposition and early diagenesis. On the other hand, the paler, coloured kutnohorite laminations that alternate with the darker laminations suggest more oxygenated conditions (Figure 18d; Huckriede and Meischner 1996). What chemical–physical mechanism can explain the source and unusual enrichment of Mn in light laminae and the association of S and framboidal pyrite in higher TOC, darker sediments?

Sulphate is one of the dominant anions in sea water, and a high abundance of sulphides (S) suggests a sea water source for S in pyrite, as framboidal pyrite requires a marine connection facilitating S resupply. The abundance of framboidal pyrite within the Stuart Range Formation implies sulphate reduction, which is energetically favoured only after free oxygen is no longer available as an oxidant. The development of seasonal strong density stratification, resulting in oxygen deficiency, by can be achieved through various mechanisms. The Arckaringa Basin shows similar fjord-like steep walled troughs in seismic data that would result in restriction by end-moraine sills, formed during the termination of glacial scour (Figure 17; Menpes *et al.* 2010). Restriction due to sills, and subsequent limited sea water exchange, results in anoxic conditions and H_2S build up in many modern examples. Examples include ancient analogues, such as the Karoo Basin in South Africa (Haldorsen *et al.* 2001; Maruoka *et al.* 2003) and the East Greenland Basin in Greenland (Piasecki and Stemmerik 1991), and modern analogues, such as the Framvaren Fjord in Norway (Saelen *et al.* 1993; Meyer and Kump 2008),

the Skagerrak Fjord in Germany (Aure *et al.* 1996), the Ellis Fjord in eastern Antarctica, the Baltic Sea in central Europe (Huckriede and Meischner 1996) and the Black Sea in southeast Europe (Murray *et al.* 2007). These are restricted from the open ocean by a sill or landmass, and are characterised by strong density stratification and S-rich euxinic conditions that generate high TOC values. Within the Stuart Range Formation, geochemical evidence supports the notion of periodic restriction and euxinia with a build up H_2S. This would explain the high S composition evidenced by abundant pyrite framboids and association of S with OM.

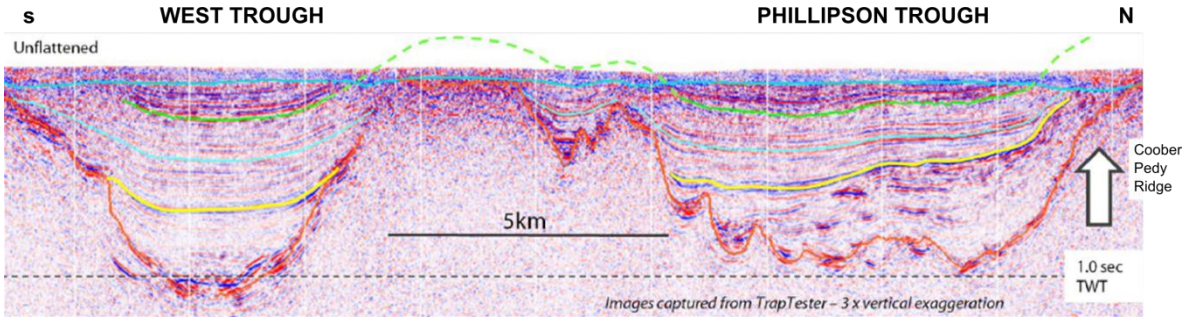

Figure 18: Interpretation of seismic line 86AK-7 of the Southern Arckaringa Basin troughs (West Trough and Phillipson Trough), showing the current geometry of the troughs (unflattened). These troughs have been interpreted as incised glacial valleys, i.e. fjords. From Menpes *et al.* (2010).

Schematically shown in Figure 19, restricted water exchange leads to density stratification, an elevated pycnocline, deep water oxygen depletion, and microbial sulphate reduction. H_2S builds up and pyrite precipitates until the depletion of Fe^{+2}. However, enhanced water exchange across the sill with sea level change re-oxygenates the bottom waters, resulting in a downward shift of the pycnocline to interstitial waters a few centimetres below the sediment–water interface (Meyer and Kump 2008; Howe *et al.* 2010). Changes in oxygenation in the benthic environment are recorded by intermittent intervals of bioturbation in the bioturbated facies (Figure 17c).

Bioturbation causes mixing, homogenisation and irrigation, allowing oxygenated water to penetrate the sediment (Aller 1984). This can impede OM preservation by remineralising OM at a more rapid rate (Aller 1994; Hartnett *et al.* 1998). Exchange with open ocean waters and flushing of stratified waters can occur periodically or aperiodically, depending factors such as tide, season, fresh water input, and seasonal heating (c.f. Howe *et al.* 2010).

Manganese has a short oceanic residence time (5–25 years) and therefore the fate of Mn is largely dependent on the capture and stabilisation of Mn in marine sediments (Klinkhammer and Bender 1980; Burke and Kemp 2002). The kutnohorite laminations that alternate with the darker laminations in the Stuart Range Formation cyclic varve unit (pelagic facies) are similar to those described from modern sediments in the anoxic Baltic Sea (Huckriede and Meischner 1996), which contain high concentrations of dissolved Mn, but experience seasonal oxygenation resulting in the oxidation of manganese (Mn^{2+}) to fine-grained particulate oxides. With a return of anoxic conditions, manganese oxides dissolve and Mn^{2+} accumulates in shallow sediment. Bacterial sulphate reduction, in combination with the Mn^{2+} liberated from manganese oxides, results in highly alkaline conditions. These conditions will promote kutnohorite precipitation above the anoxic sediments in the Baltic (Huckriede and Meischner 1996). Kutnohorite laminae form on seasonal timescales as varves (Burke and Kemp 2002), related to late winter–spring flooding events. By analogy, the rapid alteration between pyrite/OM rich laminae and kutnohorite laminae suggests seasonal oscillation in benthic redox conditions in the Stuart Range Formation pelagic facies. This implies a physical barrier, such as a sill, which would enhance sensitivity to changes in sea level and

climate. Sea level fluctuations influence the magnitude of bottom water exchange over time, as recorded in the pelagic facies, and may consequently explain the variation in the types of OM preserved.

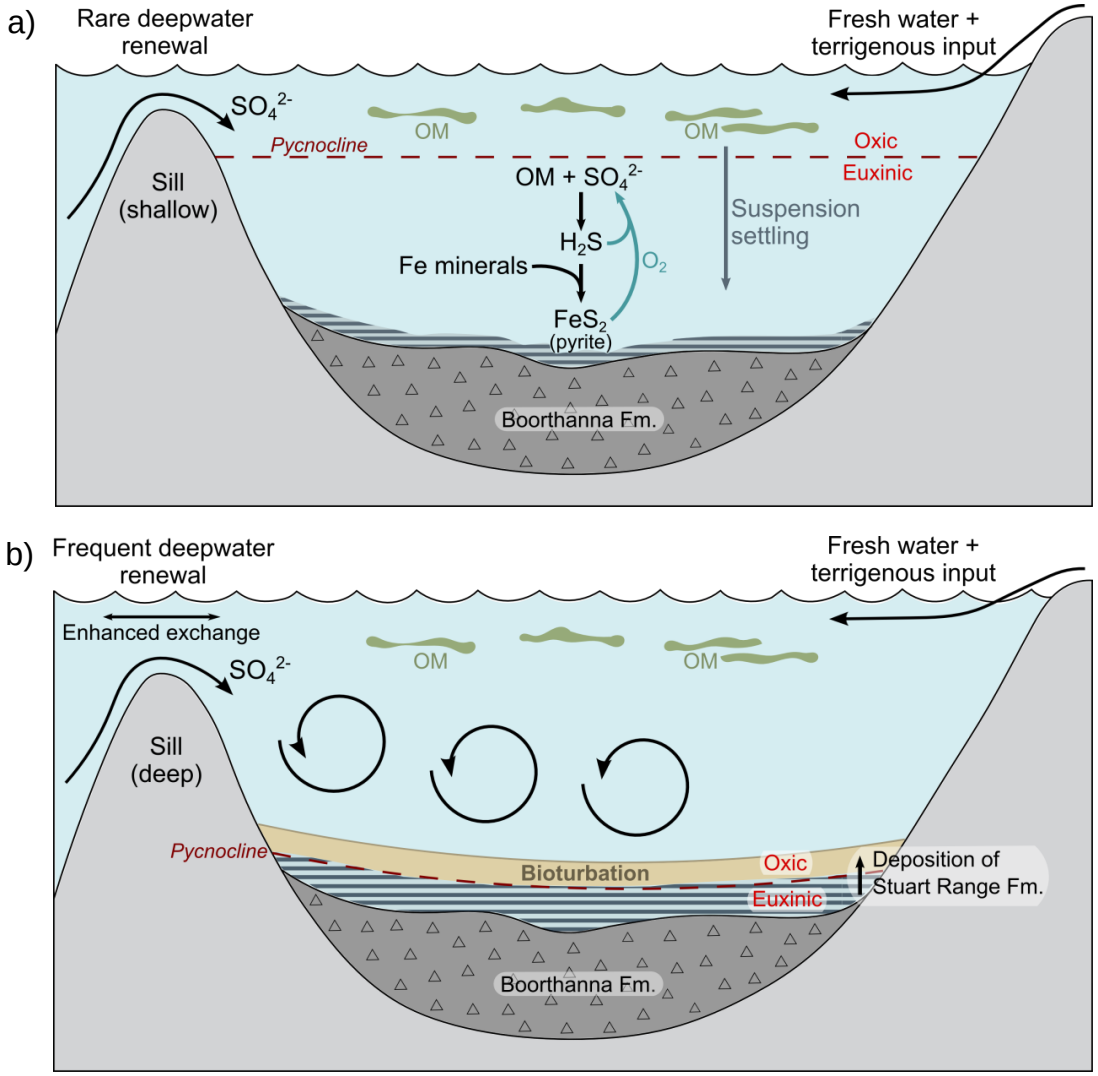

Figure 19: Schematic diagram illustrating the changes in water exchange across the sill and changes in bottom water redox conditions, as sea level rises and falls. Connection with the open ocean water across the sill allows sulphate (SO42-) replenishment. This diagram also shows the fluxes of fresh water, terrigenous material, and organic matter (OM) during deposition of the Stuart Range Formation, within the Arckaringa Basin troughs. (a) Low sea level, shallow sill conditions. Rare deep water renewal and a shallow pycnocline, promotes the development of stratified, euxinic bottom water conditions. The sulphur cycle, occurring within the euxinic zone, shows the partial removal of SO42- by bacterial sulphate reduction to make sulphide or hydrogen sulphide (H2S). H2S can then react with the iron (Fe) minerals within the water column to precipitate pyrite (FeS2). Fine-grained sediments are deposited as laminations in this undisturbed setting. (b) High sea level, deep sill conditions. Frequent deep water renewal and a pycnocline within the interstitial waters a few centimetres below the sediment–water interface. Mixing of the water column with oxygen and nutrients promotes benthic fauna activity within the oxic sediments (bioturbation).

Vulcanization reactions (also known as sulfurization) result in the enrichment of S in OM and involve the incorporation of inorganic S into lipids and carbohydrates to form organosulphur compounds during early diagenesis (Burdige 2007). Microbial sulphate reduction during early sediment burial [1],

$$2CH_2O + SO_4^{2-} \rightarrow 2HCO_3^- + H_2S, \quad [1]$$

results in H_2S build up below the pycnocline, leading to water column formation of pyrite in small (10 μm) framboids and the incorporation of S into OM. Vulcanization has been shown to increase carbon preservation in recent sediments (Wakeham *et al.* 1995; Adam *et al.* 1998 and references therein). A study by Tegelaar *et al.* (1989) indicates that, in certain environments, these reactions can facilitate the preservation of structural information in reactive biomarkers, by preventing the degradation and remineralisation of sulphurised biolipids. Studies on the Karoo Basin (Maruoka *et al.* 2003), East Greenland Basin (Piasecki and Stemmerik 1991; Syvitski *et al.* 1996), Ellis Fjord (Sinninghe Damsté *et al.* 2007), and Black Sea sediments (Wakeham *et al.* 1995) show incorporation of reduced inorganic S in OM as a result of vulcanization during early diagenesis. The former three settings are of particular relevance to the Arckaringa Basin as these are associated with glacial, cold climate conditions within a restricted marine environment, providing an alternative mode of black shale deposition to greenhouse conditions responsible for the majority of source reactions.

It is envisaged that vulcanization was influenced cyclically by sea level change, which enhances or restricts water exchange across a sill at the head of the fjord, influences the depth of the pycnocline and influences the efficiency of sulphur bonding as a preservational mechanism. In the Stuart Range Formation, unlike the labile sporinite

and algal macerals with incorporated S, the refractory terrestrially-derived OM does not appear to be vulcanized, and does not seem to need vulcanization for preservation. Thus, it appears that when the system does not have the capacity for vulcanization, the sporinite and algal macerals are not preserved. In a preservation context, this explains changes in OM type through the Stuart Range Formation as a function of sea level fluctuations. At a facies level, it would be expected that within the pelagic facies the less oxygenated sediments (with lower kutnohorite concentrations) would have greater hydrogen indexes due to more labile OM. However, the pelagic sub-facies have similar distributions do not show this association (Figure 15). Undetected finer-scaled variations in OM type and geochemical trends may explain this.

Source rocks within the Cooper Basin, 350 km north-east of the Arckaringa Basin, comprise feldspathic immature mineralogy, similar thermal maturities to the Stuart Range Formation, and were deposited during the waning stages of the Pennsylvanian to early Permian glaciation (Hill *et al.* 2011). However, unlike the marine Arckaringa Basin, the equivalent Cooper Basin source rocks were deposited in freshwater lacustrine conditions. There is a dominance of Fe sulphides (pyrite) in the Arckaringa Basin, whereas Fe-rich siderite cement is common in the Cooper Basin, indicating S limitation typical of freshwater environments (Rezaee and Schulz-Rojahn 1998). While similar physical conditions governed deposition of sediment in the Cooper Basin during deglaciation, OM is highly oxidised even though anoxia also occurred in this setting. OM within the Cooper Basin consequently has very low hydrocarbon generation potential even though similar TOC values are recorded (Granger 2013). The lack of

abundant S from sea water likely made OM more labile without vulcanization reactions common in the Arckaringa Basin.

CONCLUSIONS

The immature feldspathic composition of the Stuart Range Formation reflects limited chemical weathering typical of cold climate environments where weathering rates are low and physical weathering dominates. High surface clay minerals typically formed in soils are not significant and thus cannot account for OM preservation in the same way as the class of source rocks deposited during greenhouse conditions. OM is dominated by discrete particles of OM in contrast to organo-clay aggregates common in many source rocks. Framboidal pyrite (<5 µm) is abundant only within organic-rich laminae and there is a positive relationship between OM and S concentration in these laminae. This indicates sulphate reduction in euxinic conditions leading to abundant reduce S in the water column. Restriction of sea water exchange in to the fjord in which the Stuart Range Formation was deposited led to development of density stratification while supplying S in the form of sulphate from an intermittent connection to the ocean. The reducing conditions of the fjord provided a chemical trap for S leading to its enrichment in organic matter. Similarly, Mn within carbonates was enriched in the same manner. The intermittently restricted conditions provide a trap of Mn leading to deposition of kutnohorite laminae during oxic intervals. This suggests seasonal oscillation in benthic redox conditions, similar to annual varves in proglacial environments.

The observations presented in this study show that restriction due to sill development in a fjord, and subsequent limited sea water exchange, resulted in anoxic conditions and

accounts for the enrichment of both S and Mn during alternating redox cycles associated with varve formation. This led to periods of hydrogen sulphide build up within the water column that was annually flushed with seasonal change in temperature and runoff. Excess dissolved sulphur build up in the water column and sediments resulted in vulcanization reactions to preserve OM through the incorporation of inorganic S into lipids and carbohydrates to form organosulphur compounds during early diagenesis. Equivalent successions in the lacustrine Cooper Basin are similar in many ways to the Stuart Range Formation, though they exhibit a very low hydrocarbon generation potential even though similar TOC values are recorded. Unlike the Arckaringa Basin, the lack of abundant S from sea water likely made OM more labile without vulcanization reactions to preserve OM.

ACKNOWLEDGMENTS

I am extremely grateful to my Primary Supervisor, Professor Martin Kennedy, for providing project scope, imparting his wealth of knowledge, and for his keen interest in developing my academic and analytical skills. I am thankful to my Co-Supervisor, Dr Stefan Löhr, for providing constructive thesis support, valuable feedback, and laboratory expertise. I also thank Dr Tony Hall for laboratory management, project support, and providing me with the opportunity to develop my technical and analytical skills. Sample preparation and experimental assistance was made possible through the help of laboratory assistant, Robyn Williamson, who also provided thesis support. I offer my thanks to Sandy Menpes from DMITRE/Santos Ltd. for her advice and in depth knowledge of the Arckaringa Basin, and to Dr Rosalind King and Dr Katie Howard for providing course work guidance. Constructive criticism and project ideas developed from discussions with the Sprigg Geobiology group, James Hall, and Eavhuy Chan are also greatly appreciated.

REFERENCES

ADAM P., PHILIPPE E. & ALBRECHT P. 1998. Photochemical Sulfurization of Sedimentary Organic Matter: A Widespread Process Occurring at Early Diagenesis in Natural Environments? *Geochimica et Cosmochimica Acta* **62**, 265-271. doi: 10.1016/S0016-7037(97)00332-3.

ALEXANDER E. M., GRAVESTOCK D. I., CUBITT C. & CHANEY A. 1998 Lithostratigraphy and environments of deposition. *In* Gravestock D. I., Hibburt J. E. & Drexel J. F. eds. *The petroleum geology of South Australia. Vol. 4: Cooper Basin.* Department of Primary Industries and Resources. Report Book 98/9, South Australia.

ALGEO T. J., MEYERS P. A., ROBINSON R. S., ROWE H. G. & JIANG Q. 2014. Icehouse–greenhouse variations in marine denitrification. *Biogeosciences* **11**, 1273-1295. doi: 10.5194/bg-11-1273-2014.

ALLER R. C. 1984. The importance of relict burrow structures and burrow irrigation in controlling sedimentary solute distributions. *Geochimica et Cosmochimica Acta* **48**, 1929-1934. doi: 10.1016/0016-7037(84)90375-2.

ALLER R. C. 1994. Bioturbation and remineralization of sedimentary organic matter: effects of redox oscillation. *Chemical Geology* **114**, 331-345. doi: 10.1016/0009-2541(94)90062-0.

ANDERSON R. Y. 1964. Varve calibration of stratification. *In* Merriam D. G. ed. *Symposium on Cyclic Sedimentation.* Kansas Geological Survey Bulletin, 1-20.

AURE J., DANIELSSEN D. & SÆTRE R. 1996. Assessment of eutrophication in Skagerrak coastal waters using oxygen consumption in fjordic basins. *ICES Journal of Marine Science* **53**, 589-595.

BALLANTYNE C. K. 2002. Paraglacial geomorphology. *Quaternary Science Reviews* **21**, 1935-2017. doi: 10.1016/S0277-3791(02)00005-7.

BERNER R. A. 1982. Burial of organic carbon and pyrite sulfur in the modern ocean: Its geochemical and environmental significance. *American Journal of Science* **282**, 451-473.

BISHOP M. G. 2013. Resource and evaluation report of the Arckaringa Basin, South Australia. *Gustavson Associates LLC*. Colorado.

BRADSHAW M. T., BORISSOVA I., EDWARDS D. S., GIBSON G. M., HASHIMOTO T., NELSON G. T., ROLLET N. & TOTTERDELL J. M. 2012 Out of Gondwana. *In* Blewett R. S. ed. *Shaping a Nation: A Geology of Australia.* Geoscience Australia and ANU E Press, Canberra, pp. 332-379.

BURDIGE D. J. 2007. Preservation of organic matter in marine sediments: controls, mechanisms, and an imbalance in sediment organic carbon budgets. *Chemical Reviews* **107**, 467-485.

BURKE I. T. & KEMP A. E. S. 2002. Microfabric analysis of Mn-carbonate laminae deposition and Mn-sulfide formation in the Gotland Deep, Baltic Sea. *Geochimica et Cosmochimica Acta*, 1589-1600.

CROWELL J. C. & FRAKES L. A. 1971. Late Paleozoic glaciation: Part IV, Australia. *Geological Society of America Bulletin* **82**, 2515-2540.

DIDYK B. M., SIMONEIT B. R. T., BRASSELL S. C. & EGLINTON G. 1978. Organic geochemical indicators of paleoenvironmental conditions of sedimentation. *Nature* **272**, 216-222.

ESPITALIÉ J., MADEC M., TISSOT B., MENNING J. & LEPLAT P. 1977. Source rock characterization method for petroleum exploration. *Offshore Technology Conference*, Houston, Texas.

FREUDENTHAL T., WAGNER T., WENZHÖFER F., ZABEL M. & WEFER G. 2001. Early diagenesis of organic matter from sediments of the eastern subtropical Atlantic: evidence from stable nitrogen and carbon isotopes. *Geochimica et Cosmochimica Acta* **65**, 1795-1808. doi: 10.1016/S0016-7037(01)00554-3.

GRANGER T. 2013. Mechanisms for anomalous organic matter concentrations within the Roseneath-Epsilon-Murteree section of the Cooper Basin. Honours Thesis. The University of Adelaide, Adelaide (unpubl.).

HALDORSEN S., VON BRUNN V., MAUD R. & TRUTER E. D. 2001. A Weichselian deglaciation model applied to the Early Permian glaciation in the northeast Karoo Basin, South Africa. *Journal of Quaternary Science* **16**, 583-593. doi: 10.1002/jqs.637.

HALL P. A., MCKIRDY D. M., HALVERSON G. P., JAGO J. B. & GEHLING J. G. 2011. Biomarker and isotopic signatures of an early Cambrian Lagerstätte in the Stansbury Basin, South Australia. *Organic Geochemistry* **42**, 1324-1330. doi: 10.1016/j.orggeochem.2011.09.003.

HARRIS W. K. & MCGOWRAN B. 1968. S.A.G. Cootanoorina No. 1 Well. Upper Paleozoic and Lower Cretaceous Micropalaeontology. Grid G/3. Report 66/33. *Department of Mines*. South Australia.

HARTNETT H. E., KEIL R. G., HEDGES J. I. & DEVOL A. H. 1998. Influence of oxygen exposure time on organic carbon preservation in continental margin sediments. *Nature* **391**, 572-574. doi: 10.1038/35351.

HARVEY S. C. & HIBBURT J. E. 1999. Petroleum exploration and development in South Australia. 12th edition. Report Book 99/3. *Department of Primary Industries and Resources*. South Australia.

HIBBURT J. E. 1984. Review of exploration activity in the Arckaringa Basin region 1858 to 1983. Report Book 84/1. *Department of Mines and Energy*. South Australia.

HIBBURT J. E. 1995 Arckaringa Basin. *In* Drexel J. F. & Preiss W. V. eds. *The geology of South Australia. Vol. 2, The Phanerozoic.* South Australia. Geological Survey. Bulletin, 54, pp. 73-76.

HILL A., MENPES S., BACKE G., KHAIR H. & SIASITORBATY A. 2011. Shale gas prospectivity in South Australia. *APPEA Journal* **51**.

HOWE J. A., AUSTIN W. E. N., FORWICK M., PAETZEL M., HARLAND R. & CAGE A. G. 2010. Fjord systems and archives: a review. *The Geological Society of London, Special Publications* **344**, 5-15.

HUCKRIEDE H. & MEISCHNER D. 1996. Origin and environment of manganese-rich sediments within black-shale basins. *Geochimica et Cosmochimica Acta* **60**, 1399-1413.

INTERNATIONAL COMMITTEE FOR COAL AND ORGANIC PETROLOGY 1963. International Handbook of Coal Petrology. 2 ed. Centre National de la Recherche Scientifique, Paris.

INTERNATIONAL COMMITTEE FOR COAL AND ORGANIC PETROLOGY 1998. The new vitrinite classification (ICCP System 1994). *Fuel* **77**, 349-358. doi: 10.1016/S0016-2361(98)80024-0.

INTERNATIONAL COMMITTEE FOR COAL AND ORGANIC PETROLOGY 2001. The new inertinite classification (ICCP System 1994). *Fuel* **80**, 459-471. doi: 10.1016/S0016-2361(00)00102-2.

JARVIE D. M., CLAXTON B., HENK B. & BREYER J. 2001. Oil and Shale Gas from Barnett Shale, Ft. Worth Basin, Texas. *AAPG National Convention.*

JASPER J. P. & GAGOSIAN R. B. 1989. Glacial-interglacial climatically forced d^{13}C variations in sedimentary organic matter. *Nature* **343**, 60-62.

JENSEN-SCHMIDT B., ALEXANDER E. M. & COTTON T. B. 2006 Structural and tectonic setting. *In* Cotton T. B., Scardigno M. F. & Hibburt J. E. eds. *The petroleum geology of South Australia, Volume 2: Eromanga Basin.* 2 ed. Department of Primary Industries and Resources, South Australia., pp. 1-27.

JONES M. J. 1987. Review of palynology, Arckaringa Basin (Newmont NB/SR 12, Birribiana No. 1 and Hanns Knob No. 1). Report 542/1. *Dehli Petroleum Pty Ltd*. South Australia.

JONES P. J. 1988. Evidence for diapirism in the Arckaringa Basin, South Australia. Honours Thesis. The University of Adelaide, Adelaide (unpubl.).

KEIL R. G., MONTLUCON D. B., PRAHL F. G. & HEDGES J. I. 1994. Sorptive preservation of labile organic matter in marine sediments. *Nature* **370**, 549-552.

KENNEDY M. J., PEVEAR D. R. & HILL R. J. 2002. Mineral Surface Control of Organic Carbon in Black Shale. *Science* **295**, 657-660. doi: 10.1126/science.1066611.

KENNEDY M. J. & WAGNER T. 2011. Clay mineral continental amplifier for marine carbon sequestration in a greenhouse ocean. *Proceedings of the National Academy of Sciences* **108**, 9776-9781. doi: 10.1073/pnas.1018670108.

KLEMME H. & ULMISHEK G. F. 1991. Effective petroleum source rocks of the world: stratigraphic distribution and controlling depositional factors (1). *The American Association of Petroleum Geologists Bulletin* **75**, 1809-1851.

KLINKHAMMER G. P. & BENDER M. L. 1980. The distribution of manganese in the Pacific Ocean. *Earth and Planetary Science Letters* **46**, 361-384. doi: 10.1016/0012-821X(80)90051-5.

LUDBROOK N. H. 1961. Permian to Cretaceous subsurface stratigraphy between Lake Phillipson and the Peake and Denison Ranges, South Australia. *Transactions of the Royal Society of South Australia* **85**, 67-80.

LUDBROOK N. H. 1967. Permian deposits of South Australia and their fauna. *Transactions of The Royal Society of South Australia* **91**, 65-92.

LÜNING S., CRAIG J., LOYDELL D. K., ŠTORCHD P. & FITCHESE B. 2000. Lower Silurian `hot shales' in North Africa and Arabia: regional distribution and depositional model. *Earth-Science Reviews* **49**, 121-200. doi: 10.1016/S0012-8252(99)00060-4.

MACQUAKER J. H. S. & KELLER M. A. 2005. Mudstone sedimentation at high latitudes: Ice as a transport medium for mud and supplier of nutrients. *Journal of Sedimentary Research* **75**, 696-709. doi: 10.2110/jsr.2005.056.

MARUOKA T., KOEBERL C., HANCOX P. J. & REIMOLD W. U. 2003. Sulfur geochemistry across a terrestrial Permian–Triassic boundary section in the Karoo Basin, South Africa. *Earth and Planetary Science Letters* **206**, 101-117. doi: 10.1016/S0012-821X(02)01087-7.

MAYER L. M. 1994. Surface area control of organic carbon accumulation in continental shelf sediments. *Geochimica et Cosmochimica Acta* **58**, 1271-1284. doi: 10.1016/0016-7037(94)90381-6.

MENPES S. A., KORSCH R. J. & CARR L. K. 2010. 2008 Gawler Craton-Officer Basin-Musgrave Province-Amadeus Basin (GOMA) seismic survey, 08GA-OM1: Geological interpretation of the Arckaringa Basin. *In* Korsch R. J. & Kositcin N. eds. *GOMA (Gawler Craton-Officer Basin-Musgrave Province-Amadeus Basin) Seismic and MT Workshop 2010.* Geoscience Australia, Record 2010/39, 16-31.

MENPES S. A. 2012. Unconventional hydrocarbon potential of the Arckaringa Basin, South Australia. *In* Ambrose G. J. & Scott J. eds. *Central Australian Basins Symposium III.* Petroleum Exploration Society of Australia, Special Publication, 1-7.

MEYER K. M. & KUMP L. R. 2008. Oceanic Euxinia in Earth History: Causes and Consequences. *Annual Review of Earth and Planetary Science* **36**, 251-288. doi: 10.1146/annurev.earth.36.031207.124256.

MOODLEY L., MIDDELBURG J. J., HERMAN P. M. J., SOETAERT K. & DE LANGE G. J. 2005. Oxygenation and organic-matter preservation in marine sediments: Direct experimental evidence from ancient organic carbon-rich deposits. *Geology* **33**, 889-892. doi: 10.1130/G21731.1.

MOORE P. S. 1982. Hydrocarbon potential of the Arckaringa Region, central South Australia. *Australian Petroleum Exploration Association* **21**, 237-253.

MURRAY J. W., STEWART K., KASSAKIAN S., KRYNYTZKY M. & DIJULIO D. 2007 Oxic, suboxic, and anoxic conditions in the Black Sea. *In* Yanko-Hombach V., Gilbert A., Panin N. & Dolukhanov P. M. eds. *The Black Sea Flood Question: Changes in Coastline, Climate, and Human Settlement.* Kluwer, Dordrecth, Netherlands.

PEIZHEN Z., MOLNAR P. & DOWNS W. R. 2001. Increased sedimentation rates and grain sizes 2–4 Myr ago due to the infuence of climate change on erosion rates. *Nature* **410**, 891-897.

PIASECKI S. & STEMMERIK L. 1991. Late Permian anoxia in central East Greenland. *Geological Society Special Publication* **58**, 275-290. doi: 10.1144/GSL.SP.1991.058.01.18.

POPPE L. J., PASKEVICH V. F., HATHAWAY J. C. & BLACKWOOD D. S. 2001. A Laboratory Manual for X-ray Powder Diffraction. Open-File Report 01-041.

PRICE P. L., FILATOFF J., WILLIAMS A. J., PICKERING S. A. & WOOD G. R. 1985. Late Palaeozoic and Mesozoic palynostratigraphical units. Report 274/25. *CSR Oil and Gas Division*. (unpubl.).

REZAEE M. R. & SCHULZ-ROJAHN J. 1998. Application of Quantitative Back-Scattered Electron Image Analysis in Isotope Interpretation of Siderite Cement: Tirrawarra Sandstone, Cooper Basin, Australia. *International Association of Sedimentologists, Special Publications* **26**, 461-481.

SAELEN G., RAISWELL R., TALBOT M. R., SKEI J. M. & BOTTRELL S. H. 1993. Heavy sedimentary sulfur isotopes as indicators of super-anoxic bottom-water conditions. *Geology* **21**, 1091-1094.

SHERROD L., DUNN G., PETERSON G. & KOLBERG R. 2002. Inorganic carbon analysis by modified pressure-calcimeter method. *Soil Science Society of America Journal* **66**, 299-305.

SINNINGHE DAMSTÉ J. S., RIJPSTRA W. I. C., COOLEN M. J. L., SCHOUTEN S. & VOLKMAN J. K. 2007. Rapid sulfurisation of highly branched isoprenoid (HBI) alkenes in sulfidic Holocene sediments from Ellis Fjord, Antarctica. *Organic Geochemistry* **38**, 128-139. doi: 10.1016/j.orggeochem.2006.08.003.

STICKLEY C. E., PIKE J., LEVENTER A., DUNBAR R., DOMACK E. W., BRACHFELD S., MANLEY P. & MCCLENNAN C. 2005. Deglacial ocean and climate seasonality in laminated diatom sediments, Mac.Robertson Shelf, Antarctica. *Palaeogeography, Palaeoclimatology, Palaeoecology* **227**, 290-310. doi: 10.1016/j.palaeo.2005.05.021.

SUÁREZ-RUIZ I., FLORES D., FILHO J. G. M. & HACKLEY P. C. 2012. Review and update of the applications of organic petrology: Part 1, geological applications. *International Journal of Coal Geology* **99**, 54-112. doi: 10.1016/j.coal.2012.02.004.

SUMMERFIELD M. A. 1991 Weathering and associated landforms. *Global geomorphology : an introduction to the study of landforms.* Pearson Education Ltd., Essex, London.

SUN M., ALLER R. C., LEE C. & WAKEHAM S. G. 2002. Effects of oxygen and redox oscillation on degradation of cell-associated lipids in surficial marine sediments. *Geochimica et Cosmochimica Acta* **66**, 2003-2012. doi: 10.1016/S0016-7037(02)00830-X.

SYVITSKI J. P. M., ANDREWS J. T. & DOWDESWELL J. A. 1996. Sediment deposition in an iceberg-dominated glacimarine environment, East Greenland: basin fill implications. *Global and Planetary Change* **12**, 251-270. doi: 10.1016/0921-8181(95)00023-2.

TAYLOR G. H., TEICHMÜLLER M., DAVIS A., DIESSEL C. F. K., LITTKE R. & ROBERT P. 1998. Organic Petrology. Gebrüder Borntraeger, Berlin.

TEGELAAR E. W., DE LEEUW J. W., DERENNE S. & LARGEAU C. 1989. A reappraisal of kerogen formation. *Geochimica et Cosmochimica Acta* **53**, 3103-3106. doi: 10.1016/0016-7037(89)90191-9.

TOWNSEND I. J. & LUDBROOK N. H. 1975. Revision of Permian and Devonian nomenclature of four formations in and below the Arckaringa Basin. *South Australia Geological Survey, Quarterley Geological Notes* **54**, 2-7.

TOWNSEND I. J. 1976. A synthesis of stratigraphic drilling in the Arckaringa Basin 1969-1971. Report Book 73/98. *Department of Primary Industries and Resources*.

VEEVERS J. J. 2006. Updated Gondwana (Permian–Cretaceous) earth history of Australia. *Gondwana Research* **9**, 231-260. doi: 10.1016/j.gr.2005.11.005.

WAKEHAM S. G., SINNINGHE DAMSTÉ J. S., KOHNEN M. E. L. & DE LEEUW J. W. 1995. Organic sulfur compounds formed during early diagenesis in Black Sea sediments. *Geochimica et Cosmochimica Acta* **59**, 521-533. doi: 10.1016/0016-7037(94)00361-O.

WEAVER C. E. 1980. Fine-grained rocks: Shales or physilites. *Sedimentary Geology* **27**, 301-313. doi: 10.1016/0037-0738(80)90017-2.

WEISSERT H. & MOHR H. 1996. Late Jurassic climate and its impact on carbon cycling. *Palaeogeography, Palaeoclimatology, Palaeoecology* **122**, 27-43.

WOHLING D., KEPPEL M., FULTON S., COSTAR A., SAMPSON L. & BERENS V. 2013. Australian Government Initiative on Coal Seam Gas and Large Coal Mining: Arckaringa Basin and Pedirka Basin Groundwater Assessment Projects. DEWNR Technical Report 2013/11. *Government of South Australia, through Department of Environment, Water and Natural Resources*. Adelaide.

WOPFNER H. & ALLCHURCH P. D. 1967. Devonian sediments enhance petroleum potential of Arckaringa Sub-basin. *Australasian Oil and Gas Journal* **1**, 19-32.

WOPFNER H. 1970. Permian paleogeography and depositional environment of the Arckaringa Basin, South Australia. *In* Proceedings and Papers IUGS Sub-Commission on Gondwana stratigraphy and palaeontology. *Second Gondwana symposium.* Council for Scientific and Industrial Research, Scientia, South Africa, 273-291.

WOPFNER H. 1980 Development of Permian intracratonic basins in Australia. *In* Cresswell M. M. & Vella P. eds. *5th International Gondwana Symposium, Wellington, New Zealand, 1980.* pp. 185-190.

APPENDIX A: EXTENDED BASIN HISTORY AND INFLUENCES ON DEPOSITION

Following the amalgamation of a number of Archaean cratons and the development of the Australian continent, a series of tectonic events were initiated during the Delamerian Orogeny (Late Cambrian) that resulted in the underlying structural architecture of the Arckaringa Basin and the formation of zones of crustal weakness (c.f. Wohling *et al.* 2013). The establishment of the Arckaringa Basin and adjacent Permo-Carboniferous basins was controlled by the initiation of north-west trending lineaments and subsequent down-faulting (Wopfner 1970; Jensen-Schmidt *et al.* 2006). These structures were initially active during the Devonian along zones of early crustal weakness (Wopfner and Allchurch 1967; Jones 1988), and Jensen-Schmidt *et al.* (2006) suggest that the Devonian to Carboniferous compression and uplift associated with the Alice Springs Orogeny had a significant influence on the development of the basin. However, the development of the basin and its adjacent highlands was ultimately driven by compression plate convergence on the eastern Australian plate margin during the Palaeozoic (Wopfner 1980). This convergence was the result of the large-scale collision of Gondwana and Laurasia. As Gondwana drifted southward, changes from tropical equatorial carbonitic and evaporitic facies to high-latitude glacial and detrital facies occurred (Veevers 2006). A combination of latitudinal changes, highland development and shallow basement exposures promoted the occurrence of plateau-type glaciers during the mid-Carboniferous, evidenced by striated and fluted cobbles and boulders, glendonites (after ikaite), and dropstones (Wopfner 1970; Crowell and Frakes 1971).

According to Wopfner and Allchurch (1967), and Townsend (1976), the Arckaringa Basin troughs developed primarily along the north-west trends, which were re-activated as a result of tectonic activity during the Devonian to Early Permian. The Boorthanna Trough is presumed to have once been active as a failed rift arm and is now the largest basinal depocentre, (Jones 1988). In comparison, Ludbrook (1967), and more recently Menpes *et al.* (2010), considered the Arckaringa Basin troughs as erosional features formed by glacial scour, i.e. fjords. Deposition of the Arckaringa basin sediments and syngenetic faulting (Wopfner 1970; Harvey and Hibburt 1999; Jensen-Schmidt *et al.* 2006) has been dated from 298.9 to 290.1 Ma (Price *et al.* 1985) on the basis of palynological information. The Boorthanna Formation was deposited during glaciation and subsequent deglaciation, which was followed by deposition of the Stuart Range Formation with northwest to southeast eustatic sea level rise and tectonic subsidence (Wopfner 1970; Jones 1987; Veevers 2006). Eustatic fall or crustal isostatic recovery occurred and deltaic progradation across the system resulted in the deposition of the Mount Toondina Formation (Menpes *et al.* 2010; Menpes 2012). Menpes *et al.* (2010) suggested that the breaks and final termination in deposition may be correlated to three events; the breaks in deposition preserved within the Patchawarra Formation in the Cooper Basin, the Daralingie Unconformity (Early to Late Permian) in the Cooper Basin, or the Hunter-Bowen Orogeny (Middle Triassic).

It has been estimated that between 0.5 and 1 kilometre of the Mount Toondina Formation was removed by pre-Jurassic uplift and erosion (Harvey and Hibburt 1999; Wohling *et al.* 2013). Early-Cenozoic compression and uplift is also believed to have caused further deformation to the Permo-Carboniferous succession, including fault re-

activation and folding. Extended periods of tectonic quiescence and gradual down-warping have ultimately resulted in the deposition of sediments in the overlying Eromanga Basin and Lake Eyre Basin (Wohling *et al.* 2013).

APPENDIX B: EXTENDED METHODS

1 Sample collection and preparation

Samples were collected from two cores, Arck 1 and Cootanoorina 1, stored at the DMITRE drill core library, South Australia. Both cores were drilled within the Boorthanna Trough in the Arckaringa Basin (Figure B1) at similar depths (Table B1), although Arck 1 has undergone deeper burial. Samples were selected for geochemical, mineralogical, petrographical and petrophysical analyses to illustrate the geochemical and diagenetic variability across the Arckaringa Basin formations and the underlying Cootanoorina Formation.

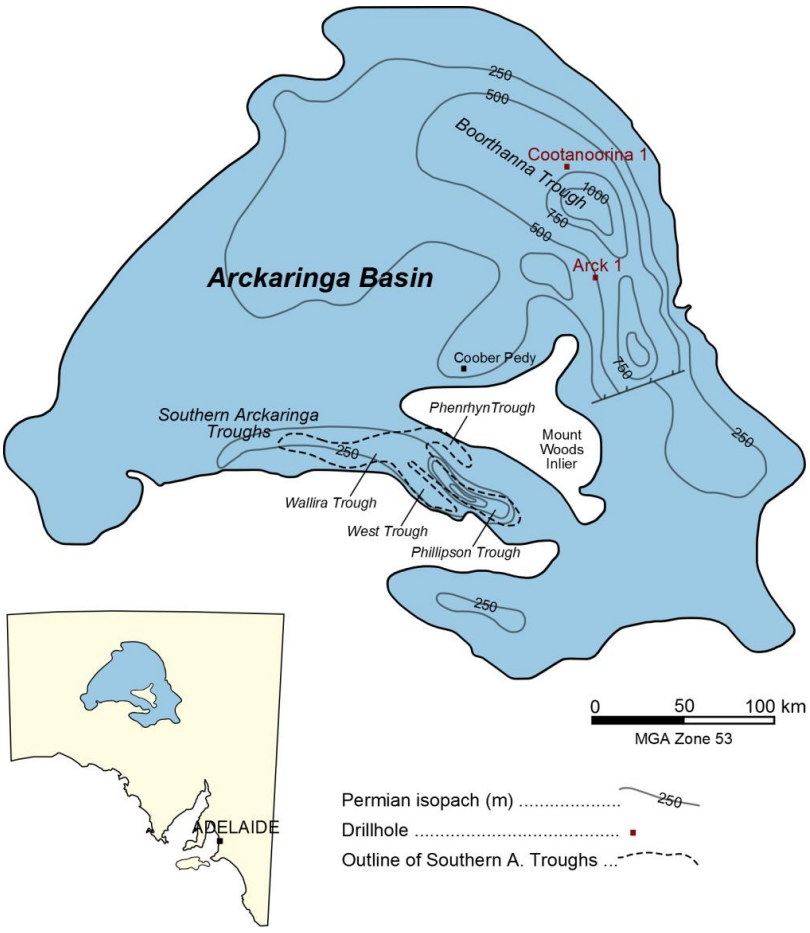

Figure B1: Location map of the Arckaringa Basin in South Australia (inset) and the position of the Boorthanna Trough and Southern Arckaringa Troughs. The locations of Arck 1 and Cootanoorina 1 within the Boorthanna Trough are also shown, intersected by section line A–B. Permian isopach lines illustrate the thickness of the subsurface Permian sediments across the basin. Modified after Hibburt (1995) and Menpes (2012).

Table B1: Summary of the drill core and sampling information for Cootanoorina 1 and Arck 1, acquired from the Cootanoorina 1 and Arck 1 well completion reports.

	Cootanoorina 1	Arck 1
Max. drilled date	15-06-1967	17-08-2011
Operator	S.A. Dept. Mines and Energy	Linc Energy Ltd.
Exploration tenement	–	PEL 122
Latitude	28° 00.5′ 23.218″ S	28° 30′ 12.48″ S
Longitude	135° 19′ 59.632″ S	135° 29′ 10.37″ E
Formations intersected	Mount Toondina Formation to Cootanoorina Formation	Mount Toondina Formation to upper Boorthanna Formation
Core depth sampled	380.09–948.06 m	876.13–994.10 m
Cutting depth sampled	701.04–871.73 m	–
Inspection number	4278	4194

Arck 1 was logged from 874–994.1m, noting the variations in lithology, diagenetic alteration features, fossils and sedimentary structures, and a total of 153 core samples were taken. Well preserved core was limited for Cootanoorina 1, so only variations in lithology could be discerned. A total of 25 core samples and 56 cutting samples were taken from Cootanoorina 1, along with 6 pre-prepared thin sections.

Prior to sampling, photographs of the core and intervals to be sampled were taken. Core samples and cuttings were acquired in accordance with the DMITRE sampling restrictions guidelines; small slithers (less than 2 cm wide) of half-core for core samples, and approximately 10 grams for cutting samples. If necessary, samples were cleaned with deionised water. Using the Labtechnics LM 1/M vibrating mill, samples were milled to a fine powder for approximately 30 seconds. Only half of each core sample was crushed to ensure that the remaining rock could be used for thin sections and polished.

2 Analyses

A variety of geochemical, mineralogical, petrographical and petrophysical analyses were conducted in order to gain an understanding of the geochemical and diagenetic variability across the Arckaringa Basin formations and the underlying Cootanoorina Formation, and these are summarised in Table 2. Data from analyses presented in the Arck 1 and Cootanoorina 1 well completion reports was used to support the analyses when necessary.

Table B2: Summary of the number of Cootanoorina 1 and Arck 1 samples for each analysis conducted. Each analysis is discussed in detail in the following sections.

	Cootanoorina 1 (No. of samples)	Arck 1 (No. of samples)
TOC	81	191
SRA (RockEval)	18	62
GC-MS (Thermal extraction)	-	7
GC-MS (Pyrolysis)	-	3
XRD (Bulk powder)	-	23
XRD (Clay mineral fraction)	-	3
Thin Section	-	14
Organic Petrography	-	11
SEM	-	11

2.1 TOTAL ORGANIC CARBON (TOC) ANALYSIS

Modified Pressure Calcimeter tests (following the standard procedure detailed below) were conducted following the method of Sherrod *et al.* (2002) in order to determine the inorganic carbon (IC) content of the samples, and an Elemental Analyser was used to determine the total carbon (TC) content. Total organic carbon (TOC) was calculated by subtracting the difference of IC from TC, and was corrected for carbonate dilution using standards;

$$TOC\ (\%) = TC\ (\%) - IC\ (\%)$$

2.1.1 Pressure Calcimeter standard procedure

1. Cut micro-centrifuge tubes above the 1 mL mark on the tubes.
2. Layout rows of small serum bottles (number of samples + number of standards and blanks).
3. Prepare an acid reagent by mixing 330 mL of concentrated (37%; 12.18 M) hydrochloric acid with 500 ml of water in a 1 L volumetric flask. Add 30 g ferrous chloride and dilute to a volume of 1 L.
4. Add 5 ml of the 4 M HCl with 3% $FeCl_2$ ($FeCl_2 * 4H_2O$) solution to each glass vial.
5. Weigh out 200 mg (± 2 mg) of each sample into a micro-centrifuge tube, record the weight, and place into the vials containing acid, ensuring that the sample does not come into contact with the acid solution.
6. Weigh out 7 $CaCO_3$ standards (approximately for every 75 samples, hence 21 standards were weighed in this analysis) into the micro-centrifuge tubes following the standards weights: 200mg, 150mg, 100mg, 75mg, 50mg, 25mg, and 10mg. Place the micro-centrifuge tubes into vials containing acid.
7. Place 4 vials as blanks (2 at the beginning of the analysis sequence and 2 at the end), containing only the acid and an empty micro-centrifuge tube in each.
8. Cap all vials with butyl rubber stoppers and aluminium tear-off seals, and crimp the foil using a hand crimper.
9. Once all vials are capped, shake each vial vigorously for several seconds to make sure that all samples and $CaCO_3$ mix and react with the acid.
10. Leave the vials for 4 hours, shaking them again at the 2 hour mark.
11. Ensure that the hose and needle is attached to a manometer.

12. Tear off the aluminium seal from the aluminium cap on the first vial, and reset the manometer to zero pressure. Pierce the butyl rubber stopper with the manometer needle and record the maximum pressure. Repeat for all vials.
13. Using the recorded weights and pressures of the $CaCO_3$ standards and blanks, graph pressure (mbar) on the x-axis and mass (mg) on the y-axis, and find the regression value and equation of the trend line (Figure 2). Calculate the $\%CaCO_3$ in each sample using the equation from the trend line that best represents the dataset (with the closest R^2 value to 1) to normalise the data and using the recorded weights and pressures for each sample. This can be done in Excel.
14. Convert $\%CaCO_3$ in each sample into %IC (inorganic carbon): $\%IC = \%CaCO_3 * 0.12$.

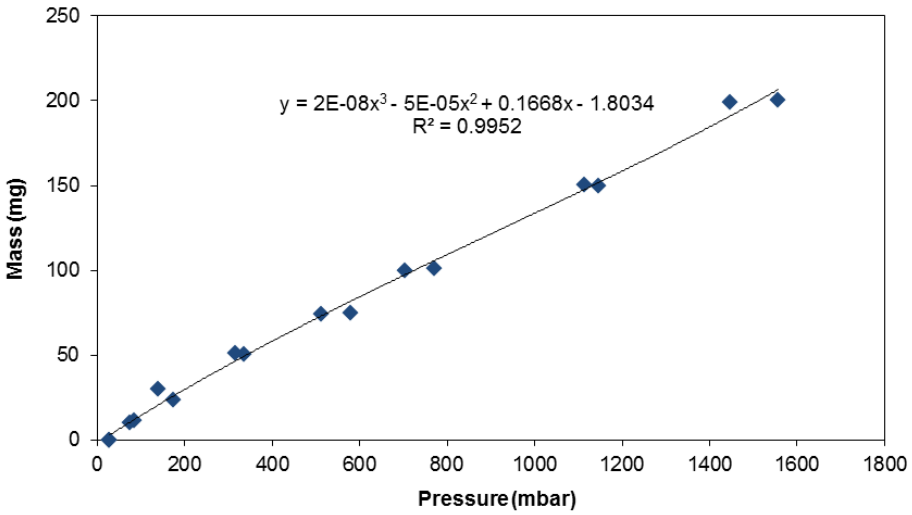

Figure B2: Pressure versus mass plot for the CaCO3 standards and blanks with polynomial regression, used to normalise to the exact mass of the weighed samples and calculate the inorganic carbon content.

2.1.2 Elemental Analyser

Once calibrated following a standard calibration procedure, the total carbon (TC) content was measured using a PerkinElmer® 2400 Series II CHNS/ O Elemental

Analyser (EA), in CHN mode. Finely milled samples were weighed to 7 mg (± 2 mg) in tin capsules, folded, and were placed in the EA carousel. Alternating S2 and $CaCO_3$ standards were run after every 10 samples to check the calibration of the EA and validate the sample readings, i.e. S2: 29.99 ± 0.3% C; and $CaCO_3$: 12.00 ± 0.3% C. If the standards were not within range, the samples were labelled as invalid and were analysed. The TC content was attained by recording the %C value for each sample.

2.2 SOURCE ROCK ANALYSER (SRA) AND ROCKEVAL ANALYSIS

To evaluate the thermal maturity, the proportion of free hydrocarbons (S_1) and the proportion of hydrocarbons with generative potential (S_2), pyrolysis-induced maturation of OM was performed using a Weatherford® Laboratories SRA TPH. The standard procedure of sample preparation listed in the Weatherford® Laboratories (December 2011) operator's manual was followed and is detailed below.

2.2.1 Sample preparation standard procedure

1. If necessary, crush or pulverise the rock material, using a mortar and pestle, and pass through a 40-mesh sieve.
2. Take the cap off and empty the contents. Do not touch the crucible with your fingers. To avoid oil contamination from the analyst's skin, either the crucibles must be handled with forceps, or the technician should wear latex or Nitrile gloves. Contamination appears as hydrocarbon traces.
3. Place an empty glass vial on the balance, press zero, and weigh out approximately 100 mg of sample into the vial. Record weight.
4. Remove the glass vial containing the weighed sample from the balance and pour the sample into a crucible (which is on the base of a metal stand and covered by a metal

funnel top). Vigorously tap the funnel to ensure that the entire sample is transferred into the crucible.

5. Remove the funnel covering and cap the crucible. Place the crucible in the auto-sampler tray. Continue weighing samples and placing them in the auto-sampler tray. A calibration standard, followed by a check standard, is run at the beginning of the sequence in the auto-sampler tray. Check standards are then run at positions 10, 20, 30, etc. and one check standard is run at the end of the entire sequence.
6. In the sequence editor, record information such as sample ID, sample weight, acquisition type, sample depth and formation, and save this information.
7. Once all of the samples have been weighed, place the auto-sampler trays in the auto-sampler rack.
8. Check the instrument gas flow rates and make adjustments to gas flows if necessary.

Air = 300 mL/min
Hydrogen = 50 mL/min
Nitrogen = 50 mL/min

9. The analytical method is set up using the Method Editor in the Thermal Station main menu.
10. Adjust the Temps tab and the Standard tab parameters as necessary.
11. Initiate acquisition after appending the information from the sequence editor.
12. The auto-sampler will transfer a crucible from the auto-sampler tray to the pedestal, which will then transfer the crucible to a 300°C oven. The oven is kept isothermally at 300°C enabling the free hydrocarbons to be volatilised. This is measured as the S_s peak by the Flame Ionisation Detector (FID).

13. The temperature of the oven is increased to 600°C at a rate of 25°C/minute. Heavy hydrocarbons ($>C_{40}$) are volatilised and non-volatile organic matter and kerogen undergo pyrolitic cracking, releasing hydrocarbons. This is measured as the S_2 peak by the Flame Ionisation Detector (FID).
14. The maximum temperature reached at the S_2 peak is recorded as T_{max}.
15. The calculation of thermal maturity (calculated $\%VR_o$) is calculated following Jarvie *et al.* (2001):

$$\text{Calculated } \%VR_o = 0.0180 * T_{max} - 7.16$$

16. The data is represented as milligrams of hydrocarbon per gram of rock and is graphed as a pyrogram.

2.3 GC-MS ANALYSIS

2.3.1 MSSV-GC-MS thermal maturity analysis

Micro-scale-sealed-vessel pyrolysis with gas chromatography mass spectrometry (MSSV-GC-MS) thermal maturity analyses were conducted utilising a Quantum MSSV injector fitted to a HP Hewlett Packard 5973 GC-MS system. Prior to every analysis, the powdered sample to undergo pyrolysis was thermally cleaned for approximately 1 hour at 300°C to remove any extractable hydrocarbons. Approximately 10 mg of the sample was loaded into a 5 cm long x 5 mm in diameter, pre-cleaned MSSV glass reactor tube. MSSV tubes have high silica purity, with an internal volume of 100 µm and are bent to 120° in the middle. Pre-cleaned 80–120 mesh glass beads were added to fill unused void volume and the tube was flame sealed using a hand-held propane torch. The sealed tube was transferred to the high precision oven and heated isothermally for 24 hours at 325°C. Separations were made with a HP5-MS capillary column (25 m

length, 0.25 mm in diameter, and 0.25 μdf phase coating) and a helium carrier gas at a constant pressure of 60 KPa. Following the methodology of Hall *et al.* (2011), the tube was inserted into the injector, heated at 300°C and taken through a cleaning cycle of the GC by heating from 45–300°C at 15°C/min before holding at 300°C for 15 minutes in order to remove any contaminants from the exterior of the tube. This also served as the thermal desorption stage for non-pyrolysed samples, with additional dwell time. The tube was cracked open inside a purpose built GC injector and operated in splitless mode for 2 minutes, with the released analytes cryofocused in the front of the capillary column using a liquid nitrogen bath. In full scan mode GC-MS analysis commenced, with temperatures programmed to range between 45–300°C at 8°C/min, then held isothermal for 17 minutes. This was repeated for all samples undergoing pyrolysis. Full scan data was acquired across a range of 45–450 amu at 3 scans/second. Tentative identifications of the resultant peak spectra were based on retention times and published mass spectra.

2.3.2 Palaeoredox determination

Sealed vessel thermal extraction (TH-GC-MS) and micro-scaled sealed vessel pyrolysis coupled to gas chromatography-mass spectrometry (MSSV-GC-MS) chromatograms were generated in order to determine the pristane (pr) and phytane (ph) ratios. Pr/ph provides a biomarker parameter for the assessment of redox conditions, where a pr/ph value >1 indicates oxic conditions and a pr/ph value <1 reflects anoxic conditions at the sediment/water interface (Didyk *et al.* 1978).

2.3.3 Solvent extraction preparation

To determine the elemental ion composition of a select sample, solvent extraction was performed on the Thermo Fisher Accelerated Solvent Extractor (ASE) 350. Analysed by the GC-MS (HP5973) 30m, 0.25mm ID, 0.25udf HP5-MS at 50C, 1ul injected at 50:1 split held for 1 minute at 8 °C/min to 300°C and held for 17.75 mins. The helium carrier gas was set at 1ml/min constant flow. The solvent extraction was set up with the following method:

1. Cell size: 22ml, and the collection vials: 60ml.
2. Heat for 5 minutes, oven temperature 100C, with a static time of 5 minutes. Cycle repeat: 3 times.
3. The Rinse volume is set to 60%, with a purge of 120 seconds.
4. The solvent 1 reservoir was filled with 9:1 optima grade DCM:MeOH .
5. The system was set to rinse in between each sample, with a rinse volume of 5ml, with 3 cycles.

2.4 X-RAY DIFFRACTION (XRD) ANALYSIS

2.4.1 Bulk mineralogy and mineral identification

The bulk mineralogy of a selection of representative and high TOC samples was ascertained by a Bruker D8 ADVANCE Powder X-ray Diffraction (XRD) with a Cu-radiation source. Prior to analysis, powdered samples were loaded into XRD sample holders using vibration to ensure a smooth surface. A standard powder sequence was run, involving a Cu-radiation source, with an angle of 3.5–50° 2theta and step sizes of 0.02° with counting times of 1 second. Bruker DIFFRAC.EVA software and

Crystallography Open Database reference patterns were utilised for identifying mineral phases.

2.4.1 Clay fraction

Clay purification for XRD analysis – Carbonate removal step:

1. Place 1 g of sample in a 50 ml centrifuge vial. If preparing more sample at once, use several centrifuge tubes.
2. Add 15 ml of 1 M sodium acetate/acetic acid buffer (confirm this amount would dissolve all carbonates in a mainly carbonate sample).
3. Loosely screw on cap and place in water bath at 90 °C.
4. Keep a close eye on the samples, if reacting too vigorously remove to cold water bath until reaction has slowed.
5. As soon as effervescence stops, remove sample from hot water bath.
6. Fill up tube to 45 ml with deionised water (DIW).
7. Centrifuge for 5 minutes at 3000 rpm and discard supernatant into appropriately marked waste container.
8. Repeat steps 2 to 7 twice (keep in hot water bath for 30 minutes during repeats) – only necessary for samples with a high carbonate content.
9. Ca-exchange sample with 10 ml 1 M $CaCl_2$.
10. Shake sample well, leave for 10 minutes.
11. Centrifuge for 5 minutes at 3000 rpm and discard supernatant.
12. . Fill up tube to 50 ml with DIW.
13. Fill to 50 ml with DIW, cap and shake sample well.
14. Centrifuge for 5 minutes at 3000 rpm, discard supernatant.
15. Repeat rinse in DIW twice (three DIW rinses total).

Clay purification for XRD analysis – Organic matter removal step:

1. Adjust the required amount of sodium hypochlorite bleach to a pH of 9.5 using 4M HCl. This needs to be done in the fume hood as it releases a dangerous gas, and should be done on the day that the solution will be used as the resulting solution is not stable. Use a calibrated pH electrode.
2. Dispense 10 ml of the pH-adjusted bleach into each centrifuge vial.
3. Loosely cap vials, place vials in a plastic rack and place in a 90 °C water bath for 15 minutes.
4. Remove vials from bath, fill to 50 ml with DIW.
5. Centrifuge for 5 minutes at 3000 rpm.
6. Discard supernatant into appropriately marked waste container.
7. Repeat steps 2 to 6 until samples no longer react upon addition of bleach and have changed colour to light grey, brown or reddish, indicating complete removal of OM. This usually requires 1-3 repeats.
8. After the last bleach repeat, rinse sample in DIW once more.
9. Centrifuge for 5 minutes at 3000 rpm and discard supernatant.
10. Fill up tube to 50 ml with DIW.
11. Fill to 50 ml with DIW, cap and shake sample well.
12. Centrifuge for 5 minutes at 3000 rpm, discard supernatant.
13. Repeat rinse in DIW twice (three DIW rinses total).

NOTE: To make up a 1M sodium acetate–acetic acid buffer with a pH of 5, dissolve 82 g of sodium acetate (CH_3COONa) in about 900 mL deionized water, then add 45 mL glacial acetic acid (the concentrated acid from the bottle) and bring the total volume of the solution to 1000 mL by adding deionised water.

Clay separation for XRD analysis – Clay (< 2 μm) separation by NaCl method followed by Ca saturation:

1. To separate out enough clay size (<2 μm) material for bulk analysis, about 5 g sample is needed, although this is quite sample dependent.
2. Place up to 1.5 g of sample into a 50 ml plastic container. 4 centrifuge tubes for each sample are needed for a total sample weight of about 5 g. The initial amount of sample is dependent on the mineralogy of the sample. If quantitative analysis is required, accurately weigh the amount of sample used.
3. Add 10ml of 1M NaCl solution to each container.
4. Shake for 10 minutes in the end over end shaker.
5. Fill each centrifuge tube to 50 ml mark with deionized water.
6. Centrifuge for 10 minutes at 3000 RPM.
7. Carefully pour off supernatant liquid ensuring that none of the material collected at the bottom of the centrifuge tube is dislodged.
8. Repeat steps 5-7 twice.
9. Wash material from the centrifuge tubes into a labelled 250 ml beaker (use one beaker for each sample, so empty 4-5 centrifuge tubes of same sample to a single beaker).
10. Fill each beaker to about 150 ml with DIW.
11. Disperse sample in each beaker using the ultrasonic probe (DO NOT use the tapered tip on the ultrasonic probe for this or the tip will be damaged. Use the flat tip for 60 seconds at 50% amplitude). Make sure the tip is immersed in the sample and does not touch the beaker.
12. Wash the sample into the corresponding centrifuge tubes and make sure they are

filled to the 50 ml mark. Clean the probe with tissue a wet tissue between samples.

13. If processing several samples simultaneously it is a good idea to complete steps 9 to 12 for each sample before proceeding.
14. Shake up all samples before placing them in the centrifuge. Then centrifuge for 4 minutes at 900 RPM.

NOTE: This speed (RPM) and time is sufficient to remove all > 2 μm diameter particles from suspension ONLY IF using the Mawson Building (Organic Geochemistry Lab) centrifuge setup. If using a different centrifuge, different centrifuge tubes or centrifuging at temperatures substantially different from 25 °C these values will need to be adjusted. This can be calculated using the Centriset program.

15. At this stage the supernatant should be cloudy or discoloured. Carefully pour approximately three quarters of the supernatant into an appropriately labelled beaker of at least 2 litre capacity (again, one beaker per sample).
16. Repeat steps 9 to 15 until the supernatant becomes clear. At this stage you have removed all the < 2 μm material from the sample.

NOTE: Ideally the supernatant should be clear when all of the relevant size fraction is collected. In practice a point of diminished returns is reached. The total amount of supernatant collected is generally around 1 litre (less for sandy samples, more for high clay content samples).

17. Flocculate the material collected in beaker by adding a teaspoon of $CaCl_2$ to each beaker. Allow the flocculated material to settle overnight and siphon off clear supernatant using the siphon attached to the vacuum pump.

18. Pour flocculated material remaining in beaker into centrifuge tubes and spin at 3000 RPM for 20 minutes.
19. Carefully discard supernatant (supernatant should be clear.)
20. Repeat steps 18 and 19 until all material has been transferred from the beaker to the centrifuge tubes. The final portion of material will need to be washed from the beaker using deionised water from a squeeze bottle.
21. Add 10ml of 1M CaCl2 solution (aqueous) to each centrifuge tube and shake up the sample using the vortex mixer. Then fill to the 50 ml mark.
22. Centrifuge at 3000 RPM for 10 minutes.
23. Carefully discard clear supernatant.
24. Fill to 50 ml mark with deionized water and disperse using vortex mixer.
25. Centrifuge at 3000 RPM for 10 minutes.
26. Carefully discard clear supernatant.
27. Repeat 24 to 26 twice.
28. Leave collected material in centrifuge tube and oven dry at 60°C.
29. For quantitative analysis weigh the amount of material recovered from each sample.

2.5 THIN SECTION ANALYSIS

Variations in composition, texture, porosity and diagenetic alteration were investigated by examining representative thin sections. Reflected and transmitted light optical petrography using a Nikon Eclipse CiPOL polarising microscope was conducted on thin sections (~30 μm) prepared by Prograding Rock Services Ltd. The thin sections were made with a blue epoxy (to spot porosity and discontinuities), had a double carbonate staining over half of each thin section, and did not have a coverslip.

2.6 ORGANIC PETROGRAPHY ANALYSIS

Transmitted white light, fluorescence (UV and blue light), and polarised light microscopy was used for organic petrography analyses in order to identify the organic matter present. Sample preparation and analyses were conducted following the methodology and identification standards of Taylor *et al.* (1998) and Suárez-Ruiz *et al.* (2012) based on the ICCP (International Committee for Coal Petrology) System 1994. Samples were cut perpendicular to the bedding plane and the polished blocks were milled using a Fischione 1010 Argon Ion Mill. The ion mill setup involved two argon beams (left and right) with voltages of 5.0 kV, a focus of 30% (hence unfocussed and covering a broader area) and an angle of 1° from the surface of the sample. The mill was set for 6 hour sequences with a continuous rotation.

A classification table for the identification of organic macerals was compiled using the identification standards of these authors (Table 3). Each petrographic analysis followed the sequence detailed below:

1. An analysis of the polished block using transmitted white light to determine the extent of reflectance (low, medium, high), then using column 1 and the 'Identification' column in Table 3 to classify the macerals into their maceral groups.
2. A classification of the macerals was made by conducting a visual analysis of the defining maceral shapes and features, using the 'Identification' column in Table 3.
3. A photograph was taken of each different maceral identified and of the representative areas.
4. Fluorescence light (UV and blue light), and polarised light if necessary, was utilised to further identify the macerals, particularly the 'liptinites' which are easier to identify using fluorescence light.

5. A photograph under fluorescence light was taken of the same area that was photographed under white light.

Table B3: Classification table for the identification of organic macerals used during organic petrographic analysis. After International Committee for Coal and Organic Petrology (1963); International Committee for Coal and Organic Petrology (1998); International Committee for Coal and Organic Petrology (2001).

Maceral	Maceral sub-group	Macerals	Identification	
Vitrinite	**Telovitrinite**: Intact cell structures	Telinite	Distinct walls in large pieces of woody tissue. Shows cell cavities.	Medium and constant reflectance Higher plant terrestrial origin
		Collotellinite	Clear, homogenous and structureless gelified remains of plant tissue.	
	Detrovitrinite: Detrital	Detrovitrinite	Fragmented vitrinite often associated with a lot of inclusions/debris.	
		Collodetrinite	Mottled, dark bands of detrital material that bind other maceral components.	
	Gelovitrinite: Dominated by colloidal gelanite material	Gelinite	Formless, structureless gels which fill formerly empty spaces.	
		Corpogelinite	Discrete and homogenous, often fills cell lumens. Can be isolated or in situ.	
Inertinite	**Telo-inertinite**: Intact cell structure	Fusinite	Empty or mineral-filled, well preserved cellular structure. Oxidised ∴ bright.	High reflect. Terrestrial origin
		Semifusinite	Squashed, broken fusinite. Cannot see distinct cell walls or structure.	
		Sclerotinite	Represents fusinised resin bodies, round or oval form, fungi/fungal spores.	
	Detro-inertinite: Detrital	Inertodetrinite	Small, discrete fragments of varying sizes, >2 µm in size.	
		Micrinite	Non-angular particles >10 µm to <2 µm in size.	
	Gelo-inertinite: Non-structured	Macrinite	Structureless and inert material, occurs as ground mass or <10 µm bodies.	
Liptinite	**Primary liptinite**: H-rich, distinct structures	Sporinite	Spores, defined by thick, distinct walls. Can occur as sporangium capsules.	Low reflect. High fluores-cence Marine and terrestrial origin
		Resinite	Often 'sausage' shaped blobs with a homogenous texture.	
		Cutinite	Upper smooth surface and lower 'saw-tooth' appendages where cuticles were.	
		Alginite	'Cauliflower' appearance. Can occur as algal colonies.	
		Lamalginite	Long and finely banded, thin-walled lamellar alginite.	
		Suberinite	Cork. Lacy/wavy continuous form, often in-filled with corpogelinite or huminite.	
		Liptodetrinite	Small, finely detrital particles that cannot be identified as a maceral.	
	Secondary liptinite: Break down of liptinite	Bituminite, fluor-inate, exsudatinite	–	

2.7 SCANNING ELECTRON MICROSCOPE (SEM) ANALYSIS

Variations in compositional, textural, porosity and diagenetic alteration were also investigated by examining representative polished blocks. Backscattered SEM imaging was performed on a selection of polished blocks using the FEI Quanta 450 SEM and Joel Neoscope JCM 6000 SEM, with a voltage set to 10 kV for all samples. The polished block samples prepared for the organic petrography analysis (detailed in section 2.6) were used for this analysis. Images were taken for areas of interest.

APPENDIX C: XRD RESULTS

Table C1: Mineral phases present within a selection of Arck 1 core samples, based on bulk powder mineralogy X-ray diffraction (XRD) results. The mineral phases have been grouped into their mineral classes and total organic carbon (TOC) values have been included to facilitate analysis. The shaded boxes marked with an 'X' represent mineral presence. The '?' indicates that a mineral phase may be present, though with uncertainty. Note that the sample numbers are prefixed with '2053' and that only the last three digits are shown below.

		SILICATE								CARBONATE					SULPHATE		PHOS-PHATE	SULPH-IDE	
Facies	Sample	Quartz	Albite	Illite /mica	K-feldspar	Kaolinite	Leucite (?)	Mixed I-S	Chlorite	Siderite	Dolomite	Magnesite	Kutnohorite	Calcite	Jarosite	Gypsum	Apatite	Pyrite	TOC
-	165	X	X	X	X	X		X	X	X						X		X	1.01
1	180	X	X	X	X	X			X		X	?	X		X	X	?	X	3.70
1	183	X	X	X	X	X			X				X		X	X	?	X	4.38
2b	188	X	X	X	X	X			X						X	X		X	8.18
2b	190	X	X	X		X	X	X							X	X		X	0.56
2b	191	X	X	X		X	X	X	X						X	X		X	8.24
-	192	X	X	X		X		?	X						X	X		X	1.81
2b	193	X	X	X		X	X	X	X						X	X		X	3.65
2a	194	X	X	X	X	X		X	X						X	X		X	3.04
3	195	X		X		X					X	X	X	?			X	X	0.11
2b	196	X	X	X		X	X	X	X						X	X		X	7.74
2a	197	X	X	X		X			X		X		X		X	X	X	X	4.78
2c	198	X	X	X	X	X	X	?	X						X	X		X	4.64
2c	307A	X	X	X		X	X	?	X				X		X	X	X	X	4.60
3	307B	X	X	X	X	X		?	X		X			X	X	X	X	X	1.76
4	311	X		X	?	X			X	X	X	X	X	X					0.23
2c	315	X	X	X	X	X		X	X	?	?	?			X	X		X	7.59
4	327	X		X	?	X	X		X	X	X	?	X	X	X		?	X	0.88
-	332	X	X	X		X	X	?	X	X	X	X	X	X	X	X	X	X	1.29
-	336	X	X	X	X	X	X	X	X	?	X	X		?	X	X		X	5.60
-	339	X		X	?	X	X	X	?						X	X	?	X	2.11
-	362	X	X	X	X	X	X	?	X	?					X	X		X	3.36
-	363	X	X	X		X		X	X	?	X	?	X		X	?	X	X	8.33
-	379	X	X	X	X	X	X	X	X	?		X			X	X		X	9.71
-	383	X	X	X		X	X	X	X	X	?	X		?	?	?	X	X	2.81

Table C2: Clay mineral fraction present within a selection of Arck 1 core samples based on randomly-orientated powdered and orientated air dried and ethylene glycol X-ray diffraction (XRD) results. Total organic carbon (TOC) values have been included to facilitate analysis. 'X' represents mineral presence and '?' indicates that a mineral phase may be present, though with uncertainty. Refer to Figure 9 in the results section.

Sample	Illite	Smectite	Mixed I-S	Kaolinite	Chlorite	TOC
2053194	X	X	X	X	X	3.04
2053196	X	?	X	X	X	7.74
2053198	X	X	X	X	X	4.64

APPENDIX D: SUPPORTING SUB-SAMPLE DATA

Table D1: Supporting data for Arck 1 core subsamples and analyses performed on each. Formations: B = Boorthanna; SR = Stuart Range; MT = Mount Toondina.

Sample	Depth (m)	To Depth (m)	Formation	TOC (mg/g)	Analysis							
					SRA	TH-GC-MS	MSSV-GC-MS	XRD (Bulk)	XRD (Clay)	Thin Section	Organic Petrog.	SEM
2053149	994.10		B	0.07								
2053150	993.36		B	-0.07						X		
2053151	990.17		B	0.08								
2053152	989.70		B	0.03								
2053153	986.40		B	0.02								
2053154	985.12		B	0.01								
2053155	985.08		B	0.04								
2053156	983.92		B	0.01								
2053157	983.32		B	0.17								
2053158	982.27		B	-0.04								
2053159	982.09		B	-0.36								
2053160	980.49		B	0.22								
2053161	980.06		B	0.45								
2053162	979.89		B	-0.10								
2053163	979.10		B	0.13								
2053164	978.05		B	0.51								
2053165	976.15		B	1.01	X						X	X
2053166	975.88		B	1.49								
2053167	975.60		B	1.93								
2053168	975.39		B	1.52	X							
2053169	975.21		B	1.60	X							
2053170	975.11		B	1.96								
2053171	974.84		B	1.35								
2053172	974.64		B	0.82								
2053173	973.96		B	0.86								

2053174	973.17		B	4.16	X					X		
Sample	Depth (m)	To Depth (m)	Formation	TOC (mg/g)	Analysis							
					SRA	TH-GC-MS	MSSV-GC-MS	XRD (Bulk)	XRD (Clay)	Thin Section	Organic Petrog.	SEM
2053175	972.82		B	2.19								
2053176	972.67		B	1.69	X							
2053177	972.56		B	0.36								
2053178	972.44		B	1.56								
2053179	972.24		B	1.87						X		
2053180	971.59		B	3.70	X			X		X		
2053181	970.14		B	0.94	X							
2053182	970.03		B	4.19								
2053183	969.98		SR	4.38	X			X				
2053184	969.38		SR	2.08	X							
2053185	969.02		SR	6.81	X							
2053186	968.96		SR	3.48	X							
2053187	968.70		SR	6.46	X	X	X					
2053188	966.35		SR	8.18	X	X		X			X	X
2053189	966.22		SR	4.19	X							
2053190	966.14		SR	0.56	X			X				
2053191	965.10		SR	8.24	X	X		X			X	X
2053192	964.71		SR	1.81	X			X				
2053193	963.04		SR	3.65	X			X				
2053194	960.82		SR	3.04	X			X	X		X	X
2053195	960.24		SR	0.11	X			X				
2053196	959.97		SR	7.74	X			X	X	X	X	X
2053197	957.60		SR	4.78	X			X			X	X
2053198	955.79		SR	4.64	X			X	X		X	X
2053307A	952.59		SR	4.60	X			X			X	X
2053307B	952.59		SR	1.76	X			X				
2053308	951.30		SR	4.91	X							
2053309	951.25		SR	4.57	X							
2053310	951.03		SR	2.90	X							
2053311	949.87		SR	0.23	X			X				

2053312	949.65		SR	1.56	X							
Sample	Depth (m)	To Depth (m)	Formation	TOC (mg/g)	Analysis							
					SRA	TH-GC-MS	MSSV-GC-MS	XRD (Bulk)	XRD (Clay)	Thin Section	Organic Petrog.	SEM
2053313	947.56		SR	4.46	X							
2053314	946.34		SR	4.05	X							
2053315	945.12		SR	7.59	X			X				
2053316	944.90		SR	5.46	X							
2053317	943.77		SR	5.93	X							
2053318	943.05		SR	6.80	X							
2053319	942.34		SR	5.78	X							
2053320	941.00		SR	-0.11	X							
2053321	940.80		SR	5.91								
2053322	940.00		SR	4.66								
2053323	938.75		SR	6.90	X							
2053324	937.52		SR	6.53								
2053325	937.15		SR	4.57								
2053326	934.76		SR	3.44								
2053327	934.59		SR	0.88	X			X		X		
2053328	934.00		SR	6.49								
2053329	932.40		SR	6.52	X							
2053330	931.10		SR	5.13								
2053331	930.65		SR	4.30	X							
2053332	928.94		SR	1.29	X			X		X	X	X
2053333	927.00		SR	1.14								
2053334	926.44		SR	5.87	X	X	X					
2053335	926.00		SR	3.28	X	X						
2053336	924.80		SR	5.60	X			X				
2053337	924.42		SR	4.55								
2053338	924.27		SR	4.04								
2053339	923.03		SR	2.11	X			X			X	X
2053340	921.81		SR	4.71								
2053341	919.60		SR	4.87	X							
2053342	918.84		SR	3.43								

2053343	918.06		SR	6.36								
Sample	Depth (m)	To Depth (m)	Formation	TOC (mg/g)	Analysis							
					SRA	TH-GC-MS	MSSV-GC-MS	XRD (Bulk)	XRD (Clay)	Thin Section	Organic Petrog.	SEM
2053344	917.49		SR	3.41	X							
2053345	917.02		SR	4.21	X	X						
2053346	916.27		SR	7.95	X							
2053347	916.05		SR	8.69	X							
2053348	915.48		SR	4.20						X		
2053349	915.36		SR	6.20								
2053350	914.66		SR	3.57								
2053351	914.56		SR	3.53								
2053352	914.32		SR	4.69								
2053353	914.03		SR	2.07	X							
2053354	913.82		SR	3.88								
2053355	913.50		SR	3.83								
2053356	912.92		SR	5.30								
2053357	912.24		SR	5.72								
2053358	911.72		SR	5.04								
2053359	911.37		SR	7.81	X							
2053360	910.37		SR	5.53								
2053361	910.00		SR	4.05								
2053362	909.18		SR	3.36	X			X				
2053363	908.00		SR	8.33	X			X				
2053364	907.53		SR	7.01								
2053365	906.33		SR	7.90	X							
2053366	906.17		SR	4.89	X							
2053367	905.63		SR	4.23	X	X	X					
2053368	905.50		SR	4.44								
2053369	904.78		SR	4.21								
2053370	904.72		SR	3.92								
2053371	904.47		SR	2.63	X							
2053372	904.27		SR	4.90								
2053373	903.72		SR	5.84								

2053374	903.08		SR	4.38								
Sample	Depth (m)	To Depth (m)	Formation	TOC (mg/g)	Analysis							
					SRA	TH-GC-MS	MSSV-GC-MS	XRD (Bulk)	XRD (Clay)	Thin Section	Organic Petrog.	SEM
2053375	901.98		SR	5.20	X							
2053376	901.70	901.63	SR	4.15								
2053377	900.73	900.76	SR	7.52	X							
2053378	899.25		SR	6.09								
2053379	898.00		SR	9.71	X			X			X	X
2053380	897.84	897.81	SR	6.88								
2053381	897.26	897.31	SR	6.11	X							
2053382	896.06	896.14	SR	2.22						X		
2053383	896.00		SR	2.81	X			X		X		
2053384	895.29	895.24	MT	0.93	X					X		
2053385	894.44	894.53	MT	1.69						X		
2053386	894.04		MT	1.85								
2053387	893.76		MT	2.74	X							
2053388	893.42		MT	1.93						X		
2053389	892.72	892.76	MT	2.25								
2053390	892.42		MT	2.39								
2053391	892.01	891.94	MT	1.73								
2053392	891.02	890.96	MT	1.04								
2053393	890.46	890.41	MT	0.98								
2053394	890.14	890.09	MT	1.39								
2053395	889.72	889.63	MT	0.94								
2053396	889.35	889.28	MT	0.64								
2053397	889.02	888.96	MT	0.28								
2053398	888.81	888.73	MT	0.89								
2053399	888.50	888.43	MT	1.40	X							
2053400	887.05	886.99	MT	1.25								
2053401	886.55	886.50	MT	4.72	X							
2053402	885.90	885.85	MT	2.65								
2053403	885.05	885.00	MT	4.10								
2053404	882.37	882.30	MT	3.39								

2053405	877.06	877.02	MT	0.15								
Sample	Depth (m)	To Depth (m)	Formation	TOC (mg/g)	Analysis							
					SRA	TH-GC-MS	MSSV-GC-MS	XRD (Bulk)	XRD (Clay)	Thin Section	Organic Petrog.	SEM
2053406	876.80	876.74	MT	2.26								
2053407	876.64	876.60	MT	2.45								
2053408	876.13	876.06	MT	2.29	**X**							
2071876	970.45		SR	5.46								
2071877	968.50		SR	2.44								
2071878	968.00		SR	8.10								
2071879	967.00		SR	10.19								
2071880	964.00		SR	8.75								
2071881	963.50		SR	8.47								
2071882	962.50		SR	4.32								
2071883	962.00		SR	9.66								
2071884	961.40		SR	4.36								
2071886	959.50		SR	6.48								
2071887	959.00		SR	8.52								
2071888	958.00		SR	6.49								
2071889	957.25		SR	6.34								
2071890	956.75		SR	6.75								
2071891	954.00		SR	8.17								
2071892	953.50		SR	5.86								
2071893	953.00		SR	4.30								
2071894	952.25		SR	4.24								
2071895	951.75		SR	5.89								
2071896	950.70		SR	6.65								
2071897	950.55		SR	4.07								
2071898	950.40		SR	3.96								
2071899	950.25		SR	6.22								
2071900	950.10		SR	2.86								
2071901	949.95		SR	6.72								
2071902	949.90		SR	0.99								
A	969.16		SR	1.28								

B	968.06		SR	1.33								
Sample	Depth (m)	To Depth (m)	Formation	TOC (mg/g)	Analysis							
					SRA	TH-GC-MS	MSSV-GC-MS	XRD (Bulk)	XRD (Clay)	Thin Section	Organic Petrog.	SEM
C	963.31		SR	1.36								
D	962.96		SR	1.29							**X**	**X**
E	961.56		SR	1.71								
F	960.03		SR	1.56								
G	960.03		SR	1.40								
H	959.03		SR	3.79								
I	957.86		SR	5.55							**X**	**X**
J	956.06		SR	3.21								
K	955.9		SR	6.16								
L	951.56		SR	6.01								

Table D2: Supporting data for Cootanoorina 1 core and cutting subsamples and analyses performed on each. Formations: C = Cootanoorina; B = Boorthanna; SR = Stuart Range; MT = Mount Toondina.

Sample	Depth (m)	To Depth (m)	Formation	Core/Cutting	TOC (mg/g)	Analysis
						SRA
2066664	948.06		C	Core	1.79	X
2066665	947.80		C	Core	1.50	X
2066666	947.34		C	Core	1.70	X
2066667	946.48		C	Core	2.16	X
2066668	945.88		C	Core	0.79	X
2066669	945.20		C	Core	1.73	X
2066670	944.45		C	Core	1.51	X
2066671	944.92		C	Core	1.51	X
2066672	944.15		C	Core	2.16	X
2066673	943.60		C	Core	1.97	X
2066674	943.00		C	Core	1.04	X
2066675	928.42		C	Core	1.33	X
2066676	927.69		C	Core	0.52	X
2066677	926.69		C	Core	1.22	X
2066678	926.23		C	Core	0.72	X
2066679	925.37		C	Core	0.09	
2066680	888.86		B	Core	0.07	
2066681	888.23		B	Core	0.03	
2066682	873.65		B	Core	0.14	
2066683	872.83		B	Core	0.13	
2066684	718.96		SR	Core	0.10	
2066685	533.90		SR	Core	2.18	X
2066686	532.25		SR	Core	2.37	X
2066687	530.96		SR	Core	2.58	X
2066688	380.09		MT	Core	0.06	
2066691	868.68	871.73	B	Cutting	0.61	
2066692	865.63	868.68	B	Cutting	0.60	
2066693	862.58	865.63	B	Cutting	0.70	
2066694	859.54	862.58	B	Cutting	0.83	
2066695	856.49	859.54	B	Cutting	0.87	
2066696	853.44	856.49	B	Cutting	0.85	
2066697	850.39	853.44	B	Cutting	0.80	
2066698	847.34	850.39	B	Cutting	0.83	
2066699	844.30	847.34	B	Cutting	0.63	
2066700	841.25	844.30	B	Cutting	0.77	
2066701	838.20	841.25	B	Cutting	0.84	
2066702	835.15	838.20	B	Cutting	0.95	
2066703	832.10	835.15	B	Cutting	0.80	
2066704	829.06	832.10	B	Cutting	0.77	
2066705	826.01	829.06	B	Cutting	0.77	
2066706	822.96	826.01	B	Cutting	0.92	
2066707	819.91	822.96	B	Cutting	0.86	
2066708	816.86	819.91	B	Cutting	1.32	
2066709	813.82	816.86	B	Cutting	1.11	
2066710	810.77	813.82	B	Cutting	0.81	
2066711	807.72	810.77	B	Cutting	0.50	
2066712	804.67	807.72	B	Cutting	0.83	
2066713	801.62	804.67	B	Cutting	0.48	
2066714	798.58	801.62	B	Cutting	0.76	
2066715	795.53	798.58	B	Cutting	1.59	

Sample	Depth (m)	To Depth (m)	Formation	Core/Cutting	TOC (mg/g)	Analysis
						SRA
2066716	792.48	795.53	B	Cutting	0.54	
2066717	789.43	792.48	B	Cutting	0.70	
2066718	786.38	789.43	B	Cutting	0.86	
2066719	783.34	786.38	B	Cutting	0.68	
2066720	780.29	783.34	B	Cutting	0.65	
2066721	777.24	780.29	B	Cutting	0.66	
2066722	774.19	777.24	SR	Cutting	0.68	
2066723	771.14	774.19	SR	Cutting	0.87	
2066724	768.10	771.14	SR	Cutting	0.75	
2066725	765.05	768.10	SR	Cutting	0.80	
2066726	762.00	765.05	SR	Cutting	0.76	
2066727	758.95	762.00	SR	Cutting	0.70	
2066728	755.90	758.95	SR	Cutting	0.73	
2066729	752.86	755.90	SR	Cutting	0.98	
2066730	749.81	752.86	SR	Cutting	0.80	
2066731	746.76	749.81	SR	Cutting	0.71	
2066732	743.71	746.76	SR	Cutting	0.87	
2066733	740.66	743.71	SR	Cutting	0.79	
2066734	737.62	740.66	SR	Cutting	0.92	
2066736	731.52	734.57	SR	Cutting	0.96	
2066737	728.47	731.52	SR	Cutting	-0.49	
2066738	725.42	728.47	SR	Cutting	1.14	
2066739	722.38	725.42	SR	Cutting	1.91	
2066740	719.33	722.38	SR	Cutting	1.48	
2066741	716.28	719.33	SR	Cutting	1.82	
2066742	713.23	716.28	SR	Cutting	2.71	
2066743	710.18	713.23	SR	Cutting	2.87	
2066744	707.14	710.18	SR	Cutting	3.44	
2066745	704.09	707.14	SR	Cutting	3.23	
2066746	701.04	704.09	SR	Cutting	3.66	